2-13-2014

Multinode Acoustic Systems for High Throughput Cellular Analysis

Pearlson Prashanth Austin Suthanthiraraj

Pearlson Prashanth Austin Suthanthiraraj
Candidate

Department of Chemical and Nuclear Engineering
Department

This dissertation is approved, and it is acceptable in quality and form for publication:

Approved by the Dissertation Committee:

Steven Graves, Ph.D., Chairperson

Andrew Shreve, Ph.D.

Dimiter Petsev, Ph.D.

Bruce Edwards, Ph.D.

James Plusquellic, Ph.D.

MULTINODE ACOUSTIC SYSTEMS FOR HIGH THROUGHPUT CELLULAR ANALYSIS

by

PEARLSON PRASHANTH AUSTIN SUTHANTHIRARAJ

B. Tech (Chemical Engineering), Anna University, Chennai, India

DISSERTATION

Submitted in Partial Fulfillment of the
Requirements for the Degree of

Doctor of Philosophy
Engineering

The University of New Mexico
Albuquerque, New Mexico

December, 2013

Acknowledgements

I sincerely thank my advisor Dr. Steven Graves for his constant support and encouragement throughout my doctoral program at the University of New Mexico. His guidance made my graduate research a rewarding experience and enabled me to accomplish my goals. I express my deepest gratitude to him for giving me opportunities to present and publish this research and also for his comments and suggestions while preparing this manuscript. I would like to acknowledge Dr. Andrew Shreve for his valuable advice and contribution towards my doctoral research that ensured successful completion of this dissertation. I am greatly thankful to Dr. Menake Piyasena who mentored me during my graduate program and helped me in every stage of this research work. It was a great experience working with him. I truly appreciate his patience and time devoted towards this research. I also thank Travis Woods for helping me with early research and also for the laboratory training that enabled me conduct research following all safety practices and procedures. I would like to acknowledge Harold Madsen at the Manufacturing Training and Technology Center for his advice and guidance in the cleanroom. I thank Dr. James Freyer for insightful comments on this research work and Antoinette Trujillo for preparing tumor microspheroid samples used in this research. I would like to thank my friends, fellow graduate students and also my former colleagues Dr. Robert Applegate Jr., Rath Chaleunphonh, Erik Arellano, Jose Cornejo and Andrew Goumas for their support and encouragement. I am also thankful to the staff at the Center for Biomedical Engineering and the Department of Chemical and Nuclear Engineering for paying tuition bills and processing financial assistantship contracts that ensured a

smooth journey through my graduate program. Finally, I thank all the funding agencies that contributed towards this research.

MULTINODE ACOUSTIC SYSTEMS FOR HIGH THROUGHPUT CELLULAR ANALYSIS

by

Pearlson Prashanth Austin Suthanthiraraj

B.Tech Chemical Engineering, Anna University, Chennai, India, 2009

Ph.D. Engineering, University of New Mexico, 2013

ABSTRACT

For decades, flow cytometry is used as the gold standard for cellular analyses as it measures multiple properties of single cells. Traditional flow cytometry uses the hydrodynamic focusing technique where the sheath fluid focuses cells in the sample into a narrow stream. Although such precise focusing provides accurate optical measurements, high sheath fluid pressure and high linear velocities limit analysis rate to 50,000 particles/s. Such rates are too low for detecting rare events where one cell may have to be detected in a population of about a billion cells. Therefore, it is necessary to eliminate the sheath fluid and improve throughput by several orders of magnitude by using a suitable alternate focusing mechanism that allows focusing cells in high volume samples into multiple focused streams. Toward this aim, this dissertation presents the multinode acoustic technique that uses high frequency ultrasonic waves to focus particles and cells into highly parallel focused streams. One challenge, however, is that acoustic

attenuation is significant at high frequencies. Therefore, to optimize acoustic energy density within multinode acoustic flow cells, a simple model is derived based on exhaustive literature review, suggesting that attenuation may be minimized by proper choice of fabrication material. Using such acoustically transparent materials, multinode acoustic flow cells were fabricated by three approaches, which include using machined aluminum frame and glass slides, disposable rectangular glass capillaries and etched silicon flow cells fabricated using standard photolithography and deep reactive ion etching techniques. Among these, flexibility in design using microfabrication approach has allowed fabricating etched flow cells having multiple parallel channels. Such parallelization improves acoustic energy density within each channel and precisely focuses particles at volumetric throughput of few tens of mL/min. Finally, this dissertation presents a proof-of-concept flow cytometry instrumentation using laser line generation optics and microscopy image sensors for imaging parallel focused streams in multinode acoustic flow cells. High throughput and precise focusing suggest that multinode focusing is a suitable alternative to conventional hydrodynamics, and multinode acoustic flow cells integrated with such optical imaging systems incorporating real-time signal processing circuitry will provide throughput matching that required for the detection of circulating tumor cells.

Table of Contents

List of Figures

Chapter 9 Optical analysis of parallel streams

List of Tables

Chapter 1

Introduction

1.1. Flow cytometry

Flow cytometry is a powerful analytical technique that finds use in various applications ranging from single cell analysis to pathogen detection and analysis of cancer prognosis[1]. Unlike traditional cytometry techniques, flow cytometry measures size and granularity of cells in flow, and hence its name. Almost all flow cytometers use a sheath fluid to focus the cell sample into a narrow stream of approximately cellular size by the conventional hydrodynamic focusing mechanism. Such a precise hydrodynamically focused stream is achieved in most modern flow cytometers using the nozzle-and-tubing arrangement, where the sample flows through a nozzle that opens into wider tubing consisting of fast flowing sheath fluid. The hydrodynamic pressure of the sheath is usually higher than that of the sample fluid and hence the sheath fluid accelerates particles in the sample to focus into a narrow uniform core[2]. Once positioned, the properties of cells such as fluorescence, forward and side scatter are measured using a laser, at the interrogation point defined by the intersection of the focused flow stream with the laser beam spot, using high numerical aperture objective lens. Depending on the values of these properties, cells of interest are identified. Cells exiting the interrogation region are enclosed within droplets, generated using a piezo transducer attached to the flow cell. These droplets are then charged electrostatically and cells of interest are selectively sorted from the heterogeneous population for downstream analysis[1, 3].

1.2. Need for alternate focusing techniques

Flow cytometry measures multiple parameters from cells that are precisely focused using the hydrodynamic focusing mechanism on a cell-by-cell basis. In hydrodynamic focusing, the Reynolds number of flow for both the sample and the sheath fluid correspond to laminar conditions such that they flow coaxially without mixing. Besides mixing, such laminar flow aids particle positioning into the center of the cylindrical tubing, which is the region of high velocity in the radial direction. Moreover, the pressure of the sheath fluid is usually much higher than the sample fluid. Such high sheath-to-sample pressure ratios confine the sample fluid to a narrow core that is surrounded by a cylindrical element of the sheath fluid. Such particle confinement by laminar flow profile and high sheath-to-sample pressure presents a small interrogation volume, and hence enables distinguishing free fluorophores in solution from the particle-bound fluorophore, when the centrally-focused cells are interrogated by laser. Furthermore, the sample separation from the walls from the walls prevents surface fouling of the optically transparent flow cells[4, 5].

However, the use of sheath fluid presents several disadvantages also. While the sheath fluid precisely focuses particles of dimensions up to few tens of μm's, very high flow velocities required to focus large particles causes turbulences due to linear scaling of the Reynolds number of flow with the dimensions of the flow cell. Therefore, hydrodynamic focusing is limited to particle sizes <70 μm. Despite laminar flow, the high pressure difference between the sheath fluid and the sample induces a high velocity gradient between them, which accelerates the sample medium further, thus increasing the particle linear velocity. Reducing the sheath-to-sample pressure gradient to minimize such

particle acceleration significantly either increases the focusing width of the sample stream or moves the particles into low velocity regions of the flow profile, thus interfering with the accuracy of optical measurements. Moreover, such particle acceleration result in short transit times at the interrogation volume, and therefore necessitates using low noise lasers for optical interrogation and expensive detectors for high sensitivity, speedy acquisition, i.e. to detect as much scatter signal as possible within the short time that the particle resides at the interrogation volume. Although cells cross the interrogation volume one-by-one, the rate of arrival is inconsistent and follows Poisson statistics. Such random arrival in turn interferes with particle confinement within droplets for downstream analysis, resulting in drops having either no cell or more than one cell. Furthermore, the use of sheath fluid dilutes the sample for such analysis. High sheath pressure and particle acceleration limit the analysis rate also to approximately 50,000 particles per second using a flow rate of 100 μL/min with an acceptable coefficient of variation (CV) value of 5%. Increasing the flow rate further will only interfere with sensitivity of detection and lower the CV value. For these reasons, the hydrodynamic focusing mechanism greatly limits analysis rate for rare event detection, where one abnormal cell may have to detected against a background of as many as a billion (10^9) healthy cells [1, 4].

Therefore, it is necessary to improve throughput in traditional flow cytometry. One of the ways to improve throughput includes focusing particles and cells into multiple focused streams. Such parallelization of the focused streams will provide throughput that is a few orders of magnitude higher than that of the conventional hydrodynamic mechanisms depending upon the number of focused streams. Using the hydrodynamic mechanism,

such attempts were made by flowing high volume samples through more than one flow cytometer and analyzing the sample simultaneously[6], and hence increasing the analysis rate linearly. However, using multiple flow cytometers increase the cost of operation also linearly. Therefore, a miniaturized hydrodynamic focusing flow cell having 72 channels, which focuses particles and cells into as many as 72 focused streams, was fabricated and integrated with flow cytometry optics and detectors. Simultaneous analysis of these highly parallel streams provided particle event rate as high as 0.5×10^9/s, which is seven orders of magnitude higher than achieved using conventional flow cytometers. Although doubling the number of channels could produce a two-fold increase in analysis rate, it does not eliminate issues due to the use of sheath fluid such as flow turbulence, high pressure and particle acceleration[6, 7]. For these reasons, it may be necessary to replace hydrodynamic focusing by an alternate mechanism that increases throughput, eliminates sheath, reduces cost and retains precision[8, 9].

1.3. Improving analysis rate in flow cytometry using alternate focusing techniques

As mentioned previously, despite being able to precisely identify cells and particles of interest, flow cytometry suffers from low volumetric throughput, which limits its use in high volume applications that require focusing and analyzing cells in large sample volumes. Another disadvantage of hydrodynamic focusing is the acceleration of particles and cells due to the sheath fluid. Several attempts to eliminate the sheath fluid include not focusing cells[10] prior to analysis as well as focusing them using flow[11] as well as field-based[12-14] alternate focusing mechanisms. While flowing the sample through a cylindrical tubing without focusing eliminates issues related to sheath fluid, this approach

cannot be used for high throughput applications as cells will be placed in different layers of the parabolic flow profile and cross the interrogation point with differing linear velocities, thus interfering with precision and sensitivity of optical measurements. To overcome these issues, several attempts have been made to improve throughput by using innovative alternate focusing methods, which include inertial, dielectrophoresis and acoustic focusing techniques, to position particles and cells as precisely as the hydrodynamic focusing mechanism. These techniques not only eliminate issues due to sheath fluid but also allow focusing particles into several focused streams, and hence provide higher throughput than the conventional hydrodynamic focusing technique. Besides flow cytometry, these alternate focusing mechanisms have been used in other analytical techniques also. These techniques and their numerous analytical applications are discussed in detail in the following sub-sections.

1.3.1. Inertial focusing

Any particle flowing in a channel experiences two types of forces, namely the drag and the lift forces. While the drag force acting in the direction of flow (horizontal) tends to accelerate the particle in that direction, the lift force acts perpendicular to it and tends to move the particle in the lateral (vertical) direction. The lift force is composed of two opposing components, the wall and the shear lift forces. While the wall lift moves the particle away from the wall, the shear lift acts down the shear gradient. In inertial focusing channels, particles are positioned into that layer of shear where the net effect of the above mentioned forces is zero. Such equilibrium positioning of particles also

depends on the geometry of the flow channel. For example, in cylindrical channels, the drag and lift forces balance each other at approximately 0.6 times of the radius of the channel. While rectangular channels have four equilibrium positions, square channels may have as many as eight equilibrium positions[11].

In order to demonstrate its utility in flow cytometry droplet sorting, inertial focusing was used to encapsulate particles as well as cells within picoliter droplets. The particles were focused precisely in two dimensions by virtue of the geometry of the channel. Furthermore, uniform separation between successive particles and cells prevented particle coincidences at the droplet break-off point[15]. In inertial focusing channels, the number of equilibrium positions of particles can be reduced simply by increasing the channel aspect ratio (channel height/channel width). Using this approach, massive parallel focusing of beads as well as isovolumetrically sphered red blood cells (sphered using surfactant) into 256 channels, at flow rates of a few mL/min, has been demonstrated. Such fast-flowing parallel focused streams have provided analysis rates required for rare event detection[9].

While the effect of the lift force in straight channels is to move particles into more than one equilibrium position, the addition of curvature to these channels enables focusing particles into a single equilibrium position by the additional effect of secondary force, also called the Dean force. Curvature in flow channels induces a mismatch in fluid inertia between fluid elements at the top and bottom of the channel, hence forcing particles that were previously focused into more than one equilibrium position to now move into a single plane at the center of the channel on exiting the curvature[11]. For flow cytometry, such curvature-induced focusing efficiency is comparable to that of a low-end

commercial flow cytometer[16]. With high-speed real-time imaging of secondary focused streams, rare cells have been analyzed with throughput approaching 100,000 cells/second[17].

Despite providing high throughput and precisely focusing particles, inertial focusing has certain disadvantages. First, the lift forces are dependent primarily on the geometry of the channel[11], which limits particle sizes that can be handled in a particular device. Second, focusing efficiency is dependent on sample concentration[16], which could limit its use in applications requiring very high throughput.

1.3.2.2. Dielectrophoretic focusing

Particles and cells can also be positioned using an external electric field by the dielectrophoretic focusing technique which uses a non-uniform electric field where particle migration depends on the magnitude of force experienced by it. For a spherical particle, the dielectrophoretic force is given by

$$F_{DEP} = 2\pi r^3 \mathcal{E}_m Re(f_{CM}) \nabla E_{rms}^2 \quad (1.1)$$

where

$$f_{CM} = \frac{\mathcal{E}_p^* - \mathcal{E}_m^*}{\mathcal{E}_p^* + 2\mathcal{E}_m^*} \quad (1.2)$$

where r is the radius of the particle, $Re(f_{CM})$ is the real part of the Clausius-Mossotti factor, which is a function of the complex permittivity $\mathcal{E}$ of the particle (subscript p) and the medium (subscript m) and the spatial variation of the mean square voltage of the applied electric field (∇E_{rms}^2). Depending on the sign of the Clausius-Mossotti factor,

dielectrophoresis may be classified into two types; positive dielectrophoresis where the electrical permittivity of the particle is greater than the medium which moves the particle to the region of stronger electric field just above the electrodes, and negative dielectrophoresis where the particle moves away from the electrodes. Among these, the latter is preferred to the former as it is gentle towards cells and prevents electrode fouling[12]. Using the size dependency of the dielectrophoretic force, red blood cells have been separated from platelets in laminar flow at low driving voltage and with high separation efficiency. Due to the larger force on them, the red blood cells moved away from the wall consisting of electrodes, while the smaller platelets moved closer to it[18]. Besides separation based on size, particles have also been separated by the differential force due to difference in dielectric properties. Such property dependent forces have enabled sorting dead yeast cells from live ones, and also to count them with efficiency comparable to that of impedance-based Coulter counter. However, throughput was too low for most cellular applications[19]. When integrated with hydrodynamic focusing, dielectrophoretic focusing precisely focuses particles in two dimensions in the channel depth. Such precise positioning has allowed interrogating the focused streams using fiber optics with high sensitivity[4, 20]. Using sufficiently high driving voltage, fluorescently labeled latex particles were focused into a narrow stream of width equivalent to single particle dimension. Such tight focusing provided accurate fluorescence measurements comparable to that of a commercial flow cytometer. However, throughput was low for rare event detection[21].

Although methods based on dielectrophoretic forces focus particles into a single plane and allow precise measurement of its optical properties, the resulting throughput is low

even for most cellular analysis. Hence, dielectrophoretic focusing cannot provide analysis rates required for detecting rare events.

1.3. 3. Acoustic focusing

1.3. 3.1. Acoustic standing wave and acoustic radiation force

The acoustic focusing technique establishes an acoustic standing wave in a flow channel of width half-wavelength and focuses particles and cells to different regions of the acoustic wave depending on their inherent physical properties such as density and compressibility. A standing acoustic wave can be represented as

$$y = A\ \cos\left(\frac{2\pi x}{\lambda} + \frac{\emptyset}{2}\right)\ \sin\left(\frac{2\pi t}{T} + \frac{\emptyset}{2}\right) \qquad (1.3)$$

where y is the displacement, A the amplitude of the standing wave of wavelength λ, x the position of a point, t the time, $\emptyset$ the phase difference and T the time period for one full oscillation. A standing wave consists of two regions differing in pressure; the region of low pressure is called the node and the region of high pressure is called the antinode. Equation (1.3) indicates that these two successive nodes or antinodes are separated by one half-wavelength $\left(\frac{\lambda}{2}\right)$.

Acoustic positioning of particles using standing waves was first demonstrated by Kundt. To determine the velocity of sound[22], a cylindrical glass tube was filled with dust. A sound source was placed at one end of the tube and a movable piston at the other. When the distance between the source and the piston was either half-wavelength or a multiple

of half-wavelength, resonance was established, standing waves were created and the dust particles collected into the nodes. By determining the distance between the nodes (which corresponds to half-wavelength), the wavelength (λ) of the standing wave was calculated, and hence the velocity of sound (c) in air using the relationship

$$c = f\lambda \tag{1.4}$$

where f is the frequency of the standing wave generated by the source. From Kundt's experiment, it was clear that the migration of the dust particles in the standing wave field was due to acoustic radiation force acting on it. An expression for this force was derived first by King[23]. However, his expression for acoustic force did not consider viscosity and thermal conductivity of the medium. Later, Gorkov[24] extended King's work to account for the above mentioned parameters and derived the following equation for the acoustic radiation force (F_{ac}) on a particle in a standing wave field.

$$F_{ac} = -\left(\frac{\pi p_0^2 V_p \beta_m}{2\lambda}\right).\emptyset(\beta,\rho).\sin(2kx) \tag{1.5}$$

where

$$\emptyset(\beta,\rho) = \frac{5\rho_p - 2\rho_m}{2\rho_p + 2\rho_m} - \frac{\beta_p}{\beta_m} \tag{1.6}$$

Here, p_0 is the pressure amplitude of the standing acoustic wave, λ its wavelength, k the wavenumber, x the position of a particle in the wavefield, V_p the volume of the particle, $\emptyset$ the acoustic contrast factor which is a function of density (ρ) and compressibility (β) of the particle (subscript p) and the surrounding medium (subscript m). Particle migration to the node or the antinode depends on the sign of the acoustic contrast factor, i.e., those particles that have positive value of the contrast factor migrate to the node, whereas those that have negative value migrate into the antinode of the standing wave field (Fig. 1.1).

Thus, equations (1.5) and (1.6) clearly indicate that a particle in a standing wave field experiences an acoustic radiation force that depends on the relative density and compressibility differences between the particle and the surrounding medium[25].

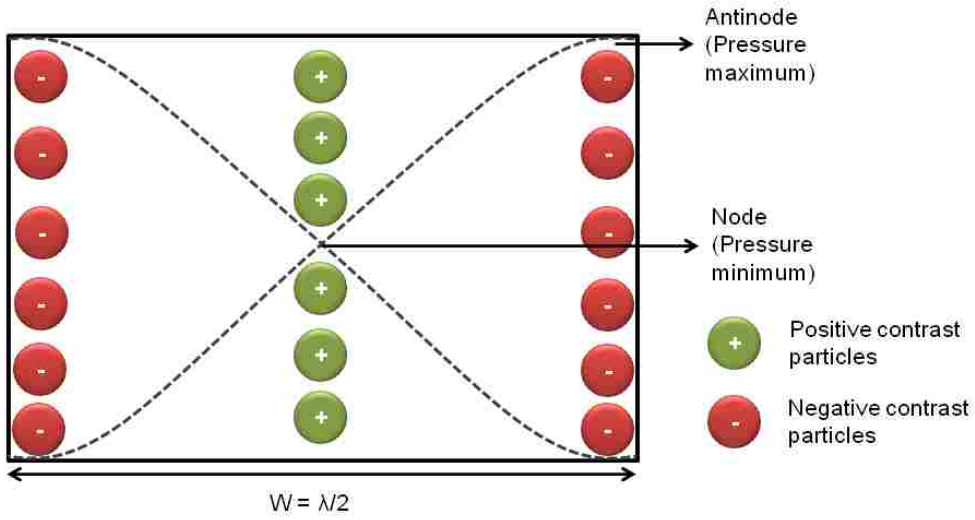

Fig. 1.1 Principle of acoustic focusing

1.3. 3.2. Manipulating microparticles in acoustic field

For manipulating microparticles in an ultrasonic standing wave field, long cylindrical tubes with transducer discs at either ends were used[26]. At the third harmonic resonance of the transducers, the suspension of 9μm polystyrene particles concentrated into three columns across the height of the cylindrical tube separated by half-wavelength distance from each other. However, when the frequency of one transducer was increased with respect to the other, (higher than third but non-harmonic), the particle columns migrated towards the lower-frequency transducer, and the rate of particle column migration was found to linearly increase with difference of frequencies of the two transducers. Furthermore, at very high frequency difference, the particle columns moved off-axis.

With frequency sweeping, the particles formed a thick central clump that could be moved both toward as well as against gravity. Short pulse tone bursts resulted in break-up of particle clumps and subsequent settling of particles at the bottom end of the cylindrical tube. While placing the tube with its axis horizontal to the tube length, the particles again formed columns at half-wavelength separations. However, clump formation and migration with frequency ramping observed previously by placing the tube vertically were not observed when it was placed horizontally. Also, using the vertical arrangement, it was observed that optimal frequency difference between the two transducers forced the clumps to settle faster than gravity sedimentation[26]. However, the clumps formed at half-wavelength separations were not quite uniform and presented challenges in settling. To improve the uniformity of clump formation, the radial standing wave field in the tube was optimized using thin-walled glass tubes and rear-electrode transducers[27]. These modifications resulted in more uniform striated pattern at half-wavelength distances, even with red blood cells, yeast and bacteria. However, bacterial migration to the standing wave columns required high drive voltages. Furthermore, acoustically activated settling has enabled saving time in two-phase separations[28]. Phase separation using acoustic standing waves was first demonstrated using a mixture of polyethylene glycol (PEG) and dextran. Application of acoustic energy resulted in alternating bands of PEG and dextran. To efficiently separate the two-phase system, the ultrasonic field was turned ‘on’ and ‘off’ alternately in short time sequences. During the ‘on’ mode, bands of both PEG and dextran were formed while the ‘off’ enhanced settling of dextran alone since it is the heavier of the two phases. Yeast and bacteria were separated using the same principle by suspending them in the PEG-dextran mixture. On acoustic excitation, yeast collected into

the dextran-rich bands while bacteria collected into PEG-rich bands. Enhanced two-phase separation of yeast and bacteria was observed on turning ‘off’ the acoustic field, when yeast collected into the bottom of the vessel while the relatively smaller bacteria floated at the surface[27, 28]. Such band formation, with both bacteria and yeast, was observed even in relatively less dense suspension medium such as distilled water[29]. Acoustic activated concentration and settling further allowed harvesting microorgansisms such as bacteria and yeast. Despite their smaller size, at higher cell concentrations, the time required for concentrating bacteria into the node was comparable to that of relatively larger yeast cells[30]. Aggregation of microparticles to the nodal regions in the standing wave allowed performing latex agglutination assays, using latex (polystyrene) microparticles coated with antigen-specific antibodies. Video microscopy confirmed increased sensitivity for such immunoassays due to acoustic particle concentration[31]. Moreover, very low levels of antigens were successfully detected[32], which allowed extending the principle of ultrasonic aggregation to detecting bacterial meningitis[33] with efficiencies comparable to that of polymerase chain reaction (PCR) which is usually the gold standard for such assays. Acoustic forces have also been used for analytical scale applications for culturing hybridoma cells, filtering and clarifying turbid suspensions[34].

1.3. 3.3. Acoustic focusing for flow cytometry

Acoustic focusing of particles for flow cytometry was first demonstrated using cylindrical capillaries, constructed of soft glass and quartz, having an inner diameter of 2 mm. Both these capillaries were actuated by a 30mm long piezo transducer crystal glued

to the wall of these capillaries and having a thickness mode resonance around 420kHz, which corresponds to the fundamental resonance mode for the capillaries' inner dimensions[35]. Surface vibration was measured using an oscilloscope and particle migration was recorded using a high resolution camera. While flowing a dilute sample of polystyrene particles using a peristaltic pump through the cylindrical capillary, the resonance frequency was determined by gradually tuning the driving frequency to determine the frequency at which the particles concentrated into the center of the capillary, which occurred at 417 kHz with a drive voltage of 10-12 V_{pp}. Similar results were observed even with a concentrated sample. While the particle concentration times were similar for both diluted and concentrated samples, the width of the focused particle stream at the center was approximately few particle dimensions for the concentrated sample. Furthermore, particle agglomeration was observed with the concentrated sample which did not dissociate below a threshold value of the acoustic power. Particle migration to the center of the capillary was observed even at higher flow rates. Also, despite using such low frequencies that have high acoustic pressure amplitudes, no cavitation was observed within the cylindrical capillaries. Theoretical calculations predicted a strong dipole at the experimentally observed values of the resonance frequency for both soft glass and quartz glass capillaries, and hence the experimental results correlated well with theory. Fluorescence from particles focused using acoustic focusing technique were measured in a subsequent work[14]. The sample was flowed through the cylindrical capillary at 500µL/min .The particle stream was interrogated using 488nm laser source with the spot size reduced to 25µm x 100µm using cylindrical lens and the fluorescence signals were read using a photomultiplier tube, with and without the acoustic signal. In

the presence of the acoustic field, the particles were focused into a 40μm wide stream at the center. While the coefficient of variation (CV) measurements for the peak height, width and area were high due to smaller depth of focusing, low linear velocities due to the absence of sheath fluid proved this focusing technique reliable for flow cytometry. The acoustic flow cell was characterized further for flow cytometry by measuring forward (90^0) and side (45^0) scatter [36]. A 488nm laser source was used for excitation and the scatter signals were read using two photomultiplier tubes, one each for forward and side scatter. However, the spot size was slightly increased to 25μm x 200μm using cylindrical lenses. Using optical filters similar to those used in commercial flow cytometers, photon incidence at the detectors was optimized. Data were acquired using a custom-built data acquisition system called DiDAC and processed using standard flow cytometry data processing software. Peak CV values were measured and limits of detection in terms of MESF were characterized using calibration beads sold commercially. The CV values for the peak height, width and area as well as the resolution of free vs. bound dye were comparable to those observed using commercial flow cytometers. Furthermore, the linear velocities of particles were several magnitudes lower than that observed using hydrodynamic focusing, and hence allowed integrating relatively less expensive detector optics and acquisition systems.

1.3. 3.4. Acoustic focusing in rectangular flow channels

While acoustic flow cytometry was demonstrated using cylindrical capillaries, acoustic radiation force-based separations were performed in rectangular capillaries. In a

rectangular flow channel of width matched to half-wavelength of the acoustic standing wave, the node is formed at the center and two antinodes at the two walls. Depending on the value of the acoustic contrast factor, the acoustic focusing technique focuses rigid (positive contrast) cells and particles to the nodal region and the relatively lower ones to the antinodal region of the standing wave. For example, red blood cells have a positive value of the contrast factor whereas lipids have a negative value[37]. Such differences in contrast factor have enabled separating blood cells from lipids using a 350μm wide rectangular channel actuated using a 2 MHz piezo crystal, trifurcating beyond the focusing region to collect the nodal and the antinodal streams. While the cells and lipids migrated respectively to the node and antinode, the lipids formed clusters at the wall, thus disturbing the laminar flow in the channel[37]. In order to overcome such lipid stenosis, the flow cell was redesigned to direct the sample flow into eight parallel channels. This allowed a relatively dilute solution of lipids to enter each channel, and hence reduced lipid clusters effectively. Despite using low flow rate and hence allowing greater particle residence time in the acoustic field, the separation efficiency of lipids and blood was only 80%. Furthermore, the separation efficiency decreased with increasing hematocrit[38], which limited the maximum efficiency to 85% mean erythrocyte separation[39]. To further improve erythrocyte separation, the focusing region was made longer with one or more meanders and the concentrated erythrocyte fractions were collected periodically from the channel without disturbing both laminar flow and acoustic energy in the channel. Erythrocyte suspensions of varying hematocrits were tested in separation channels of varying lengths. While the erythrocyte separation efficiencies were higher than those observed previously, higher hematocrits required very long separation

channels. Furthermore, the meandering design of the separation channels limited flow rate to < 80μL/min[40].

1.3. 3.5. Medium exchange using acoustic focusing

Under laminar flow conditions, particles suspended in one medium can be moved into another in an acoustically actuated rectangular channel. A proof of concept experiment of this medium exchange principle was demonstrated using a rectangular flow channel consisting of three inlets and three outlets. The particle-free clean medium was flown through the center inlet and the particle-rich contaminated medium through the two side inlets. The laminar flow in the channel sealed the two media and minimized diffusion of molecules of the two media. However, on acoustic actuation, particle in the contaminated medium migrated into the clean medium. Separation efficiencies, as high as 95%, were observed with minimum contamination of the medium[41]. To demonstrate its use in post-operative blood wash procedures, this principle was applied to exchange red blood cells in the contaminated plasma with clean plasma[42]. Characterization studies performed by varying drive voltages as well as varying erythrocyte and contaminant concentrations showed that low drive voltages were necessary to prevent particle mixing. While the medium exchange efficiency decreased with increasing particle concentration, it increased with contaminant concentration and remained above 90% for almost all contaminant concentrations[42]. Using a two-step procedure, washing and extraction of bioaffinity beads have been demonstrated using the same principle[43]. A mixture of metal oxide affinity capture (MAOC) beads incubated with both unphosphorylated as

well as phosphorylated peptides was subject to acoustophoretic washing. In the first step, the unphosphorylated peptides were removed and the second step involved eluting the phosphorylated peptides. Analysis of the eluted component using mass spectra yielded results comparable to manual superparamagnetic washing procedures. However, for affinity extraction of bacteriophages, the acoustic power in the acoustophoretic wash-device was increased further using a bigger transducer and higher drive voltage[43]. Size dependence of the acoustic radiation force together with the buffer medium exchange principle enabled separating larger cells in the G2 phase from the relatively smaller cells in the G1 phase for cell-synchronization studies[44]. The same buffer medium exchange was performed in multiple stages using cross-flow of buffer during each stage. While high washing efficiencies were observed with beads, such efficiencies were relatively low with erythrocytes. Furthermore, the multi-stage technique rendered washing sensitive to cross-flow rate[45]. Recently, this principle was used to separate somatic cells from lipid-rich raw milk using acoustophoresis. On acoustic actuation, the lipids in raw milk moved into the antinodes. The lipid rich fraction was collected through the side outlets. Downstream analysis of the cell-rich center fraction using phase microscopy, flow cytometry and Coulter counter indicated high cell concentrations and negligible lipid concentration[46].

1.3. 3.6. Size-based manipulation using acoustic radiation force

The acoustic radiation force is dependent on the volume of the particle, and hence its size. Equation (3) shows that the larger particles experience a relatively larger force than

the smaller particles. Hence, on acoustic actuation, the larger particles move to the node or the antinode depending on their contrast factor value quicker than the smaller ones. The size-dependent differential migration of particles in the acoustic field was used to separate the smaller particles from the larger ones[47] using a device having three inlets and multiple outlets for collecting the separated fractions. Of the three inlets, the center one was much larger than the two side inlets. A sample consisting of beads ranging in sizes from 3-10μm was flown into the side inlets while a bead-free suspension flowed into the center inlet. Laminar flow in the rectangular channel together with acoustic force field resulted in particle migration toward the nodal region. Due to differential acoustic forces, the larger 10μm particles moved to the center while the smaller particles moved relatively smaller distances and hence remained separated from the larger ones. Analysis of particles collected at the outlets using Coulter counter showed successful separation at low Reynolds number flow. This principle yielded satisfactory results while modifying density of the suspension medium using caesium chloride for separating blood components such as red blood cells, leukocytes and platelets[47]. Furthermore, this principle was demonstrated successfully to separate large circulating tumor cell lines from the relatively smaller healthy white blood cells[48]. Size-based differential migration has been demonstrated in a two-stage system, with each stage operating at a different resonant frequency (non-harmonic) and with different drive voltages, using a mixture of beads (3-10μm). This technique allowed preferential selection of particles in each stage, i.e., the combination of frequency and drive voltage determines the range of particle sizes to be removed in the first stage. Flow cytometry analysis of the separated fractions showed effective separation[49]. Furthermore, preferential migration was also

used to develop an acoustic fluorescence activated cell sorter (AFACS) to sort rare cells[50]. Prior to sorting, the cells were first focused to the wall of the channel using sheath fluid. The cells so focused then entered the acoustic focusing region where the standing wave concentrated the cells at the center of the channel. These cells then entered a relatively larger channel, having a lower resonance frequency. Differential migration of cells in this region enabled sorting rare cells. However, frequency switching limited analysis rates[50].

1.3. 3.7. Acoustic manipulation using higher harmonics

When the width of the rectangular channel corresponds to an integer multiple of half-wavelength of the acoustic standing wave, multiple nodes and antinodes are formed, depending on the harmonics of the standing wave. Thus, when rigid particles in a standing wave field at the fundamental harmonic focus into a single node at the center of the flow channel, when operated at higher harmonics (say n where n=2,3,4…), they will be focused into ‘n’ nodal streams (and ‘n+1’ antinodal streams)[25]. Acoustic focusing at higher harmonics was demonstrated using both rectangular glass capillaries and silicon-based devices[51]. These have been shown to reduce lipid clogging at the channel wall considerably[52] compared to resonance at fundamental harmonic[37]. While higher drive voltages may be required to move particles and cells into more than one stream, precise monitoring and control of temperature using appropriate Peltier elements will help in overcoming adverse effects due to heating[53]. By frequency switching between fundamental and higher harmonic resonances, particles were separated by virtue of their

size-dependent migration in the acoustic field[13]. Initially, a mixture of beads was flown through the side inlets and bead-free suspension through the center inlet. When the channel was excited at the second harmonic frequency, the beads focused into the two nodes in the channel. However, while switching frequency between the second harmonic and the fundamental resonance, the larger particles moved to the channel center due to the greater acoustic force on them, and the smaller particles remained focused in the two nodes of the second harmonic resonance frequency. Size separation using frequency switching was demonstrated using 3 and 8μm beads with 80% efficiency[13]. Although successful, this mechanism is sensitive to duration of the frequency pulse.

1.3. 3.8. Acoustic separation in quarter-wavelength channels

Particles can be separated by acoustic radiation force in quarter-wavelength channels also where the standing wave establishes a single node and antinode. The acoustic radiation force in these channels is relatively higher than those observed in half-wavelength channels which enabled effective size-based separation of blood in multiple stages, with the removal of the focused fraction in each stage. Despite successfully separating particles in a flow cell fabricated using polymer, flow splitting at each stage limited flow rate[54]. Furthermore, unlike half-wavelength resonators, these quarter-wavelength channels do not support resonance at higher harmonics.

1.3. 3.9. Two-dimensional acoustic focusing

Almost all acoustic force-based manipulations in rectangular channels discussed thus far focused particles to the node or the antinode only in the width of the channel. Most of these experiments have suffered either from low efficiencies due to poor focusing or high efficiencies with very low sample throughput. To enhance both separation and throughput, particles should be focused precisely in two dimensions (width and height), which can be achieved simply by fabricating channels that correspond to half-wavelength dimensions in both the dimensions and create acoustic standing waves in these two dimensions by driving them at appropriate resonance frequencies[55]. Recently such two-dimensional acoustic focusing provided very high volume concentration factors with dilute cell suspensions. Uniform laminar flow was maintained by injecting the sample with positive-pressure injection at the inlet with sample suction at the outlet. Two-dimensional focusing, together with particle-free suspension removal in multiple stages enabled achieving nearly two-hundred fold concentration factors with dilute suspensions of red blood cells and prostate cancer cell lines[55].

1.3. 3.10. Positioning microparticles and cells in acoustic field

The acoustic force on particles has also been used to position them precisely in two-dimensional arrays. Even though the magnitude of acoustic force required for such positioning is very high, this technique is still non-invasive[56]. Initial experiments of acoustic cell trapping and positioning were performed using two glass plates and four transducers, all driving the same frequency. The transducers were glued to one of the

glass plates, called the active plate, which is the plate through the which the acoustic wave is transmited to the layer beside it, and the reflective plate was called the passive plate. The gap between these two plates formed the fluid layer. Cells of the He La cancer cell lines and mesenchymal stem cells that are few microns in diameter were trapped precisely in lines in two-dimensions within the fluidic layer[57]. Proper selection of suitable glass plate thickness resulted in the formation of clumps of particles at the focal point of the two-dimensional force field and enabled cancer cell lines of the human liver (HL 60) and epithelial cell line (MCF10A) to be trapped first in lines in two dimensions, and then in clumps using two transducers placed opposite to each other[58]. Attempts have been made to reduce the number of transducers used for such positioning, and hence improve the viability of cells. Using two interdigital transducers, one each for the two acoustic fields acting either opposite or orthogonal to each other, in a poly dimethyl siloxane (PDMS) based device, super-positioning of acoustic force fields trapped cells and particles in arrays. Cells differing in shape and size, such as red blood cells and E.coli have been trapped in two-dimensional arrays. Flow cytometry analysis of such trapped cells showed viability of cells under suitable temperature and drive voltage intensities[56]. Acoustic trapping for bioassays in flow-through format was demonstrated by performing biotin-avidin binding assay. The suspension of fluorescence-labeled biotin-coated beads was first flown through a PDMS flow channel and trapped in the region above the transducer array, followed by the suspension containing avidin. The decrease in fluorescence intensity for the experimental beads was similar to that of the control[59]. Acoustic trapping using wet etched glass channels with appropriate temperature control systems has also enabled live culturing of yeast cells[60]. Acoustic

trapping was also used to separate red blood cells from plasma. Diluted red blood cell suspension was first aspirated into a disposable glass capillary, driven at frequency greater than 10 MHz, corresponding to the third harmonic in the depth of the capillary. The cells formed elliptical clusters at the three nodal regions. Free plasma was removed by reversing the flow[60]. Acoustic devices fabricated in silicon were used even for sequential focusing of epithelial cell lines first into focused streams and then into clumps[61].

Acoustic radiation force can be used to both focus and trap cells and particles larger than 1μm diameter. However, even large trapping forces are not suitable for submicron particles. Besides the primary radiation force, these submicron particles experience secondary radiation force, which may be either attractive or repulsive in nature, depending upon the orientation of these particles in the applied acoustic force field and the inter-particle distance. In a highly attenuated medium, acoustic streaming or rolling flow of the liquid in the fluidic channel occurs. However, acoustic cell trapping together with acoustic streaming and inter-particle interactions were successfully used to trap submicron particles such as E coli and nanoparticles approaching 100nm over acoustically trapped larger 10μm seed particles[62].

1.4. Modeling acoustic resonators

The acoustic focusing technique finds use in micro- as well as analytical scale applications and hence researchers have attempted to model acoustic resonators to optimize acoustic energy density. In acoustically excited chambers, the variation of

energy density is similar to that of the velocity amplitude, being a maximum at the node. Various factors such as the dimensions of the channel, boundary conditions of the coupling and reflector layers and physical characteristics of the transducer influence acoustic energy density[63]. Several models aimed at optimizing these parameters, and hence the acoustic energy density in fluidic channels, are discussed below.

In order to determine qualitatively the magnitude of acoustic force that is required to move the particle depending on its physical characteristics in the acoustic field, a suspension of 5 μm particles was acoustically actuated in a circular chamber without flow. Particle image velocimetry (PIV) measurements indicated static patterns for the suspension. However, when a mixture of 1 μm and 5 μm particles were actuated in a circular chamber, vortices were observed with 1 μm particles, while static patterns similar to those obtained earlier were observed again for 5 μm particles, thereby indicating that for a fixed frequency and drive voltage, the acoustic force acting on 5 μm particles is relatively stronger than that on 1μm particles where vortex motion of the suspension medium, commonly known as acoustic streaming occurs. Furthermore, these measurements showed that as acoustic radiation force acts throughout the fluidic chamber, geometrical symmetry of the chamber was important in optimizing the force on a particle, i.e. acoustic field was relatively weaker in asymmetric fluidic chambers[64]. A quantitative model for optimal acoustic radiation force suggests that a threshold pressure amplitude exits below which the particle will not be influenced by the acoustic field. Thus, particles of different sizes have different threshold values of sound pressure amplitude. This difference in threshold pressures enables size separation of particles in the acoustic field. The model further predicts a threshold drive voltage for band and

column formation of particles at higher harmonics[65]. Surface amplitude measurements of the transducer, the reflector and the fluidic chamber were also used to model acoustic resonators. The amplitude of oscillation of the liquid is a maximum at nodes, the regions of high energy density, and lower at other regions of the fluidic chamber. Hence, polystyrene particles on acoustic actuation collected at the regions of high oscillation velocity amplitude[63]. The product of stored energy and frequency is another indirect method of optimizing the acoustic field intensity in the channel. For a particular frequency, this product should be a maximum. While the stored energy cannot be measured directly, acoustic intensity can be optimized and measured in terms of impedance, i.e. a lower value of impedance indicates a high acoustic energy in the channel. This approach was successful in modeling an acoustic resonator for industrial filtering[66]. Impedance measurements can also be used to determine appropriate thicknesses of the fluid chamber and the reflector[67] to optimize acoustic energy in the channel. While a half-wavelength chamber generates a node at the center of the channel, the model based on impedance measurements showed that pressure nodes exist, though at arbitrary positions and not at the center, in those channels that deviate from half-wavelength dimension. Furthermore, this model indicates that resonant modes exist in the fluid chamber irrespective of its thickness, whereas the thickness of the reflector plays an important role in determining the field strength and the position of the pressure node. For example, in half-wavelength channels, when the reflector thickness is either a quarter-wavelength or its multiple, the pressure node is formed perfectly at the center of the channel. However, when the thickness of the reflector is a half-wavelength, no resonant mode exists in the channel. Furthermore, the fluidic chamber can also have a quarter-

wavelength dimension or less, with half-wavelength reflector thickness, and the pressure node will be established at the reflector surface[67]. However, unlike half-wavelength channels, the energy density of quarter-wavelength chambers is dependent on the thickness of both the matching layer and the reflector, and hence lower[68]. In all one-dimensionally excited acoustic flow channels, a lateral acoustic field, perpendicular to the primary acoustic field is created. The strength of this field is determined by the geometry of the channel as well as the material of construction of the acoustic resonator. Finite element analysis (FEA) of an acoustic resonator fabricated using silicon at one boundary and pyrex at the other with acoustic transmission through silicon and reflection at the pyrex layer showed that proper selection of the previously mentioned parameters (geometry and materials) generates a lateral acoustic field of strength as high as 85% of the primary acoustic field. Also, silicone elastomer when used as acoustic reflector, yields a more uniform lateral acoustic field[69].

While the acoustic radiation force is significant for particle dimensions greater than 1 μm. proper selection of various parameters such as the resonator geometry, its dimensions and material of construction of the matching layer and the reflector influence the acoustic energy density and also the positioning of nodes and antinodes within the fluid chamber. Furthermore, these models also indicate the presence of a lateral field orthogonal to the the plane of excitation of the fluid chamber. As mentioned previously, precision and sensitivity of flow cytometry measurements depend partly on the two-dimensional positioning of particles within the flow cell. In acoustic flow cells, such precise positioning can be obtained using a high lateral field strength. However, these models consider the fundamental resonance mode alone.

1.5. High throughput cellular analysis using advanced imaging techniques

While both microscopy and flow cytometry are commonly used for quantitative cytological measurements, they suffer from certain limitations. Microscopy commonly suffers from low throughput and even sensitivity has to be compromised to avoid photobleaching. Flow cytometry measures multiple parameters of single cells, however morphological and subcellular fluorescence characterization is impossible. These challenges can be overcome using image flow cytometry that combines the advantages of both the above mentioned cytological measurement techniques[70]. Such image-based flow cytometers are capable of detecting fluorescence as well as forward and side scatter as with any commercial flow cytometer,. Such systems employ time-delay integrated charge-coupled detectors (TDI-CCD's) that provide high image read-out rates, while preserving the image quality of conventional CCD's. As many as 12 images of individual cells are obtained in brighfield, darkfield and fluorescence modes. These images are further decomposed into subsets based on their spectral signatures. Furthermore, these flow cytometers use data software that not only allow visualizing individual cells in the population of interest, but also provide fluorescence and scatter plots and subcellular and morphological classification.

Microfluidic systems permit high parallelization of flow channels and easy integration of fluidic components, optics and electronics. These characteristics allowed fabricating as many as 384 parallel channels, and integrating the device with a setup consisting of a laser scanning system for optical interrogation and four photomultiplier tubes (PMT's) for spectral measurements. The channels were loaded using micro-titer well-plates. The highly parallel channels merged at the detection point with a small clearance between

them. Laser light from a rotating head fitted with suitable lens scanned the channels regularly at short intervals. Fluorescence emission from the sample was collected using high numerical aperture lens and focused into the PMT's. This system was used successfully to demonstrate high content screening as well as the detection of rare osteocytes at rates much higher than commercial flow sorters[71, 72].

Recently, high speed cell imaging was demonstrated by integrating array-based optics with parallel flow channels. The microfabricated flow channel, consisting of 16 parallel channels, was attached to one side of a cover glass slide, and imaged using a 4x4 array of diffraction limited microlenses, placed on the other side of the glass slide (one lens per channel). High speed images of flowing latex particles were obtained using high frame-rate complementary metal oxide semiconductor (CMOS) camera and the images were processed using Image Processing tool in MATLAB to identify and quantify them. While the side scatter plots indicated singlets and clusters, throughput was comparable to that of commercial flow cytometers using photodetectors and much above commercial image flow cytometers[73].Such an array-based lens system was also used to demonstrate parallel imaging of hydrodynamically focused flow streams. A linear array of microball lenses, each having high numerical aperture, were embedded below 32 parallel channels by using standard lithography, such that one lens imaged one focused stream in each channel. These lenses provided high throughput (384000 particles/sec) and high sensitivity with fluorescently labeled polystyrene particles. Furthermore, they were also used successfully to demonstrate live cell imaging[74].

The utility of high speed imaging techniques for rapid cellular analysis was demonstrated by integrating advanced image sensors with alternate focusing techniques. In an attempt

to demonstrate high throughput capability of inertial focusing, high speed short-exposure images of inertially focused particle streams of particles as well as blood cells in 256 parallel channels were obtained and analyzed later using standard code written in the programming tool MATLAB to determine particle velocity and their position in the z-plane. For the blood suspension, using pre-written MATLAB script, cell size and number were measured and also differentiated based on fluorescence intensity measurements[9]. In a subsequent work, advanced imaging optics and fast image processors were integrated to such inertial focusing flow cells. High speed and high resolution images of focused cells were obtained using serial time encoded amplified microscopy (STEAM) technique, which uses a high speed, broadband, short laser pulse that is spatially dispersed to obtain one-dimensional electronic slides (image scans) of flowing particles. These image slides are reflected onto an optoelectronic time-stretch image processor that converts the one-dimensional image into a pixel stream at low speed to allow real-time processing. The processor is incorporated with suitable electronics to amplify the signal and cancel out any noise in the image slides. This noise-free signal was fed into a single-pixel photodetector that read the optical signature of individual cells. The analog data were then converted into digital format and fed to a field-programmable gated array (FPGA) circuit that acts as the decision tree and processes only those images that have particles, converts them into electronic slides and distinguishes particles based on morphological and biochemical signatures using pre-coded algorithms. The fast shutter speed of the STEAM system together with signal amplification provides the high throughput analysis rates required for rare event detection[17].

All of the above attempts have involved obtaining images of particles and analyzing them either post-acquisition using image processing tools or in real time by integrating advanced processing circuitry with the image sensors. These attempts have provided analysis rates ranging from few to several orders of magnitude higher than traditional flow cytometry with both conventional hydrodynamic focusing and advanced alternate focusing mechanisms. Such high analysis rates are truly useful for applications that require focusing cells in large sample volumes such as those used in the detection of circulating tumor cells. Although the speed and sensitivity of traditional flow cytometry detectors have improved over decades, they are expensive, and unlike imaging systems, they do not permit morphological identification. Hence, these imaging flow cytometry systems would be highly beneficial for high volume flow cytometers in providing appreciably high sensitivity at a relatively lower cost.

1.6. Preface to the dissertation

Although the traditional hydrodynamic focusing mechanism offers precise focusing of particles and cells into a single-plane in the core of the cylindrical tubing[1], it suffers from particle acceleration by sheath fluid and low throughput[2]. The alternate focusing mechanisms discussed here aimed at overcoming these issues by manipulating particles in flow[11] or by using external fields such as in dielectrophoresis[12] and acoustic focusing[14, 35, 36]. All of the above mentioned alternate mechanisms eliminate sheath fluid and hence prevent particle acceleration, however, they have their own limitations. While the inertial focusing mechanism provides high throughput, the magnitude of lift

force on the particle depends on the dimensions of both the particle as well as the channel, hence limiting the range of particle dimensions[11]. On the other hand, using an external field to position particles does not present such limitations. However, both dielectrophoretic and acoustic forces are dependent on the volume of the particle[12, 13], and hence present challenges while handling submicron particles. While size sensitivity issues in acoustic focusing were overcome by using high energy radiation force and larger seed particles[62], such manipulative mechanisms do not exist to handle submicron particles by dielectrophoresis. Furthermore, throughput observed with dielectrophoretic focusing is lower than commercial flow cytometers and hence this is not suitable as an alternate focusing mechanism. Additionally, acoustic focusing allows positioning cells and particles into more than one focused stream in rectangular channels driven at higher harmonics of the fundamental resonance frequency[52]. Hence, any attempt to increase throughput using this mechanism should be directed towards increasing the number of focused particle streams within single channels to a few tens or by focusing particles into highly parallel channels as demonstrated using both hydrodynamic[6] and inertial focusing[9] techniques. Furthermore, unlike the traditional hydrodynamic focusing mechanism where the sheath fluid imparts a non-uniform spacing between successive particles and hence randomized particle arrival at the interrogation volume, the acoustic focusing technique concentrates the particles towards the node or the antinode depending upon their acoustic contrast factor value, which minimizes the time interval between successive particles relatively, and hence improves throughput for a single focused stream. As acoustic technique allows focusing particles into highly parallel streams, throughput may be increased by few orders of magnitude simply by increasing the

number of particle focused streams. This dissertation discusses parallelizing both focused particle streams and flow channels to improve throughput in flow cytometry. Although parallelization could improve sample throughput, such design approaches should be accompanied by supporting models accounting for energy density within these flow channels. While previous models have demonstrated success in designing acoustic resonators operating at the fundamental resonance, none of these models account for energy losses in these resonators which scale with increasing frequencies[75], and hence are not valid for acoustic flow cells operating at higher harmonics. Although several approaches exist to model these flow cells, this dissertation aims at characterizing the material of fabrication for acoustic flow cells operating at higher harmonics. While using high image acquisition and real time processing electronics[17] is truly useful, it is not cost-effective. Hence, preliminary data were obtained using an inexpensive commercially marketed video camera. Once the preliminary work was successfully demonstrated, for further imaging, a high sensitivity electron-multiplying charge-couple device (EMCCD) integrated to an epifluorescence microscope was used to obtain relatively high quality images and also to process them wherever necessary. At the end, this dissertation presents a proof-of-principle imaging flow cytometry instrumentation setup using high sensitivity and high frame rate sensors for imaging parallel focused streams generated using the multinode acoustic technique.

Chapter 2

Objectives and Overview of this work

Although flow cytometry is a powerful analytical technique used in various applications which include detection of pathogens, rare events and molecular assemblies, the use of sheath fluid interferes with sample flow, particle arrival characteristics and cell viability and also limits throughput in high volume applications. While previous attempts to improve throughput by parallelizing the focused particle streams have been successful in improving throughput, these have their own limitations in that they either use the sheath fluid, and hence issues related to sheath persist, or present limitations in particle dimensions for analysis. Therefore, an alternate sheathless focusing technique that eliminates all of the above mentioned problems would be truly useful for high volume cellular analysis. Toward this aim, this dissertation introduces the multinode acoustic technique where particles and cells will be focused into several highly parallel streams depending upon the relative density and compressibility of the particle and the surrounding medium (Fig. 2.1). The primary objective of this work is to develop multinode acoustic flow cells that support parallel flow cytometry and hence improve throughput. I hypothesize that particles and cells will be focused into highly parallel streams at high flow rates using the multinode acoustic technique. Such highly parallel streams permit high volume throughput, and integration of suitable interrogation and detection optics will provide high analysis rates. Such high analysis rates are required for rare event analysis such as the detection of circulating tumor cells and fetal cells in maternal blood, where one cell has to be counted in a population of about a billion healthy cells. Multinode acoustic focusing for high throughput flow cytometry was

demonstrated by fabricating flow cells using three different approaches which include (i) using micromachined metal frame with laboratory glass slides, (ii) using rectangular glass capillaries and (iii) etching flow cells in silicon using standard photolithography and deep reactive ion etching techniques. This dissertation devotes separate chapters for each of the above mentioned approaches and discusses qualitatively the characterization of material of construction with respect to acoustic losses, the fabrication procedures, and the experimental methods and results observed with particles as well as with cells. Finally, this dissertation presents a proof-of-concept imaging flow cytometry custom instrumentation that uses laser line optics and commercially available microscopy cameras to image the highly parallel focused streams generated using multinode acoustic focusing technique.

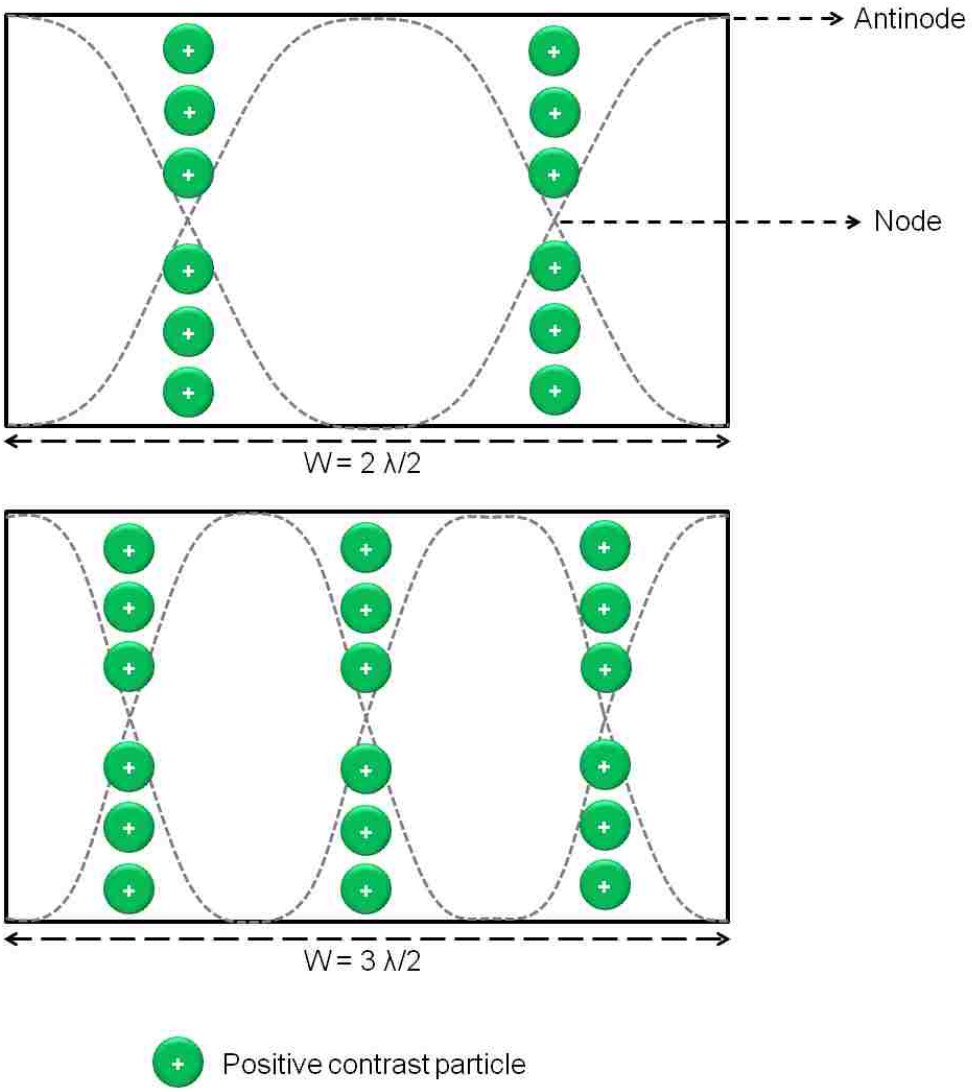

Fig. 2.1 Principle of multinode acoustic focusing

Knowledge of the acoustic losses in multinode acoustic flow cells provide a better understanding of acoustic wave propagation in multinode acoustic flow cells. These losses occur in the transducer, the material of the flow cell as well as the sample. Almost all these losses are dependent on the driving frequency and hence cannot be eliminated. However, proper selection of the material of construction helps in restricting these losses

to a minimum. For this reason, Chapter 3 discusses the mechanism of each of these losses and finally characterizes the material of construction for multinode acoustic flow cells.

Chapter 4 demonstrates multinode acoustic technique that this dissertation suggests as an alternative to the conventional hydrodynamic focusing technique to improve sample throughput in flow cytometry, using the prototype multinode acoustic flow cell fabricated using machined aluminum frame and commercially marketed laboratory glass slides. This chapter proposes a methodical approach to increase throughput, which includes increasing the number of focused particle streams simply by increasing the driving frequency of the transducer. Using this approach, particles and cells have been focused into highly parallel streams with throughput comparable to that of commercial flow cytometers using hydrodynamic focusing. Preliminary results with this flow cell have been published in Analytical Chemistry (ME Piyasena, PP Austin Suthanthiraraj, RW Applegate Jr, AM Goumas, TA Woods, GP Lopez and SW Graves, *Anal. Chem.* 2012, **84**(4), pp 1831-1839).

Chapter 5 introduces the commercially available rectangular glass capillaries for demonstrating multinode acoustic focusing technique. These capillaries are made of borosilicate and have lower acoustic losses than metals. Besides providing appreciable throughput, they are optically transparent and hence allow easy integration with commercial flow cytometers. The results observed herein were published in an article in the Methods journal (PP Austin Suthanthiraraj, ME Piyasena, TA Woods, MA Naivar, GP Lopez and SW Graves, *Methods* 2012, **57**(3), pp 259-271).

Chapter 6 introduces flow cells fabricated using standard photolithography and deep reactive ion etching techniques. These flow cells provided much higher throughput than the two flow cells fabricated previously. This approach was used to fabricate two different types of flow cells. The first includes fabricating single wide channels that accommodate multiple focused streams. The second includes directing inlet fluid flow into several parallel channels where each channel accommodates fewer focused focused streams, and using a transducer with a natural frequency that matches the dimensions of the channels. While both these designs have allowed higher throughput than the flow cells used previously, the latter has performed better. Data observed with a flow cell consisting of 13 parallel channels were published in the Methods journal (PP Austin Suthanthiraraj ME Piyasena, TA Woods, MA Naivar, GP Lopez and SW Graves,, *Methods* 2012, **57**(3), pp 259-271). Furthermore, the parallel design has allowed massive parallelization of the multinode acoustic technique, which is discussed in Chapter 7. The massively parallel flow cell consists of 100 parallel channels, and hence generates a few hundreds of focused streams when driven at the resonance frequency of the transducer. Furthermore, this flow cell focuses particles and cells at a few tens of mL/min, which is few orders of magnitude higher than that of commercial flow cytometers. For this reason, these flow cells are excellent candidates for high throughput cellular analysis, and can replace the conventional hydrodynamic focusing technique for such analyses.

In flow cytometry, the particles are positioned into a single plane, which allows measuring the optical properties of every cell crossing the interrogation region with high accuracy. To replace the conventional hydrodynamic focusing technique for flow cytometry, such precise focusing must be achieved using alternate techniques. For this

reason, Chapter 8 discusses two-dimensional acoustic focusing of particles using two flow cells used previously in Chapter 6. However, these flow cells are etched to one half-wavelength dimensions such that a standing wave of fundamental resonance frequency is established in the channel depth, which in turn will focus all the particles into a single plane.

Although the multinode acoustic technique provides high throughput by focusing particles and cells into highly parallel streams, high analysis rates required for detecting rare events can be achieved only by interrogating these focused streams simultaneously and integrating signals from suitable detectors. Almost all flow cytometers use either circular or elliptical laser beam spots and hence cannot be used to analyze these parallel focused streams. To demonstrate such analysis, this dissertation introduces a proof-of-concept imaging flow cytometry instrumentation in Chapter 9 that uses a laser line to interrogate the parallel focused streams. Proof-of-principle experiments were performed using a glass capillary flow cell and the focused particle streams were imaged using commercially available microscopy camera.

Chapter 10 summarizes the results observed with multinode acoustic flow cells and suggests future directions for work with these flow cells. Therefore, this dissertation concludes that the multinode acoustic technique developed herein and demonstrated using flow cells fabricated using different techniques, is a suitable alternative to the conventional hydrodynamic focusing technique for those applications that require high analysis rates. These flow cells, when integrated with suitable optical elements and detectors, will provide high analysis rates that are required for the detection of rare events for flow cytometry.

Chapter 3

Acoustic energy losses in multinode acoustic flow cells

3.1. Importance of acoustic losses

The acoustic standing acoustic wave is a mechanical wave that requires a medium for propagation. While propagating through a half-wavelength flow channel, it creates a region of low pressure at the center of the flow cell called the node and two regions of high pressure near the walls of the channel called the antinodes. Due to the force acting on particles suspended in the medium, they migrate either to the node or the antinode depending upon the relative density and compressibility of the particle and the medium. However, only a fraction of the input energy from the driving transducer is transmitted into the flow cell The amount transmitted depends on factors such as the material of construction of the transducer as well as the flow cell and also characteristics of the particles and the suspension medium. In other words, energy losses in the transducer and the flow cell limit the net acoustic radiation force within the flow cell. Almost all these losses depend on the driving frequency and hence significant for half-wavelength flow cells. However, these losses increase with increasing frequency and also with increasing harmonics even for low driving frequencies. As multinode acoustic flow cells are driven at higher harmonics and higher frequencies than those used in half-wavelength resonators, these energy losses are significant. Although acoustic losses in the sample are inevitable, knowledge of acoustic energy losses in materials will help in optimizing energy transmission in multinode acoustic flow cells.

3.2. Acoustic losses in multinode acoustic flow cell components

The generic power law equation for acoustic losses is

$$\alpha = \alpha_0 |\omega|^y \qquad (3.1)$$

where α is the overall acoustic attenuation, α_0 is a constant, ω is the angular frequency and *y* is a real finite number [76]. When the value of *y* is closer to either 0 or 2, dispersion, i.e. change in the velocity of the ultrasound wave through the material or medium due to attenuation, can be considered negligible. For example, distilled water has a frequency-squared dependence, and hence dispersion in a suspension medium of distilled water is usually neglected. However, for most solids and other liquids, $y \geq 1$, and hence the acoustic energy losses become significant. The value of *y* depends on the various loss mechanisms[76] that occur in the components of the flow cell (Fig.3.1), which may be broadly classified as follows:

i. Transducer losses
ii. Impedance mismatch losses at the interface between
    - the transducer and the material of the flow cell
    - the flow cell and the sample medium
iii. Material losses
iv. Medium losses

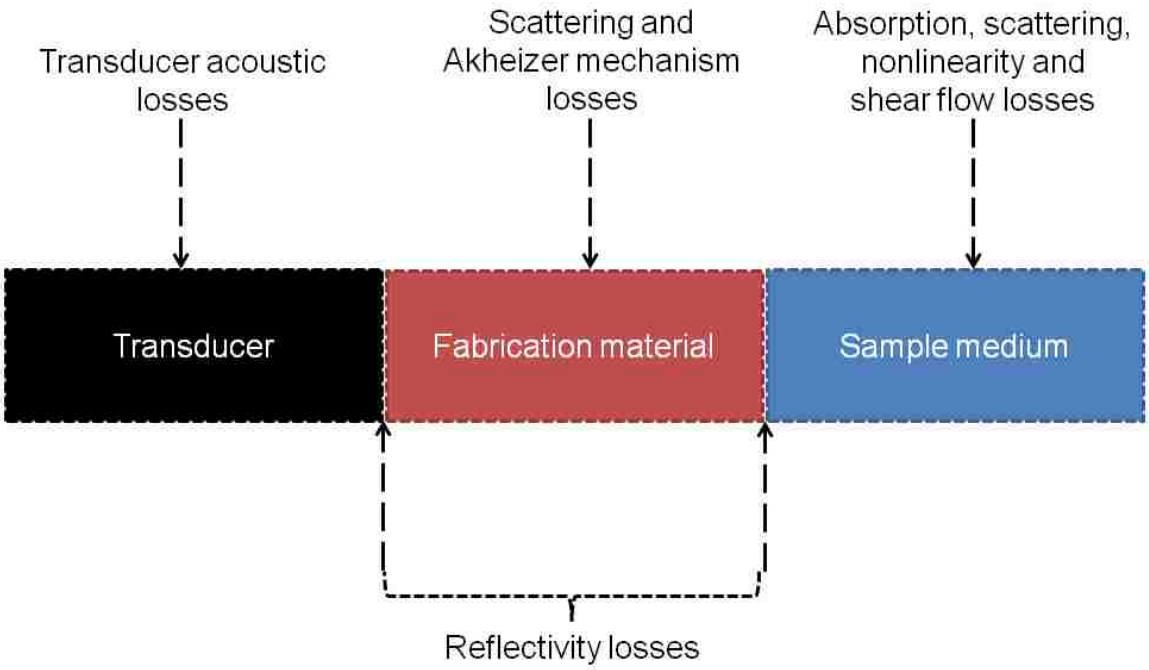

Fig. 3.1 Schematic representation of the various losses in the transducer, fabrication material, the sample medium and their respective interfaces

The nature and mechanism of these losses are discussed in detail in the following paragraphs.

3.2.1. Transducer losses

Ultrasonic transducers use the principle of reverse piezoelectric effect where electrical energy is converted into mechanical energy. As transducers are fabricated of crystalline materials, they experience compressions and rarefactions. In multinode acoustic flow cells, these are transmitted continuously into the flow cell, thus creating alternating nodal and antinodal regions within the flow cell. Irrespective of the value of Q-factor of the driving transducer, power losses occur in the material of the transducer. For a given applied voltage, the power input to the transducer[77] is given by

$$W_E = I^2 R_A/2 \quad (3.2)$$

where

$I(=\omega C_0)$: current,

$R_A(= R_{A0} sinc^2\left(\frac{\omega}{2\omega_0}\right))$: radiation resistance,

ω : angular frequency,

ω_0 : angular frequency of the fundamental harmonic,

C_0 : clamped capacitance,

$R_{A0}(= \frac{2k_T^2}{\pi\omega_0 C_0})$: fundamental resistance and

k_T : coupling constant for the transducer.

However, a fraction of the input power is lost due to impedance depending on the transducer's resonance frequency, expressed as

$$A_L(\omega_0) = Z_R/(Z_L + Z_R) \quad (3.3)$$

where $$Z = \rho v \quad (3.4)$$

is the impedance of the transducer made of a material having density ρ and sound velocity v. Subscripts R and L denote the transducer acoustic ports[77].

3.2.2. Impedance mismatch losses

Besides transducer losses, impedance mismatch losses due to differential impedance of materials and media occur at the interfaces of the transducer, flow cell and the medium. For example, at the interface between the transducer and the flow cell, due to impedance mismatch between the material of the transducer and that of the flow cell, a certain amount of the transmitted acoustic power is reflected. These reflectivity losses are expressed as

$$R_{tfc} = \frac{Z_{fcm} - Z_{tm}}{Z_{fcm} + Z_{tm}} \quad (5)$$

where *Z*, as in equation (3.4) is the impedance, and subscripts *fcm* and *tm* indicate material of construction of the flow cell and the material of the transducer. Similar losses that occur at the interface between the flow cell and the medium can be given by

$$R_{sfc} = \frac{Z_{sm} - Z_{fcm}}{Z_{sm} + Z_{fcm}} \quad (6)$$

where *sm* denotes the sample medium.

3.2.3. Material losses

Besides the transducer, additional losses occur in the material of construction of the flow cell. While frequency dependence is the common denominator for all these losses, the mechanism underlying each and the magnitude of frequency dependence differ, as different materials respond differently to acoustic propagation. These mechanisms may be broadly classified into 3 types:

i. Scattering

ii. Thermoelastic loss

iii. Akhiezer mechanism

3.2.3.1. Scattering

For metals, the frequency-dependent acoustic attenuation in equation (3.1) may be rewritten as

$$A = B_1 f + B_2 f^4 \tag{3.7}$$

where B_1 and B_2 are constants that depend on the grain size of the metal and f is the frequency. Each term on the right hand size of equation (3.7) represents a different mechanism - the first term represents linear hysteresis losses in the metal while the second represents scattering losses that depend on the fourth power of frequency. Therefore, the highest contribution to losses in a metal is from the scattering term, which is significant in the frequency range of 2-15 MHz. For this reason, the hysteresis term in is neglected and equation (3.7) reduces to

$$A = B_2 f^4 \tag{3.8}$$

Besides frequency, scattering depends on the grain size of the metal also, and is significant when the grain size is less than one-third of the wavelength of the acoustic wave. These grains scatter the incident acoustic wave in different directions, and also exhibit anisotropy, i.e. they have different values of elastic constants in different directions, which increases scattering losses further. Moreover, frequency dependence

diminishes with increasing grain size. However, among metals, aluminum, magnesium and tungsten have low scattering losses[78].

3.2.3.2. Thermoelastic loss

Besides scattering, acoustic energy in metals is attenuated by the thermoelastic phenomenon. Sound energy is longitudinal in nature and consists of regions of compressions and rarefactions. Hence, when sound is incident on metals, thermal energy flows from the compressed hot region towards the relatively cooler expanded region, which attenuates sound, which is quantified as

$$A = \frac{\omega^2 \langle \gamma \rangle^2 KT}{2\rho v^5} \tag{3.9}$$

A : acoustic attenuation in neper/cm

ω : angular frequency

$\langle \gamma \rangle$: average Gruneisen parameter

K : thermal conductivity

T : absolute temperature

ρ : density

v : sound velocity

Gruneisen parameter (γ) represents the change in the volume of the metal as a result of propagation of sound. However, these losses are negligible in glass and silicon.

3.2.3.3. Akhiezer mechanism

Glass and silicon are the amorphous and crystalline structures of silica respectively. When sound propagates through these solids, the atoms in their lattice structure are displaced and vibrate or oscillate about their mean positions. The energy associated with these vibrations is discrete and stored in packets or quanta termed as phonons. The time that an atom displaced from its equilibrium position takes to reach its original position is called the relaxation time (τ). Unlike metals, the change in volume of the lattice structure due to vibrations is not only dependent on frequency (ω), but also on temperature (T), and described by Gruneisen parameter (γ). In glass and silicon, in the Akhiezer regime where $\omega\tau \leq 1$, two different mechanisms contribute to sound attenuation. The first mechanism involves heat conduction between the regions of compressions and rarefactions results in loss of sound energy, given by

$$\Gamma_h = \left(\frac{\omega^2}{\rho v^3}\right)\left(\frac{KT\alpha^2\rho^2 v^2}{C^2}\right) \tag{3.10}$$

In the second mechanism which is called internal friction, heat is dissipated as the vibrating phonons reach equilibrium, and given by

$$\Gamma_i = \left(\frac{\omega^2}{\rho v^3}\right)(CT\tau\gamma^2) \tag{3.11}$$

Γ_h : sound attenuation by heat conduction

Γ_i : sound attenuation by internal friction

C : specific heat per unit volume

α : coefficient of thermal expansion

From equations (3.10) and (3.11), the ratio of acoustic losses by these two mechanisms is given as

$$\frac{\Gamma_h}{\Gamma_i} = \frac{K\alpha^2\rho^2v^2}{C^3\tau\gamma^2} \tag{3.12}$$

By definition, the coefficient of thermal expansion,

$$\alpha = \frac{C\gamma}{\rho v^2} = \frac{C\gamma}{B} \tag{3.13}$$

where

$$B = \rho v^2 \tag{3.14}$$

is the bulk modulus, and the thermal conductivity

$$K = CD \tag{3.15}$$

where D is diffusivity of the material. Hence, equation (3.12) reduces to

$$\frac{\Gamma_h}{\Gamma_i} = \frac{D}{v^2\tau} \tag{3.16}$$

The denominator in equation (3.16) denotes energy absorption by the vibrating phonons. In glasses, this ratio of attenuation is negligible, whereas it tends to unity for crystalline silicon. The combined attenuation due to these two phenomena is given by

$$\Gamma = \Gamma_h + \Gamma_i \tag{3.17}$$

$$\Gamma = \frac{\omega^2}{\rho v^3}\gamma^2 TC\left[\frac{D}{v^2} + \tau\right] \tag{3.18}$$

Equation (3.18) shows that acoustic attenuation in glass and silicon has a squared dependence on frequency(ω) as well as the Gruneisen parameter(γ). Compared to silicon, glass has a higher value of γ, and hence higher attenuation[79].

3.2.4. Medium losses

Like the fabrication material, the sample medium also contributes to total acoustic energy losses. Although most samples used herein such as distilled water and phosphate buffered saline have negligible losses[76], energy losses occur due to particles and cells suspended in the medium. These losses may be caused by various mechanisms such as

i. Absorption
ii. Scattering
iii. Flow velocity
iv. Temperature
v. Nonlinearity (of sound pressure amplitude and density of the medium)

Hence, the energy intensity of an acoustic wave propagating through a distance x in the sample medium is given by

$$I(x) = I_0 \exp[-2(\alpha_a + \alpha_v + \alpha_s)x] \quad (3.19)$$

I_0: unattenuated amplitude of the incident acoustic wave

α_a: attenuation by cellular absorption

α_v: attenuation by viscous relative motion

α_s: attenuation by scattering

3.2.4.1. Absorption

Absorption refers to the degradation of acoustic energy into other forms. These losses are mainly due to relaxation where the time delay in the recovery of kinetic energy results in conversion of sound energy into other forms, mainly heat. Absorption losses occurring in the sample medium may be broadly classified into two categories, namely cellular level and molecular level losses[80].

At the cellular level, the two mechanisms that contribute significantly to absorption losses are viscous relative motion and thermal diffusion[80]. In blood, viscous relative motion is mainly due to the difference in density between the red blood cells and plasma. On sound propagation, the red blood cells and plasma oscillate with a phase difference due to different vibrating energies, which causes a transfer of momentum over time when acoustic energy is lost by relaxation. The magnitude of losses due to viscous relative motion decreases with frequency. Within the range of 1-10MHz used in acoustic focusing, these losses may be as high as 25% at the lower frequency and decrease to 5% for higher frequencies. Besides frequency, viscous relative losses depend on haematocrit. For example, at low concentrations, these losses vary linearly with haematocrit. However, these losses become negligible with increasing haematocrit (40-50%). Furthermore, these losses increase linearly with saline concentration also where there is a greater density difference between the cells and the surrounding saline medium. Thermal diffusion occurs due to temperature difference between intracellular and extracellular fluid. In comparison to losses due to viscous relative motion, these losses are low in most cells and hence can be neglected.

The net cellular level absorption losses in blood[81] can be given by the equation

$$\alpha_{cell} = \alpha_{tr} + \alpha_{vrm} \tag{3.20}$$

where $$\alpha_{tr} = h_r\left(\frac{\rho_c c_c}{\rho_l c_l}\right)\alpha_r \tag{3.21}$$

where $$h_r = \frac{4}{3}\pi a^3 N$$

and $$\alpha_{vrm} = \frac{1}{2}h_r(1-h_r)^2\left(\frac{\rho_c-\rho_l}{\rho_l}\right)^2 K \frac{s}{s^2+[\tau+\left(\frac{\rho_c}{\rho_l}\right)(1-h_r)]^2} \tag{3.22}$$

where $$\tau = \frac{1}{2} + \frac{9}{4\beta a} \tag{3.23}$$

$$s = \frac{9}{4\beta a}\left(1 + \frac{1}{\beta a}\right) \tag{3.24}$$

$$\beta = \left(\frac{\omega\rho_c}{2\eta}\right)^{\frac{1}{2}} \tag{3.25}$$

α_{cell} : absorption losses by cellular mechanism

α_{tr} : absorption losses by thermal relaxation

α_{vrm} : absorption losses by viscous relative motion

h_r : volume concentration of red blood cell suspension

a : equivalent radius $(= 2.4)$ for a red blood cell

N : number of cells per unit volume

η : coefficient of viscosity of the liquid

At the molecular level, acoustic energy losses occur mainly due to viscosity and thermal conduction rather than structural and thermal relaxation[80]. Absorption viscosity losses occur due to varying shear between molecules of the medium that results in diffusion of momentum between them. Besides shear viscosity, bulk viscosity that signifies the resistance to compression in the medium, contributes further to attenuation. The difference between the experimentally measured values of attenuation and that given theoretically by Stokes law of acoustic attenuation (that assumes attenuation by shear viscosity alone) results from bulk viscosity[82]. Besides viscosity losses, thermal diffusion occurs from the region of compression to the region of rarefaction in the medium. However, commonly used media have negligible thermal relaxation times, hence these losses are neglected.

3.2.4.2. Scattering

Ultrasonic scattering losses refer to scattering of incident acoustic wave by particles and cells suspended in the medium, and depend on frequency, concentration and flow conditions. Within the frequency range used in multinode acoustic focusing, scattering losses in blood are negligible, and increase only above 10 MHz. However, a higher haematocrit in blood could increase scattering losses even at lower frequencies due to greater shear between individual red blood cells[80, 83]. Furthermore, they increase with increasing fibrinogen content in blood[84].

The scattering cross-section for a red blood cell[81] is given by

$$\sum s = 2\pi a^2 (ka)^4 \int_0^{\pi} (\nu_k + \nu_\rho \cos\theta)^2 \frac{(b\cos b - \sin b)}{b^3} \sin\theta \, d\theta \tag{3.26}$$

where $$b = 2ka \ \sin\frac{\theta}{2} \tag{3.27}$$

$$\nu_k = \frac{K_r - K_l}{K_l} \tag{3.28}$$

$$\nu_\rho = \frac{\rho_r - \rho_l}{\rho_l} \tag{3.29}$$

θ : angle between incidence and scattering directions

K_r : compressibility of red blood cell

K_l : compressibility of liquid suspension

ρ_r : density of red blood cell

ρ_l : density of liquid suspension

Equations (3.27) and (3.28) are valid only within the cell and become zero outside the cell.

3.2.4.3. Shear flow losses

The flow of a fluid of density ρ_f and viscosity μ_f through a closed duct of dimension D with a velocity v_f is characterized by its Reynolds number

$$Re = \frac{\rho_f v_f D}{\mu_f} \tag{3.30}$$

This dimensionless number describes whether the flow is laminar or turbulent. In a uniform parabolic flow, a constant shear gradient exists from the wall of the duct to its geometric center. Hence, when sound is refracted through the shear layers in the medium, it is gradually attenuated as it propagates through the layers of differing shear. The extent of attenuation is dependent on another dimensionless number called the Mach number (M) that is defined as the ratio of the velocity of the particle (v_p) in the fluid to the velocity of sound (c) in the same fluid.

$$M = v_p/c \tag{3.31}$$

Usually, acoustic energy losses by shear flow increase with increasing Mach number (and hence with increasing flow rate) and increasing frequency[75], and are written in terms of intensity[85] as

$$I = \frac{p^2}{2\rho_l c}|\alpha|\, q \left|\frac{(1-M^2)}{(1-\alpha M)}\right|^2 \tag{3.32}$$

where

$$\alpha = 1 - \left[\left(\frac{kc}{\omega}\right)^2 (1 - M^2)\right]^{\frac{1}{2}} \tag{3.33}$$

$$q = 1 - r^2\left(\frac{1-\alpha M}{1+\alpha M}\right)^2 \tag{3.34}$$

$$r = e^{-2\eta} \tag{3.35}$$

I : intensity of the incident acoustic wave

p : pressure amplitude of the incident wave

ρ_l : density of the liquid

q : energy transmission coefficient

r : modal reflection coefficient

η : phase difference

Under low Mach conditions ($M < 0.05$), as observed in acoustic focusing, shear flow losses increase with increasing harmonics of the resonant frequency. However, as the Mach number approaches the upper limit ($M \sim 0.05$), the slope gradually decreases[86]. Also, shear flow losses which increase with boundary layer thickness (as observed in more realistic slip flow conditions) are relatively low at low Mach numbers[87].

3.2.4.4. Temperature

Besides frequency, acoustic attenuation is a function of temperature also for most human and animal tissues[88]. In the frequency range of 1-10MHz, acoustic attenuation coefficients of different tissues such as spleen and liver over temperatures ranging from 4-37^{0}C have been shown to be dependent on temperature, having very high attenuation constants at low temperatures which decrease gradually with increasing temperature. Such temperature dependence may be due to the transition of inherent lipids in these tissues from the gel phase to the liquid phase over this temperature range. With increasing temperature, while the velocity of sound through the medium increases with temperature at the rate of 4 m/s/K [64], the pressure amplitude decreases by a few decibels at temperatures above 37^{0}C[89, 90].

3.2.4.5. Nonlinearity losses

It is often assumed that the driving frequency alone propagates through the medium at any given time and also that the amplitude is the same throughout its path. However, these assumptions have failed due to non-linearity losses in the medium, which include the effects of amplitude distortion, harmonic decomposition and shock wave formation. When sound propagates through a medium, the amplitude of the input sound wave is distorted which results in decomposition of the incident sound wave into several other frequencies that are harmonically related to the frequency of the incident wave. The extent of amplitude distortion is characterized by a constant called the shock wave factor, which increases with increasing frequency and sound amplitude. However, beyond the saturation level, this distortion is unaffected by increasing frequency and amplitude. These effects modify the linear relationship between sound pressure and density of the medium, thus introducing a nonlinearity factor[91]

$$p = c^2\rho + \frac{1}{2}\frac{c^2}{\rho}\left(\frac{B}{A}\right)\rho^2 + \cdots \tag{3.36}$$

where $\frac{B}{A}$ is the ratio of the quadratic terms and represents the magnitude of losses due to all the effects just mentioned. For most suspension media, these losses have a strong dependence on concentration and temperature. For example, the B/A factor is 5.2 for distilled water and much higher for fatty tissues[91, 92].

3.3. Considering design parameters for multinode acoustic flow cells

The discussion thus far shows that the acoustic losses in the transducer, material of construction, medium and their interfaces increase with increasing frequency. As multinode acoustic focusing usually involves generating highly parallel streams at higher harmonics of the fundamental resonance frequency, all these losses are significant in multinode acoustic flow cells. The general equation for acoustic losses in multinode acoustic flow cells is

$$Total\ loss = Transducer\ loss + \ Material\ losses + Medium\ losses + Impedance\ mismatch\ losses \tag{3.37}$$

While the transducer, reflectivity and the inherent medium losses are intrinsic and hence inevitable, proper selection of the fabrication material will help in minimizing these losses significantly. For this reason, multinode acoustic focusing flow cells were fabricated using three different approaches that include

i. Glass-metal flow cell fabricated using micro-machined aluminum frame and glass slides
ii. Glass capillary flow cell using commercially available rectangular borosilicate glass capillaries
iii. Etched silicon flow cells fabricated using photolithography and deep reactive ion etching techniques

The influence of material losses in each type of flow cell is qualitatively explained in the following sub-sections.

3.3.1. Glass-metal flow cell

The prototype multinode acoustic flow cell was fabricated using a precision machined aluminum frame and commercially marketed glass slides. Although this flow cell uses different fabrication materials, namely metal and glass, the material losses in this flow cell occur predominantly in the metal frame, as the acoustic wave propagates through the metal frame only. For this flow cell, aluminum was chosen as the primary material of construction due to its low scattering losses[78]. However, attenuation in metals has a greater dependence on frequency (f), given by

$$\alpha_{metals} \sim f^4 \tag{3.38}$$

Hence, to minimize acoustic losses, the flow cell must be driven at low megahertz resonance frequencies. Therefore, in this flow cell, multinode acoustic focusing was demonstrated using particles and cells and with driving frequencies less than 2MHz using a 1" circular transducer having a low value of Q-factor. Such transducers are commonly used in non-destructive testing. Although they generate a lower acoustic energy, these transducers have a large surface area of contact that provides efficient coupling with the machined glass-metal flow cell, and hence drive almost all their energy output into the flow cell.

3.3.2. Glass capillary flow cell

To minimize the frequency-dependent material losses further, a commercially available glass capillary having rectangular cross-section was chosen to demonstrate multinode

acoustic focusing. In the glass capillary flow cell, Akhiezer mechanism (described in 3.2.3.3) is the only source of loss and has frequency dependence described by

$$\alpha_{glass} \sim f^2 \tag{3.39}$$

Thus, frequency-related energy losses in glass capillary flow cells are relatively lower than in glass-metal flow cells. This permitted use of a relatively high driving frequency generated by a piezo ceramic crystal having a high value of Q-factor. The width of the glass capillary was chosen to permit generation of a few focused streams.

3.3.3. Etched silicon flow cells

These flow cells use silicon as the acoustic coupling layer and are fabricated by standard photolithography and deep reactive ion etching (DRIE) techniques. The fluidic channels are formed by sealing the etched silicon wafer with a Pyrex glass slide of appropriate dimensions. Like the glass capillary, Akhiezer mechanism losses influence material losses in these flow cells. Although these losses have a frequency-squared dependence, they are relatively lower in silicon. Furthermore, as silicon is the coupling layer, the material losses in these flow cells are primarily due to silicon, and hence lower than losses in glass-metal and glass capillary flow cells. Multinode acoustic flow channels etched in silicon were driven at lower as well as higher driving frequencies using piezo ceramic transducer crystals and with low and high drive voltages. Furthermore, to explore parallelization using this fabrication technique and also to examine the extent of losses resulting from such parallelization, two flow cells, one consisting of 13 parallel channels, and the other consisting of as many as 100 parallel channels were fabricated. The

efficiency of focusing of the particles into such highly parallel streams was evaluated by image analysis.

Therefore, it can be concluded that proper choice of the fabrication material minimizes the total acoustic losses considerably. The inherent acoustic attenuation of the three fabrication materials used in multinode acoustic flow cells, namely aluminum, glass and silicon is low, and hence these materials when used for acoustic coupling permit maximum energy transmission into the flow cell. The general equation for net power transmission is given by

$$Net\ power\ transmission = Power\ input\ into\ the\ transducer - Total\ acoustic\ loss \tag{3.40}$$

Therefore,

$$W_{net} = W_E - \sum Acoustic\ losses \tag{3.41}$$

The quality of sound energy produced by the ultrasonic transducer is defined by its Q-factor, which is the ratio of the resonance frequency of the transducer to its frequency bandwidth.

$$Q - factor = \frac{Resonance\ frequency}{Frequency\ bandwidth} \tag{3.42}$$

Usually, those transducers that have high bandwidth, i.e. those that produce appreciable energies at various harmonics, like the one used to drive the machined glass-metal flow cell, have a low Q-factor. Equation (3.41) suggests that acoustic transmission in multinode acoustic flow cells may also be improved using transducers having high values

of Q-factor such as the piezo ceramic crystals used in glass capillary and etched silicon flow cells.

Chapters 4-6 in this dissertation discuss the multinode acoustic flow cells fabricated using the above mentioned approaches along with their fabrication procedure, experimental methodology, results and discussion.

Chapter 4

Machined multinode acoustic flow cell

4.1. Introduction

Multinode acoustic focusing involves focusing particles and cells into highly parallel streams at higher harmonics of the fundamental resonance frequency, which in turn increase the acoustic radiation force on the particles. Such parallel streams provide high throughput such as those required for rare event analysis. The preliminary attempt towards developing a high throughput multinode acoustic flow cell involved using precision micromachining technique. The fabrication procedure and the experimental methodology and observations have been discussed below.

4.2. Methods

4.2.1. Device design and fabrication

The basic components used in fabricating this flow cell are a machined metal frame and two commercially available glass slides. The frame was micromachined from a single block of aluminum. The thickness of the frame varies from approximately 2 mm at its extreme ends to approximately 700μm towards the flow area. The main flow channel is approximately 1.6 cm wide, 5 cm long and 700μm deep. The flow channel has a rectangular cross-section having two openings, one each for fluid inlet and outlet, where flexible silicon tubing was inserted and glued using epoxy. The frame is precisely machined to fit commercially available glass slides perfectly on either side of the fluidic

channel (Fig. 4.1). The glass slides were glued using super glue to the metal frame, and sealed further using epoxy glue. The finished flow cell was allowed to dry at room temperature for a few hours.

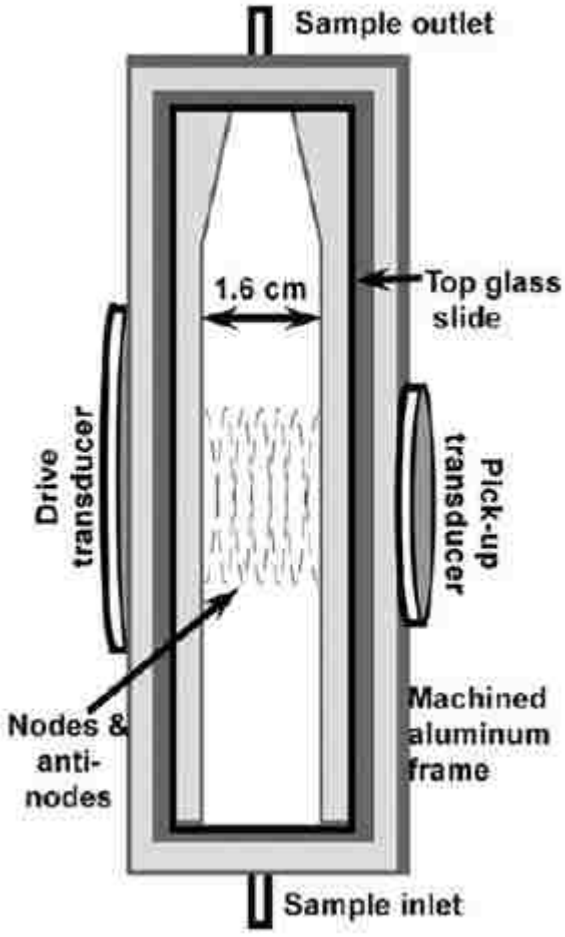

Fig. 4.1 Schematic of the glass-metal flow cell

4.2.2. Experimental setup

The flow cell was held vertically between a 1" and a 0.5" circular transducer (Panametrics Inc., Waltham, MA) , both having a resonance frequency of 1 MHz. The transducers were gel-coupled to the flow cell for maximum acoustic power transmission

into the flow cell. The flow cell was driven using the 1" transducer. The acoustic signal was produced by a waveform generator (33250A, Agilent, Santa Clara, CA). The input acoustic signal was amplified using a radio-frequency amplifier (Empower RF Systems, Inglewood, CA) before transmitted into the flow cell. The 0.5" transducer was coupled across from the driving transducer and was connected to an oscilloscope (Tektronix Inc, Beaverton, OR) to measure the strength of the acoustic signal within the flow cell (Fig. 4.2). A syringe pump was used to inject the sample from a syringe. The images of the focused particle streams were recorded using a commercial video camera (JVC, Wayne, NJ) interfaced to a computer via Windows based imaging software. While the wide-field images that capture all the focused streams in the flow cell were recorded directly using the camera, a magnified image of a few focused streams was recorded using a 4x objective placed in front of it.

Fig. 4.2 Experimental setup of the glass-metal flow cell

4.2.3. Experiment

4.2.3.1. Demonstration of multinode acoustic focusing

Multinode acoustic focusing in this micromachined flow cell was demonstrated by flowing a concentrated ($1.36 * 10^5$/mL) sample of 10.2μm Nile Red polystyrene particles

(Spherotech Inc, Lake Forest, IL) at 250μL/min. Keeping the gain constant, the driving frequency was increased gradually from 1 MHz to 1.7 MHz to obtain increasing numbers of focused streams with increasing harmonics of the fundamental resonance frequency (1 MHz) of the transducer. At each resonance, the signal strength from the 0.5" transducer was nearly a maximum. The driving frequency was gradually decreased to produce focused streams for resonance frequencies below 1 MHz. From the images recorded using the video camera, the number of focused streams observed at each harmonics of resonance was counted. Experiments were repeated for higher flow rates and for lower sample concentrations (~10^3-10^4/mL). Furthermore, multinode acoustic focusing of a sample consisting of a mixture of positive and negative contrast factor particles was demonstrated by adding few drops of the commercially marketed 2% fat milk to the sample of polystyrene particles.

4.2.3.2. Characterization plot

The number of streams generated at each resonance frequency increase with frequency according to the equation

$$n_{nodes} = 2Wf/c \qquad (1)$$

where n_{nodes} is the theoretical number of the nodes in a flow cell of width W at frequency f of the acoustic standing wave in a medium having a sound velocity c. The polystyrene particles have a positive value of the acoustic contrast factor and hence focus into the nodes. Hence, this multinode acoustic flow cell was characterized by plotting the observed number of focused particle streams against the theoretical resonance frequency.

The theoretical fit of the observed resonance frequency (represented by solid dots) was plotted to determine their conformance to theory. For calculations, the value of sound velocity in medium (distilled water) was assumed to be ~1480 m/s.

4.2.3.3. Multinode acoustic focusing with biological samples

Once the multinode flow cell was characterized, the efficiency of the device in focusing biological samples was tested. The flow cell was cleaned with a dilute solution of milk to remove any residue from samples used previously, and a sample of concentrated human whole blood, prepared by using standard protocols, was flowed at ~1 mL/min. The resonance frequency of the transducer was tuned to approximately 1.54 MHz. The sample exiting the flow cell after focusing was collected into a tube. Besides whole blood, multinode acoustic focusing of large samples was tested by flowing tumor microspheroids of different sizes (>60μm upto ~250μm) and of varying concentrations, prepared using standard protocols at 250μL/min flow rate and at 1.54 MHz. Finally, multinode acoustic focusing of microorganisms was demonstrated using a concentrated sample of the algae Dunaliella. These are green micro-algae that usually measure < 10 μm in size. As these algae produce carotenoids, they are commonly used in cosmetics and in dietary supplements. These were grown in the laboratory under suitable salt and light conditions for a few days. The sample was flowed through the flow cell at 100 μL/min and both wide-field and magnified images of the focused streams were recorded.

4.3. Results

The polystyrene particles are denser than the surrounding medium and have a positive value of the acoustic contrast factor. Hence, they migrate into the nodes in an acoustic standing wave field. While increasing the driving frequency of the transducer, the first resonance frequency for the device occurred at 1.025 MHz where 22 focused streams of polystyrene particles was observed. Increasing numbers of focused particle streams were observed with increasing harmonics of the fundamental resonance frequency (Fig. 4.3a). However, the output signal strength, measured using the 0.5" transducer decreased at frequencies much higher than the transducer's rated frequency of 1 MHz. For example, beyond 1.715 MHz where 37 focused streams were observed, the signal strength was too low and hence the particles were poorly focused. Similarly, on decreasing the frequency below 1 MHz, the lowest resonance frequency for optimal signal strength was 784 kHz. At this frequency, the polystyrene particles focused into 17 nodal streams. Furthermore, the near-range images of the focused streams indicated tight particle focusing at all frequencies (Fig. 4.3b). Particles were focused tightly at low sample concentrations, and also for flow rates up to 1 mL/min. For the lipid rich mixture of 2% fat milk and polystyrene particles, the positive-contrast polystyrene beads focused into the nodes while the negative-contrast lipids in milk focused into the antinodes (Fig. 4.3c).

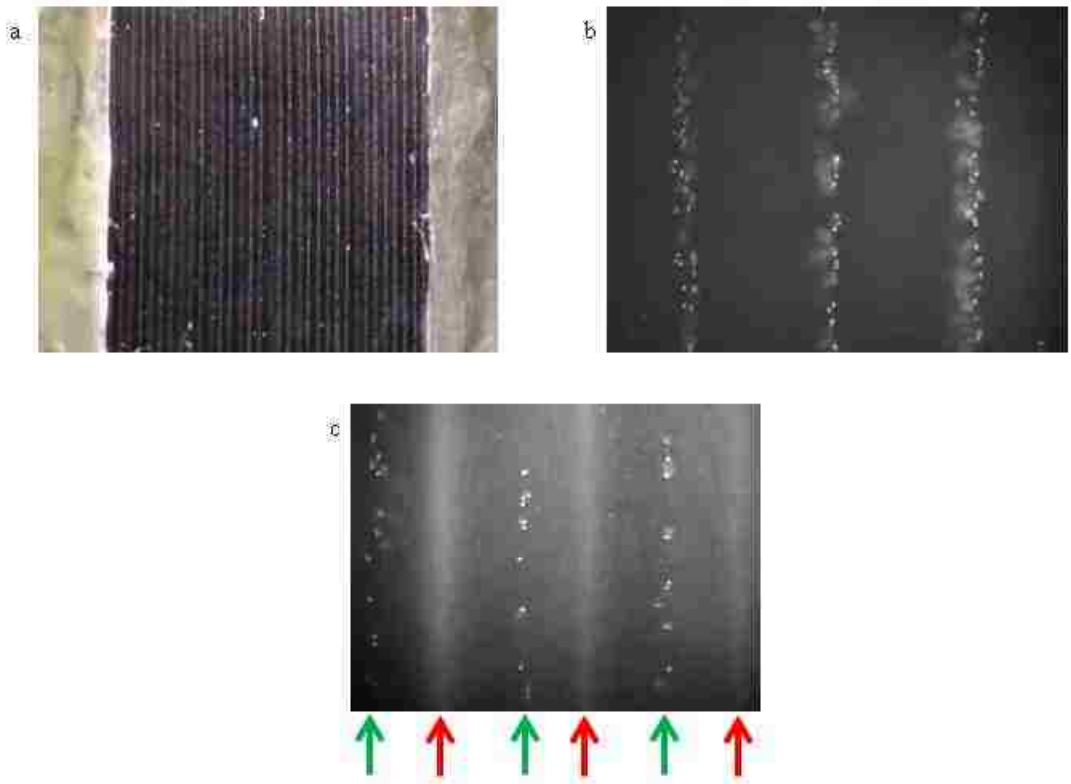

Fig. 4.3 (a) 10.2 μm Nile Red polystyrene (NR-PS) particles focused into 33 parallel streams at 1.54 MHz (b) Image of 3 focused streams using a 4x objective lens (c) Image of nodal (green arrows) and antinodal (red arrows) streams of 10.2 μm NR-PS and lipids in whole milk respectively using 4x objective

The characterization plot (Fig. 4.4) for the device indicates appreciable conformance between theory and experiment within the range of the observed values of resonance frequency.

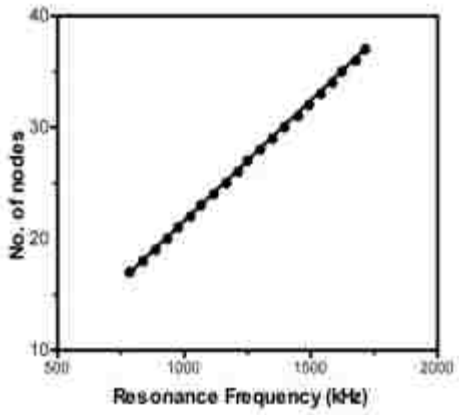

Fig. 4.4 Plot of theoretical number of nodes versus observed resonance frequency

While particles were focused well through the range of frequencies used herein, very tight focusing of particles into the individual nodal streams was observed in the 1.5-1.6 MHz frequency range. Therefore, for experiments with biological samples, the resonance frequency of 1.54 MHz was chosen, which corresponds to the 33rd harmonic. Hence particles and cells (most cells are rigid and have a positive value of contrast factor) focused into 33 nodal streams at this frequency. At ~1mL/min and with relatively higher amplification than that used previously, the blood cells focused into 33 nodal streams (Fig. 4.5a). Despite using high gain, the individual focused streams observed in a magnified image of a few focused streams were broad, indicating relatively poor focusing than the polystyrene particles. However, tumor microspheroids of all sizes were well focused at the resonance frequency of 1.54 MHz. Fig. 4.5b shows focused streams of spheroids ~95μm diameter at 1.54 MHz. While the wide-angle image shows 33 well-focused streams of these spheroids, the image of individual streams confirm tight focusing. The inherent high lipid density of algae not only limited the maximum flow rate to 100μL/min but also required very long times for focusing into the individual streams.

For example, the image of focused algal streams (Fig. 4.5c) shown here was not obtained until ~30min after the acoustic field was turned on. However, algal cells were focused just like the polystyrene particles, despite their small size.

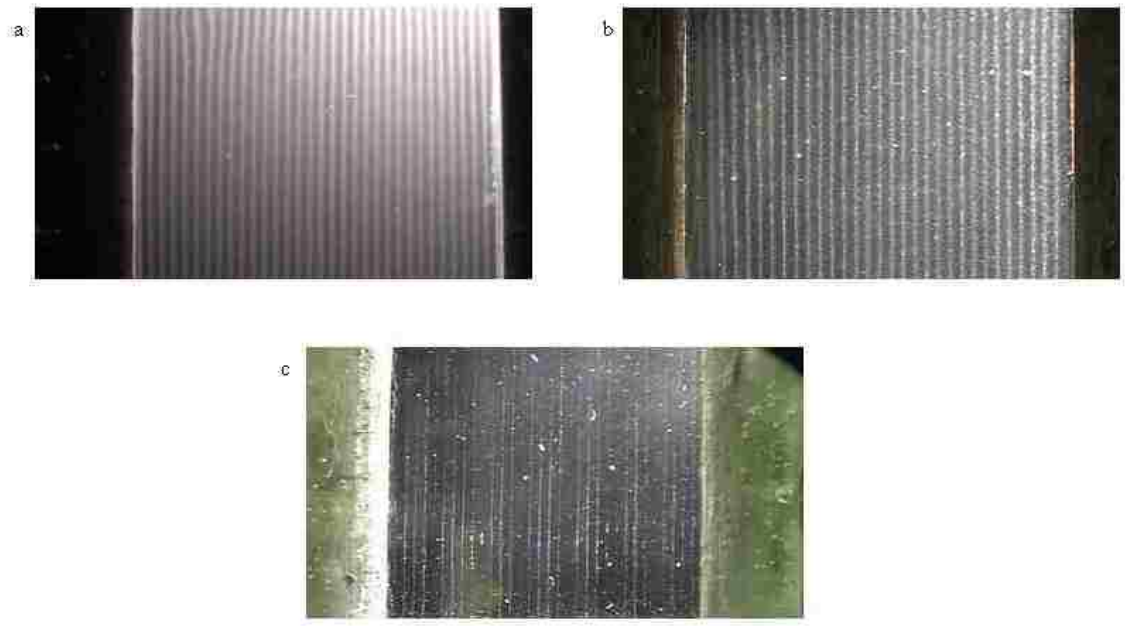

Fig. 4.5 33 parallel streams of (a) human whole blood (b) spheroids (95μm mean diameter) and (c) algae at 1.54 MHz

4.4. Discussion

The primary aim of the multinode acoustic technique is to increase the analysis rates in flow cytometry by few orders of magnitude by focusing particles and cells into multiple parallel streams. Toward this aim, the glass-metal flow cell was fabricated. A flow channel, a few cm wide, was selected in order to demonstrate this technique at increasing harmonics of the fundamental frequency of the transducer. Also, the materials of construction, namely aluminum and glass, were chosen to minimize acoustic losses and enhance acoustic energy transmission, while minimizing costs. Furthermore, the larger

the driving transducer, the greater the area of contact with the flow cell and hence greater is the acoustic energy penetration.

A machined flow cell 1.6 cm wide permitted generation of as many as a few tens of focused streams at higher harmonics of lower resonance frequencies. Such highly parallel focused streams allowed focusing of cells in large volume samples and hence promised to be truly useful for rare event detection. Also, the large lateral dimensions of this flow cell allowed handling of particles with diameters ranging from a few microns to hundreds of microns. Furthermore, the flow cell was optically transparent and hence may be easily integrated with flow cytometry optics and detectors.

As most cells and particles have a positive value of the contrast factor, they migrate into the nodal plane of the acoustic standing wave. The polystyrene particles used here have positive contrast factor value and have been used previously for demonstrating acoustic focusing at fundamental as well as higher harmonics[13, 35]. Hence these particles were chosen here also to demonstrate the multinode acoustic focusing technique.

Previously researchers elsewhere have successfully driven narrow flow channels at the very low harmonics of resonance frequency using high quality (i.e. high Q-factor) transducer crystals[51, 52]. However, focusing particles at lower harmonics produced only a small improvement in throughput. In comparison, this machined flow cell was driven using a low Q-factor transducer. However, this flow cell successfully generated as many as 37 focused particle streams. This indicates that transducer coupling and not necessarily transducer Q-factor value influences acoustic transmission into the flow cell. In other words, gel-coupling the transducer to the flow cell and increasing the surface

area of contact of the transducer with the flow cell improves acoustic transmission even while using a transducer having low Q-factor. The appreciable correlation between theory and experiment as observed in the characterization plot is an indicator of precise functioning of this glass-metal flow cell for multinode acoustic focusing technique. Furthermore, this flow cell focuses both low and high concentrations of particles (range = x to y cells/ml) as well as precisely focusing cells at flow rates up to 1mL/min. Also, the particles were tightly focused in both the nodal as well as the antinodal streams. This flow cell also generated highly parallel focused streams over a range of driving frequencies. This range was limited by the rated resonance frequency and the bandwidth of the transducer, and hence, if driven using a transducer having a higher bandwidth, this flow cell may function over a wider range of frequencies, thereby generating more parallel focused streams. Finally, the optical transparency of the glass slides used herein allowed interrogating the focused particle streams using flow cytometry optics.

Despite generating highly parallel streams, this flow cell presents limitations with respect to both design as well as focusing. Although the depth of this flow cell allows handling particles few hundred microns in diameter, it limits particle flow rate to 1 mL/min for polystyrene particles and large cells (> 5μm), and much lower for smaller biological samples such as algae. The low flow rate observed with algae may however be justified by the dependency of the acoustic radiation force on the volume of the particle. While polystyrene particles and most cells (spheroids and algae) were tightly focused into the individual streams, the blood cells were relatively poorly focused. Such imprecise focusing may be due to acoustic losses that occur in the material of the flow cell and the medium. Although scattering losses in aluminum are low, these losses scale with the

fourth power of frequency, and hence are greater in magnitude than other material losses[78]. Hence, for a particular frequency, the acoustic energy transmission into the flow cell is lower. Besides material losses, the inherent nature of cells suspended in the medium contribute further to the total acoustic loss. For example, red blood cells have a tendency to agglutinate under suitable conditions. Visual analysis of a few focused streams at high magnification indicated dense focused streams of blood. At such high concentrations, blood cells agglutinate, which increases scattering losses in the medium[83]. While previous studies have shown negligible scattering losses for the range of frequencies used here[80], scattering losses increase with particle concentration, and hence can become significant. Furthermore, this flow cell generated multiple focused streams across its width at a few tens of harmonics. As non-linearity losses become significant at higher harmonics of megahertz frequencies[91], these losses may further limit the acoustic energy within the flow cell. Considering the design of the flow cell, the individual streams are very closely spaced at higher frequencies. Such narrow clearance between the focused streams may present challenges while redesigning this metal frame with outlet ports for collecting the individual streams for downstream analysis. Although manual fabrication of this flow cell using epoxy adhesives is crude, such issues can be overcome by using rubber clamps or seals to hold the glass slides in place. However, additional fabrication materials could contribute further to acoustic attenuation. Therefore, better fabrication approaches that generate highly parallel focused streams with relatively lower energy losses must be adopted for multinode acoustic flow cells.

Chapter 5

Glass capillary for generating multiple focused streams

5.1. Introduction

Using the machined flow cell described in Chapter 4, particles, cells, spheroids and unicellular algae were focused into highly parallel streams in a flow channel of rectangular cross-section. However, qualitative examination indicated high acoustic losses, mainly due to fourth-power frequency-dependent scattering losses in the micromachined aluminum frame. Furthermore, high manufacturing cost involved in precision machining precludes disposing these flow cells. Hence, the aim of this chapter is to present an alternate fabrication approach that not only generates multiple focused streams but is also easy to fabricate, optically transparent and potentially inexpensive enough to be considered disposable. Toward this aim, commercially available rectangular glass capillaries have been used to demonstrate multinode acoustic focusing. Unlike the glass-metal flow cell, this flow cell is relatively compact in design and optically transparent, besides being disposable. Furthermore, acoustic losses are relatively minimal as this flow cell is fabricated homogeneously of glass, where scattering losses are negligible. Thus, the glass capillary flow cell will generate multiple focused streams, just like the micromachined glass-metal flow cell, but with lower acoustic losses.

5.2. Methods

5.2.1. Device design and fabrication

A commercially available borosilicate glass capillary of rectangular cross-section was used to fabricate the flow cell used here. In order to minimize effects due to flow and achieve a uniform parabolic profile, care was taken to select the glass capillary (Friedrich and Dimmock Inc, Millville, NJ) of appropriate dimensions. The glass capillary is 2 mm wide and 200μm deep. A 2.91 MHz piezo transducer crystal (30.32mm long, 5.05mm wide and 0.46mm thick, Boston Piezo-Optics Inc, Bellingham, MA), glued to one of its walls using cyanocrylate glue (commercially sold as "super glue"), drives the acoustic energy into the flow cell. A similar transducer glued to the other wall of the capillary served as the feedback transducer to measure the strength of the acoustic signal. Next, flexible silicone tubing of 1.6mm inner diameter were glued to the inlet and outlet of the glass capillary. Finally, the glass capillary with tubing was mounted over two baked polydimethylsiloxane (PDMS) slabs and sealed to a commercially available glass slide. Fig. 5.1 shows a snapshot of the finished glass capillary device.

Fig. 5.1 Snapshot of the glass capillary device

5.2.2. Experimental setup

The sample was injected into the flow cell using a syringe pump. The input acoustic signal from the waveform generator (33250A, Agilent, Santa Clara, CA) was amplified

using a radio frequency RF amplifier (Empower RF Systems, Inglewood, CA) having fixed gain. The amplified input signal to the driving transducer and the resulting output signal from the feedback transducer were monitored using an oscilloscope (Tektronix Inc, Beaverton, OR). For imaging the focused particle streams, the glass capillary flow cell was placed in the optical path of a 4x objective fitted to an epifluorescence microscope (Axio Imager-2, Carl Zeiss, Inc) incorporating an electron multiplying charge-coupled device (EMCCD) camera (Luca S, Andor Technology, Belfast, N.Ireland).

5.2.3. Experiment

Multinode acoustic focusing in the rectangular glass capillary flow cell was demonstrated using a concentrated sample of 10.2μm Nile Red polystyrene particles (Spherotech Inc, Lake Forest, IL) flowing at 1mL/min. The width of the glass capillary is the 8^{th} multiple of half-wavelength for the driving frequency of 2.91 MHz and hence the flow cell generates 8 focused streams when driven at the resonant frequency of the transducer. However, due to structural resonance, a shift in actual resonance frequency may be expected. Hence, the driving frequency was gradually increased above the transducer's resonance frequency to determine the actual resonance frequency for the flow cell. Once this frequency was determined, the amplitude of the input acoustic signal was adjusted to further improve particle focusing in the individual streams. Once the particles were focused well, they were imaged using the epifluorescence microscope and the EMCCD camera with 545/25 and 605/70 band-pass filters for excitation and emission respectively.

5.3. Results

Without acoustic actuation, the polystyrene particles were randomly dispersed across the flow channel (Fig.5.2a). On gradually increasing the driving frequency, the particles were found to appreciably focus into 8 individual streams at 3.12 MHz. However, the particles were focused well only at the input drive peak-to-peak voltage of $50V_{pp}$ (Fig. 5.2b).

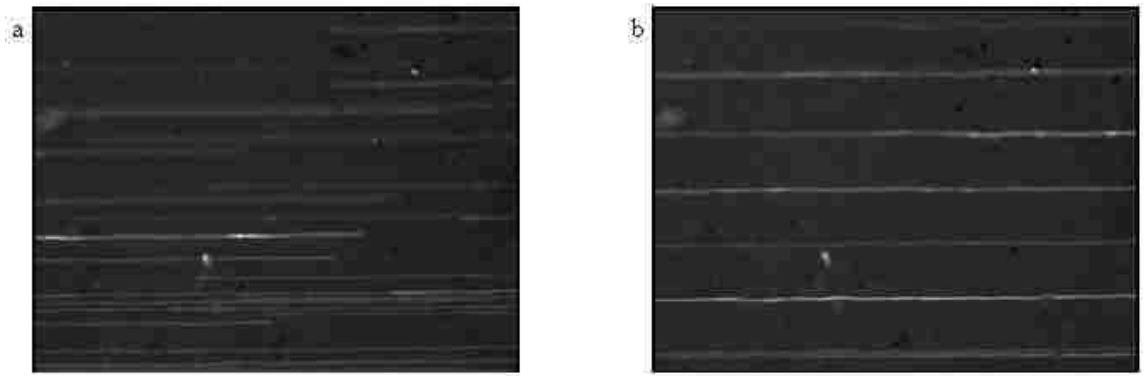

Fig 5.2. (a) Randomly moving 10.2 μm Nile Red polystyrene particles are (b) focused into 8 streams at 3.12 MHz and drive voltage of 50 Vpp. Only 7 streams are imaged due to limited field of view

5.4. Discussion

The rectangular glass capillary flow cell discussed here generates multiple focused streams of particles just like the glass-metal flow cell used previously. Besides being useful for parallel flow cytometry, such flow cells are disposable, easy to fabricate and more importantly, they have relatively minimal acoustic energy losses due to lower scattering losses. Furthermore, the optical transparency of glass allows easy integration with flow cytometry interrogation and detection optics This flow cell has all the attributes of flow cells used in the commercial acoustic flow cytometer, and has the added advantage of focusing particles and cells into multiple streams.

Despite being suitable for parallel flow cytometry, the glass capillary flow cells have certain limitations. First, experimental observations show that particle focusing in these rectangular glass capillaries is very sensitive to the orientation of the transducer, i.e., the transducers have to be glued perfectly orthogonal to the wall of the capillary. Misalignment of the transducer is quite unforgiving and particles are either unfocused or poorly focused even in the presence of a strong acoustic field. Second, despite having relatively lower frequency dependent acoustic losses than metals[79], very high input power (drive voltage) is required to focus particles even with proper orientation of the transducer. For example, with polystyrene beads, despite using a high Q-factor transducer, an input peak-to-peak voltage of 50V was required to generate just 8 focused streams, unlike the glass-metal device where, except for unicellular microorganisms, as many as 37 focused streams were obtained at half that input voltage and by using a low Q-factor transducer. Reasoning similarly, energy requirements for biological samples in these glass capillary devices would be very high and may not be compatible with most cells and tissues. Such a difference could arise due to the surface area of contact between the transducer and the flow cell. In the glass capillary flow cell, the piezo ceramic transducer is in contact with only a small surface of the wall of the glass capillary, unlike the machined flow cell where the surface area of the transducer is much larger. While only 8 focused streams were generated in this flow cell, use of a wider flow channel and an appropriate transducer might allow generating as many streams as observed with the glass-metal device, and perhaps even more. However, based on the observations made here, increasing parallelization of the focused particle streams would likely also increase power requirements. Although these capillaries allow easy integration with optics and

involve simple fabrication procedures, they consume high power which could increase the cost of operation of a commercial parallel flow cytometer. Therefore, future attempts should aim at fabricating flow cells that have relatively lower material acoustic losses and provide more optimal acoustic coupling while using piezo ceramic crystals.

Chapter 6

Etched silicon devices for high throughput applications

6.1. Introduction

Thus far, multinode acoustic focusing has been demonstrated using micromachined glass-metal and rectangular glass capillary flow cells. Although successful for multinode acoustic focusing, they suffer from certain limitations. Besides others, these fabrication approaches do not support incorporation of multiple physical flow channels in parallel. Previously such parallelization using conventional hydrodynamic focusing and inertial focusing techniques have improved throughput by few orders of magnitude. While the hydrodynamic mechanism suffers from the use of sheath fluid, the inertial focusing technique is limited by particle and channel dimensions. Furthermore, a volume throughput several orders of magnitude higher is necessary for high volume applications. As the multinode acoustic technique is free of the above mentioned limitations, and allows focusing particles into more than one focused stream within a channel (unlike the traditional hydrodynamic mechanism), a several fold increase in volumetric throughput is possible. Application of multinode acoustic technique to parallel flow channels also results in increased acoustic energy density within each channel to better facilitate tight focusing of streams. This chapter presents an alternate approach that supports such parallelization.

6.2. Methods

6.2.1. Device design

Parallelization of the fluidic channels as discussed above can be achieved using a microfabrication approach. Such an approach provides flexibility in designing flow cells of any dimension and complexity as required by its intended application. For example, shallow channels may be sufficient to handle cells a few microns in diameter whereas deeply etched channels may be necessary to handle larger objects such as cell clusters and eggs of Drosophila. Hence, the microfabrication approach will allow fabricating high throughput and high energy multinode acoustic flow cells compatible with use in parallel flow cytometry for the detection of rare events. Toward this aim, two different types of multinode acoustic flow cells, classified as type-1 and type-2, have been designed and fabricated using etching techniques:

Type-1: Multinode flow cells having a single wide channel, and

Type-2: Multinode flow cells having multiple parallel channels, each channel generating a few focused streams

Two different designs for each type were fabricated to test the hypothesis that these microfabricated flow cells minimize acoustic energy losses and improve throughput.

6.2.2. Fabrication procedure

These multinode acoustic flow cells were fabricated using standard photolithography and deep reactive ion etching procedures. First, the design of the flow cell was drawn in

AutoCAD (Autodesk Inc, San Rafael, CA) (Fig. 6.1). This design was then printed on a high resolution photomask (10,000 dpi), through a commercial source (CAD/ Art Services Inc, Bandon, OR). Once printed, the photomask can be used for photolithography procedures. The steps involved in microfabrication, from photolithography through etching and finally anodic bonding (Fig. 6.2), are described in detail in the following paragraph.

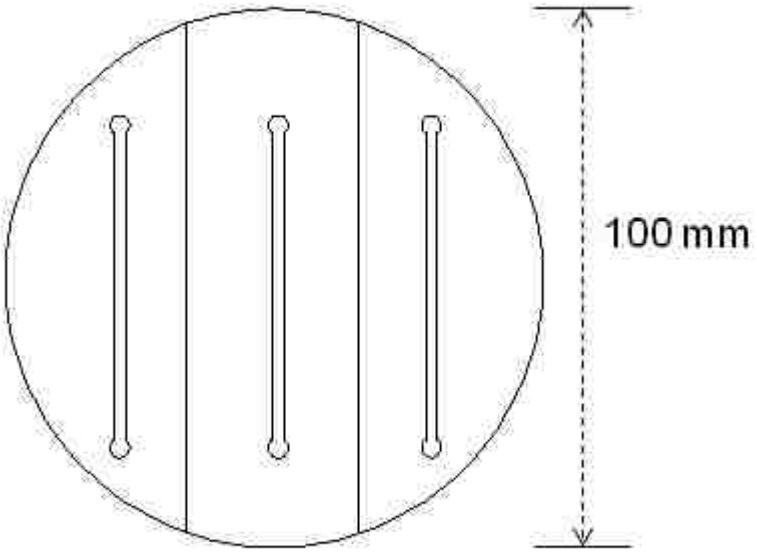

Fig. 6.1 Design of a flow cell drawn using AutoCAD for photomask

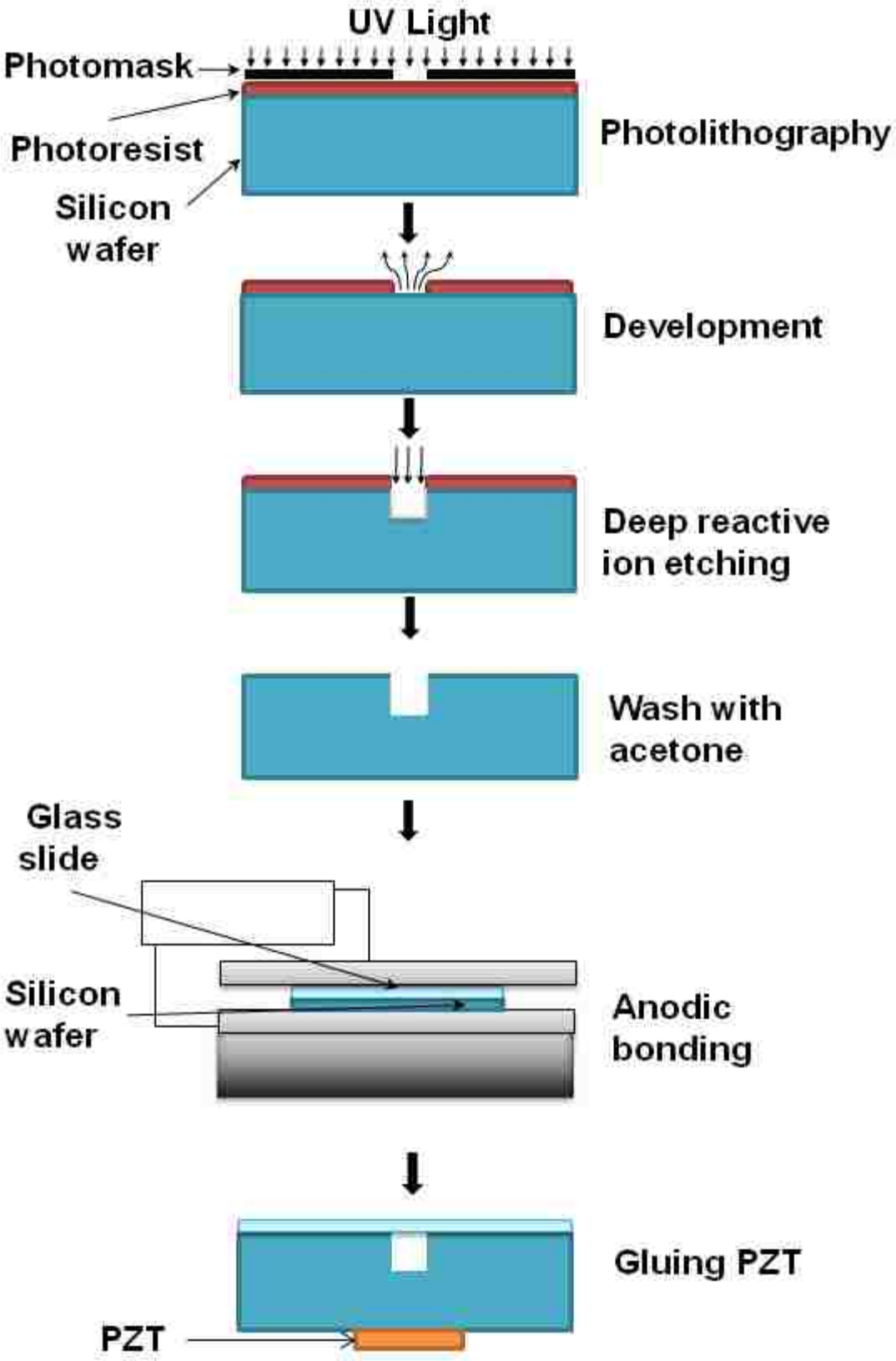

Fig. 6.2 Steps involved in the microfabrication of multinode acoustic flow cells etched in silicon

A uniform layer of hexamethylene disilazane (HMDS) was coated on a 100mm diameter silicon wafer (WaferNet Inc, San Jose, CA, test grade, N or P type). Next, positive photoresist (AZ 9260, Microchemicals GmbH, Germany) was spin coated onto the HMDS-treated wafer in two cycles. In the first cycle, the spin coater (Cee® 200X, Brewer Science) was spun at 500 rpm with an acceleration of 5000 rps for 5s, whereas in the second cycle, the coating was performed at a higher spin velocity of 2000 rpm with the same acceleration, but for about 60s. The spin coated wafer was baked over a hot plate at 120^0C for 5 minutes, and cooled at room temperature for atleast 20 min. Once cooled, the design on the photomask was printed onto the wafer by exposing it to high energy ultraviolet light (365nm, 4.5 mW/cm^2) in a mask aligner (Karl Suss MA6, SUSS, MicroTec AG, Germany). The exposed photoresist on the wafer was removed using a diluted developer (AZ 400K, Microchemicals GmbH, Germany, 1:4 dilution with distilled water). The developed wafer was washed with distilled water and dried in a stream of nitrogen. Once dried, the pattern on the wafer was etched to the desired depth using a DRIE etcher (Alcatel AMS 100, Alcatel Micro Machining Systems, Annecy, France). Residual photoresist left after etching was removed by washing the wafer with acetone and deionized water. Holes of diameter ~1mm were drilled using a hand drill (Dremel Rotary 300 Series, Dremel) on a customized borosilicate glass slide (Borofloat 33, Schott North America Inc., Elmsford, NY) for inlet and outlet tubing connections. The drilled glass slide and the etched silicon wafer were washed and cleaned by immersing them in a glass vessel consisting of a mixture of 30% hydrogen peroxide and 70% sulfuric acid, commonly known as the Piranha etch. The drilled glass slide and the etched wafer were bonded finally using a custom anodic bonding setup that consists of

two metal plates maintained at high voltage (~1.2kV) and high temperature (400-425^{0}C). Finally, lengths of flexible silicone tubing were attached to the inlet and outlet and a piezo ceramic transducer (Boston Piezo-Optics Inc, Bellingham, MA) was glued beneath the silicon wafer (Fig. 6.3).

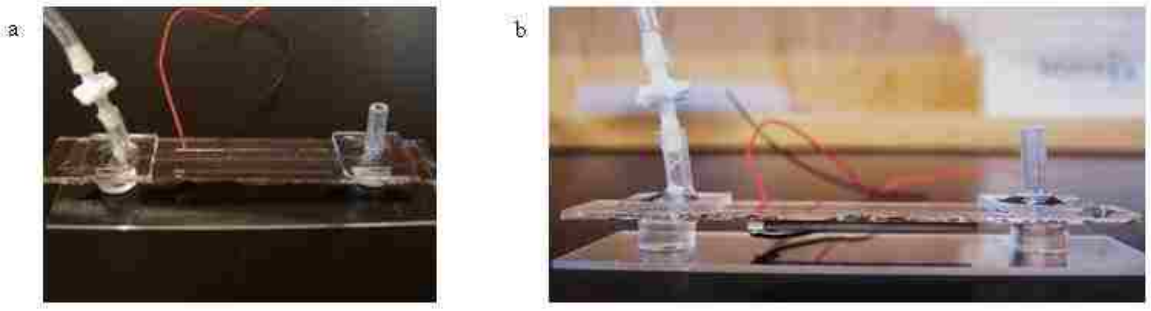

Fig. 6.3 (a) Top and (b) side views of a microfabricated device

6.2.3. Experiment

6.2.3.1. Acoustic focusing in etched silicon devices

As mentioned earlier, the microfabrication approach for multinode acoustic flow cells was demonstrated using two devices for each type described in 'device design' section (6.1.1.).

Type-1: Multinode flow cells having a single wide channel

First, a 2cm wide channel (Fig. 6.4a) was fabricated and a 2.91MHz transducer was glued beneath the etched channel. The width of the channel corresponds to the 40th harmonic resonance for the natural frequency of the transducer, and hence this flow cell should generate 40 focused streams of cells and particles. A sample of 10.2μm Nile Red polystyrene particles of approximately 10^5/mL concentration was flowed through the

device to demonstrate multinode acoustic focusing. Images of focused particle streams were recorded using a 4x objective in an epifluorescence microscope fitted with an electron-multiplying charge-coupled device (EMCCD) camera.

Next, to demonstrate multinode focusing at relatively higher frequencies, a 2mm wide flow channel (Fig. 6.5a) was fabricated. This flow channel was driven using a 4.48MHz transducer, which corresponds to the 12^{th} harmonic resonance frequency for the channel dimensions. Hence, this flow cell should generate 12 focused streams when driven at 4.48MHz. This flow cell was also tested using 10.2μm Nile Red polystyrene particles and images were recorded using a 4x objective in the epifluorescence microscope fitted with an EMCCD camera. Furthermore, precise focusing of particles in the z-plane was examined by imaging a few focused streams using a 10x objective in the epifluorescence microscope.

Type-2: Multinode flow cells having multiple parallel channels

To demonstrate parallelization of multinode acoustic focusing technique using the microfabrication approach, a flow cell consisting of 13 parallel channels was fabricated (Fig. 6.6a). This flow cell was driven using a 4.48MHz transducer glued beneath the channels. In this flow cell, each channel is 500μm wide, which corresponds to the 3^{rd} harmonic resonance for the driving frequency, and etched to 100μm. Therefore, when driven at 4.48MHz, each channel should generate 3 focused streams across its width. When every channel in this flow cell resonates at the driving frequency, the particles focus into 39 streams. Again, the flow cell was tested by flowing 10.2μm Nile Red

polystyrene particles. Images of the focused particle streams were recorded using a 10x objective in the epifluorescence microscope.

6.3. Results

Multinode acoustic focusing was demonstrated successfully using type-1 flow cells. The 2cm wide channel focused 10.2μm Nile Red polystyrene particles into 40 streams at flow rates up to 12.5mL/min (Fig. 6.4b). However, magnification produced by the 4x objective restricted the field of view and hence only 7 streams were captured in an image frame. Even the 2mm wide channel focused particles into 12 streams as predicted. However, smaller dimensions of the flow cell limited the flow rate to 500μL/min. Fig. 6.5b shows 10 focused streams that were captured in the field of view of the 4x objective in the epifluorescence microscope. Furthermore, the magnified image of few focused streams (Fig. 6.5c) captured using the 10x objective showed that almost all particles were focused into a single plane in the channel depth.

a

b

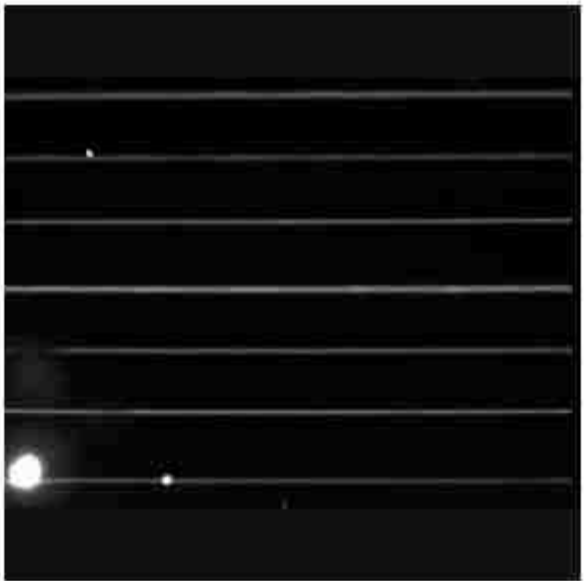

Fig. 6.4 (a) Snapshot of the 2 cm wide channel (b) Image of 7 streams of 10.2 μm Nile Red polystyrene particles flowing at 12.5 mL/min

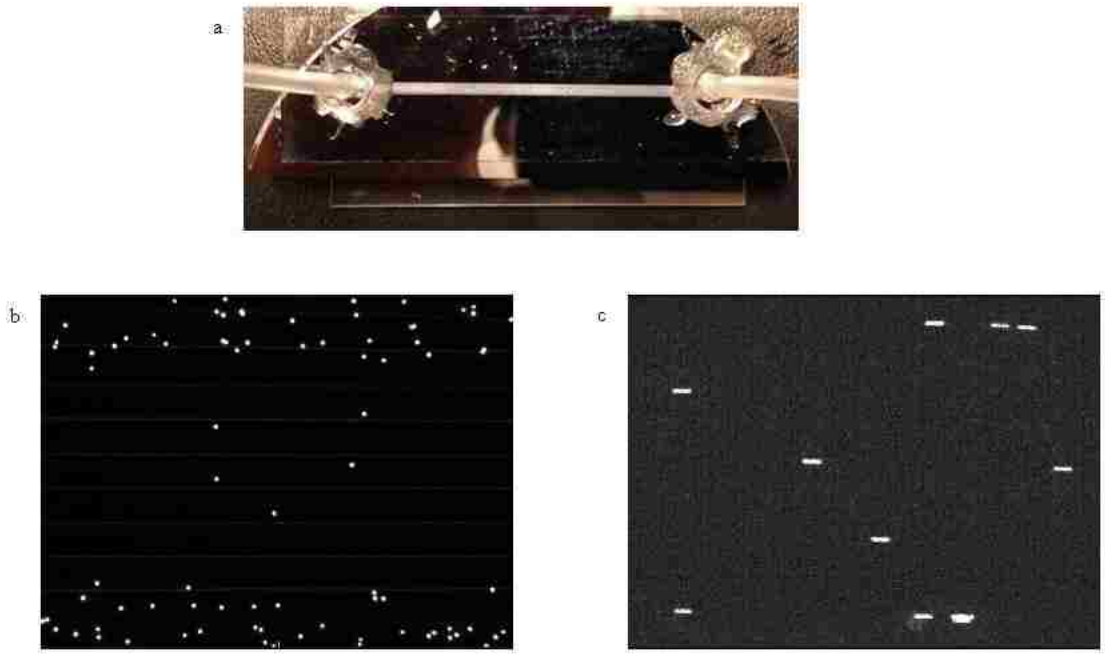

Fig. 6.5 (a) Snapshot of the 2 mm wide channel (b) Image of 10 focused streams of 10.2 μm NR-PS particles flowing at 500 μL/min taken using 4x objective (c) Image of 5 streams at the center of the channel showing precise focusing of particles in the z-plane taken using 10x objective

Parallelization in type-2 flow cell also showed success in multinode acoustic focusing. In the type-2 flow cell, the particles were focused tightly into 3 streams in every channel at 1.5mL/min. Hence, this flow cell successfully generated 39 highly parallel streams.

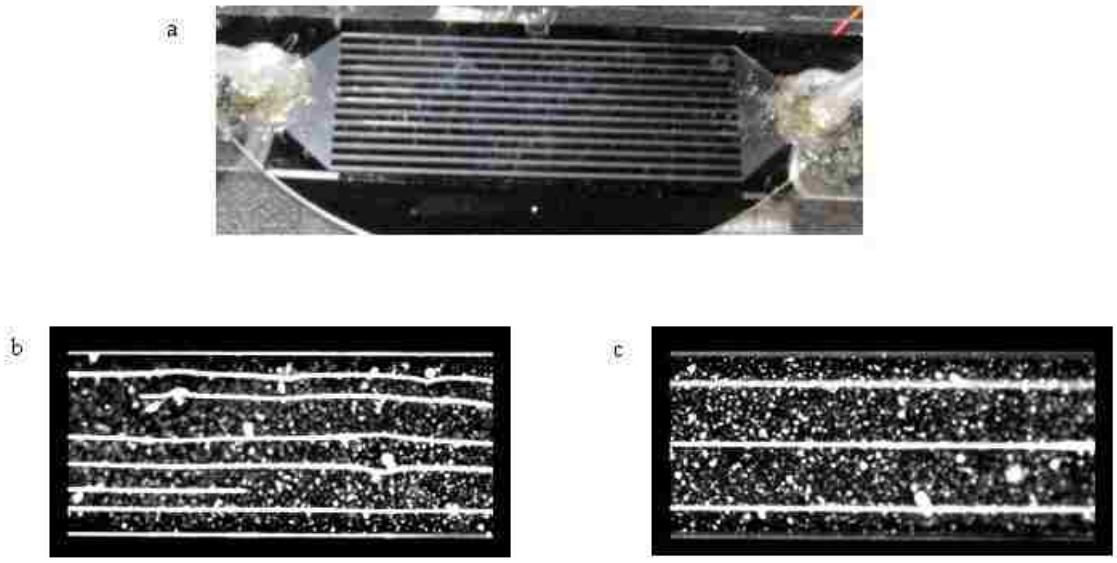

Fig. 6.6 (a) Snapshot of the 13-channel 3-streams per channel device (b) Unfocused 10.2 μm NR-PS particles flowing at 1.5 mL/min are (c) focused into 3 streams in one of the channels at 4.48 MHz.

6.4. Discussion

The microfabrication technique used here for multinode acoustic flow cells offer flexibility in designing flow cells for multinode acoustic focusing. For example, as demonstrated here, this approach may be used to fabricate flow cells having a single wide channel that accommodates multiple focused streams within it as well as parallel flow channels where each channel accommodates a few focused streams. This approach further allows easy integration of fluidic ports. Despite being time-consuming and requiring professional training, flexibility in design makes this approach suitable for fabricating high throughput flow cells for flow cytometry. Although these flow cells are fabricated using both silicon and glass, acoustic attenuation occurs mainly in silicon, the material with the lowest acoustic energy loss among those used to fabricate multinode acoustic flow cells[79].

Like the micromachined and glass capillary flow cells, the single channel (type-1) flow cells fabricated using this technique also successfully generated multiple focused streams. Although these flow cells focus particles up to 12.5mL/min, focusing efficiency of individual streams at the channel center was poor compared to those near the walls. Furthermore, particle settling was more pronounced in these flow cells. Such particle settling is not due to acoustic trapping as settling was observed in images recorded with and without acoustic field.

In comparison to type-1 single-channel flow cells, the 13-channnel flow cell of type-2 provided a better focusing efficiency. Such precision in focusing may be attributed to at least two reasons. First, the acoustic energy is more concentrated within each channel in

type-2 flow cell than type-1 flow cell where acoustic energy, besides being attenuated with increasing propagation distance by nonlinearity losses, is divided among all the focused streams within the wide channel. These nonlinearity losses, which increase with increasing harmonics, and hence increasing number of focused particle streams, may actually be negligible in the 13-channel flow cell, where each channel resonates independently. Second, every channel in the type-2 flow cell has a more uniform parabolic flow profile by virtue of its dimensions. Although both type-1 and type-2 flow cells are etched to 100μm, the width/height ratio for channels in the type-2 flow cell is relatively low, which gives rise to a more uniform laminar parabolic flow profile and hence more lift force on the particles within these channels. This positions the particles precisely into the channel depth. However, the magnitude of these lift forces is theoretically much lower than the acoustic radiation force.

Therefore, among the flow cells fabricated using microfabrication techniques, the parallel channel design performs better for multinode acoustic focusing. Although throughput obtained with the parallel channels is significant and comparable to that of hydrodynamic focusing flow cell used in commercial flow cytometers, it is still low for high throughput applications. Hence, future work with these flow cells must focus on improving throughput, either by increasing the number of channels or by increasing acoustic energy within each channel with large transducers of different geometry.. Truly high analysis rates can be achieved only by imaging all the focused streams within the flow cell simultaneously. Hence, future research should also focus on developing optical systems that allow interrogating and analyzing multiple focused streams.

In summary, in comparison with the fabrication approaches discussed previously, multinode acoustic flow cells fabricated using photolithography and deep reactive ion etching techniques provide better throughput and focusing precision, and hence will provide relatively high analysis rates in flow cytometry.

Chapter 7

Microfabricated parallel multinode acoustic flow cell for high volume cellular focusing

Pearlson P. Austin Suthanthiraraj[1], Menake E.Piyasena[2] and Steven W. Graves[1]

[1]Center for Biomedical Engineering, Department of Chemical and Nuclear Engineering, University of New Mexico, Albuquerque, NM 87106
[2]Department of Chemistry, New Mexico Institute of Mining and Technology, Socorro, NM 87801

(To be submitted for review)

Abstract

Flow cytometry is commonly used to analyze and differentiate single cells depending upon their fluorescence and scatter properties. Although efficient for rare event analysis, its low throughput caused by sheathing of the sample prolongs analysis times for such high throughput applications. In this paper, we describe a microfabricated multinode acoustic flow cell that focuses particles and cells into 300 focused streams at flow rates of few tens of mL/min using a single piezo-ceramic crystal (5mm wide, 30mm long). Our characterization studies for the efficiency of particle focusing in individual focused streams in terms of peak width at half maximum confirms tight focusing of polystyrene particles even at the highest flow rate. We have further demonstrated high throughput focusing of both small biological samples such as red blood cells and large samples such as tumor microspheroids having mean diameter of 65μm at 10mL/min. Such cell positioning into several highly ordered streams at high flow rates will provide volumetric throughput required for rare event analysis such as the detection of circulating tumor cells.

7.1. Introduction

The pathogenic stage of a disease is determined by analyzing single cells which involves measuring its intrinsic and extrinsic properties such as size, shape and the nuclear content[1].For example, a cell's DNA content may be necessary to monitor cancer progression. Such quantitative measurements can be obtained using flow cytometry that measures multiple parameters from individual cells labeled with membrane specific antibodies. Furthermore, flow cytometry also sorts heterogeneous cell populations

depending on their scatter properties, and hence allows performing downstream analysis of the sorted population[93]. The precise optical measurements together with the sorting capability of flow cytometers enable performing even rare event analysis. However, such analysis requires processing large sample volumes, which presents challenges for flow cytometry. Flow cytometry uses hydrodynamic focusing mechanism that focuses particles and cells into a single narrow stream by using the sheath fluid at specific ratio of the hydrodynamic pressure of the sheath fluid and the sample. While such precise focusing permits accurate measurement of the cell's properties, it presents challenges in throughput, mainly due to the sheath fluid[2]. Besides large volumes of the sheath fluid, such high throughput applications also require processing large sample volumes for prolonged time periods to achieve the desired accuracy and precision. Furthermore, the sheath fluid accelerates cells in the sample, hence requiring expensive fluorescence detection elements. For these reasons, research in recent years has focused on both improving analysis rates and throughput in hydrodynamics as well as developing alternate focusing techniques that eliminate the sheath fluid.

Attempts to improve throughput and analysis rates by hydrodynamic focusing include using commercial flow cytometers as well as using microfabricated flow cells. One of the simplest ways to improve throughput is by parallelizing the fluidic systems which includes focusing particles into more than one stream. Such an attempt was made using hydrodynamics where particles were focused in four separate flow cells and these flow streams were analyzed using different optical heads that included similar excitation and detection elements. Simultaneous focusing and analysis produced a linear increase in

analysis rates (~280,000 cells/s), and hence this approach was extended to microfabricated flow cells generating parallel hydrodynamically focused streams. While such focused parallel streams are predicted to yield a 10-fold increase in throughput, complexity in the flow cell design is certain[6]. Hydrodynamic focusing in commercial flow cytometers is achieved using a nozzle-and-tubing arrangement, the sample flowing from the tubing completely ensheathed near the nozzle.

Sheathing produced by using nozzle and steel capillary[94] has been reproduced in microfabricated devices fabricated using polydimethylsiloxane (PDMS) mold sealed to a cover glass slide. The flow cell has a rectangular cross-section, 300 μm high and 110 μm wide. Sheath flow from three inlets positioned the particles tightly (5-10 μm width) and also precisely in two dimensions in the flow channel. The focused stream was interrogated using a 12 μm laser beam spot. Using conventional flow cytometry detectors, the flow cell provided particle event rates up to 17000 cells/s. Despite yielding linear velocities of 8 m/s, throughput limits its use for high volume applications[95]. Such precise focusing have also been demonstrated by designing flow channels with grooves and chevrons, and by using relatively fewer inlets for the sheath fluid[96]. A T-shaped flow cell of rectangular cross-section was fabricated using both soft lithography and laser ablation. In this flow cell, the sheath fluid and the sample were flown from opposite ends. Initially, the sheath fluid and the sample flowed side by side. On entering the grooved region, the sheath fluid was transferred over and under the sample, thus separating it from the walls, and focusing it into the center of the channel. Increasing the sheath-to-sample flow rates caused stretching of the sample stream. Another flow cell

was fabricated consisting of pairs of chevrons at the top and bottom of the channel, instead of the grooves. In this flow cell, the sheath fluid flowed from the two side inlets and the sample flowed from the center. In the region of the chevrons, the sample stream was compressed vertically and isolated from the top and bottm of the channel by the sheath fluid[96]. Although using these structure-influenced sheathing reduces the complexity of design considerably, they still limit throughput.

Although the above mentioned approaches have provided higher analysis rates than conventional flow cytometers, they are still low and can achieve higher throughput. Hence, research in recent years has focused on positioning particles without using the sheath fluid. These involve manipulating particles in flow depending upon the magnitude of the inertial lift forces acting on them. Any sample flow is characterized by two dimensionless numbers, namely the channel and the particle Reynolds number. When the particle Reynolds number approaches unity, the inertial forces dominate particle behavior, and focus particles into equilibrium positions, where the components of the lift force, namely the wall and the shear lift force balance each other[97]. While the number of equilibrium positions depends on the geometry and dimensions of the channel, in two-dimensional channels, they may vary from one to four depending on the channel aspect ratio, and hence allows focusing particles into more than one stream in a single channel[11]. Such effects are observed in curved channels also where secondary forces called the Dean drag forces act on the particles, besides the primary inertial lift force. At the curves, mismatch of inertia between the fluid elements at the channel center and the channels walls at the curved causes recirculation of the fluid, and equilibrium positioning

of particles occur where the inertial lift force and the Dean drag force balance each other[11]. These flow manipulated particle positioning have allowed encapsulating beads and cells in picoliter droplets[15] and separating particles based on density and size differences[98]. Furthermore, they have been successfully used to focus particles and cells into 256 parallel channels at mL/min flow rates[9], and improve throughput for high volume cellular analyses. While this technique uses neither the sheath fluid nor an external field to focus particles, the lift force depends on the dimensions of both the particle as well as the channel, and hence limits the range of particle dimensions.

While using alternate focusing mechanisms improve sample throughput, using scanning optics and advanced imaging systems enhance analysis rates. Toward this aim, attempts have been made to image focused particle streams in a microfabricated flow cell. Sample injected from well plates flows into 384 parallel channels which are imaged using laser optics scanning at rates as high as 12 MHz across a 80 mm field of view and relaying fluorescence signals to four photomultiplier tubes. Such scanning systems have been demonstrated to be useful for high throughput screening and rare event detection[72] [71]. In high throughput screening, these high scanning rates have provided better signal-to-noise ratio and have also enabled sorting the screened population[71]. Furthermore, attempts have been made to improve throughput by integrating microfabricated imaging lenses to fluidic channels. Towards this aim, a 4x4 array of microfabricated diffractive lenses was used to image particles flowing in 16 parallel channels such that each lens obtains an image of particle stream in one channel and relays those images in real time to a complementary metal oxide semiconductor (CMOS) camera. However, throughput was

limited to 2000 cells/s, which is several orders of magnitude lower than that required for rare event detection[73]. Besides scanning, advanced imaging systems that are capable of processing images at rates of 6 million frames/s have been developed. These systems include components for obtaining images of fast flowing particles, amplifying them and also read out data in real time with low noise and high sensitivity[99]. More recently, integration of these high speed image analyzers have produced analysis rates approaching a million/s[17]. While these advanced imaging techniques can provide analysis rates few orders of magnitude higher than conventional techniques, they also increase the cost of commercial flow cytometers.

Here we present a microfabricated flow cell that uses the multinode acoustic principle to focus particles and cells into several highly parallel focused streams. Previously, we have demonstrated this technique using flow cells fabricated by micromachining, rectangular glass capillaries and microfabrication approaches[100] [101]. Among these, the microfabrication approach allowed easy parallelization while focusing particles at flow rates up to 1.5mL/min. In this work, we have used this approach to fabricate a highly parallel multinode acoustic flow cell, consisting of 100 parallel channels for handling high volume cell samples. In this flow cell, we focused polystyrene particles into as many as 300 parallel focused streams at flow rates up to 25mL/min. Here we present results of our image analysis that confirm tight focusing within individual streams even at such high flow rates. Furthermore, we have used this flow cell to focus biological samples ranging in size from a few microns to tens of microns, such as red blood cells and spheroids, at flow rates upto 10mL/min.

7.2. Theory and Background

In the multinode acoustic flow cell described here, particle focusing into the streams is controlled by the acoustic radiation force on the particle. The effect of acoustic force on particles was first noticed during the famous Kundt's tube experiment where the dust particles in a resonating tube concentrated into specific regions of the standing wave. King related such displacement of particles to second order effects and derived an expression for the radiation force on a particle in an ideal fluid[23]. Later, Gorkov included the effects of viscosity of the medium, and arrived at the following expression (Eqns. 7.1a, 7.1b) for a spherical particle[24].

$$F_{ac} = -\frac{4\pi}{3} r^3 k E_{ac} A \sin(2kx) \qquad (7.1a)$$

$$A = \frac{5\rho_p - 2\rho_m}{2\rho_p + \rho_m} - \frac{\beta_p}{\beta_m} \qquad (7.1b)$$

Equations 7.1a and 7.1b show that the acoustic radiation force (F_{ac}) depends on the dimension (r) of the particle, acoustic energy density (E_{ac}), the position of the particle (x) in the standing wave and the acoustic contrast factor (A). The sign of the acoustic contrast factor, which is a function of density (ρ) and compressibility (β) of the particle (subscript p) and the surrounding medium (subscript m), determines particle migration in the standing wave field (Fig. 7.1a); particles that have positive value of the contrast factor migrate into the node (pressure minimum), while those that have a negative value of the contrast factor migrate into the antinode (pressure maximum)[25] [102]. Usually,

standing waves are created in channels of width equal to half-wavelength for the resonance frequency[50].

Migration of polystyrene particles in the standing wave field was first observed in a cylindrical glass tube excited at the third harmonic resonance frequency when the particles collected into the nodes[26]. Such ultrasound activated concentration was observed even with red blood cells, bacteria and yeast[27], which allowed separating analytical scale two-phase mixtures of bacteria and yeast[28], culturing and harvesting hybridoma cells and microorganisms from suspensions[30] [27], besides increasing sensitivity in latex agglutination assays for detecting bacterial meningitis[31]. Furthermore, concentration of a mixture of positive and negative contrast factors has been demonstrated using a mixture of red blood cells and lipids from shed mediastinal blood for cardiac surgery procedures in a rectangular channel half-wavelength wide[37] [38] [39]. While the rigid blood cells moved to the nodes and the relatively less-dense lipids collected into the antinodes, the lipids formed aggregates at the walls[37] thus limiting efficiency. However, such clustering at the walls was overcome by focusing lipids in channels operated at high harmonic resonance frequencies[52]. Besides concentrating particles in flow, they can also be exchanged between two media in laminar flow through rectangular channels. This principle has been used to move red blood cells from contaminated to clean plasma[42].

The ability of high frequency ultrasound (hundreds of kHz) to focus particles for flow cytometry was first demonstrated using a cylindrical glass capillary of diameter equal to

half-wavelength for the resonance frequency of the transducer, glued to the wall of the capillary. Due to radial concentration of acoustic energy, the particles focused into the geometric center of the cylindrical capillary[14] [35]. Integration of this flow cell into custom flow cytometry instrumentation allowed measuring of fluorescence and scatter signals with precision comparable to that of commercial flow cytometers using hydrodynamic focusing[14] [36].

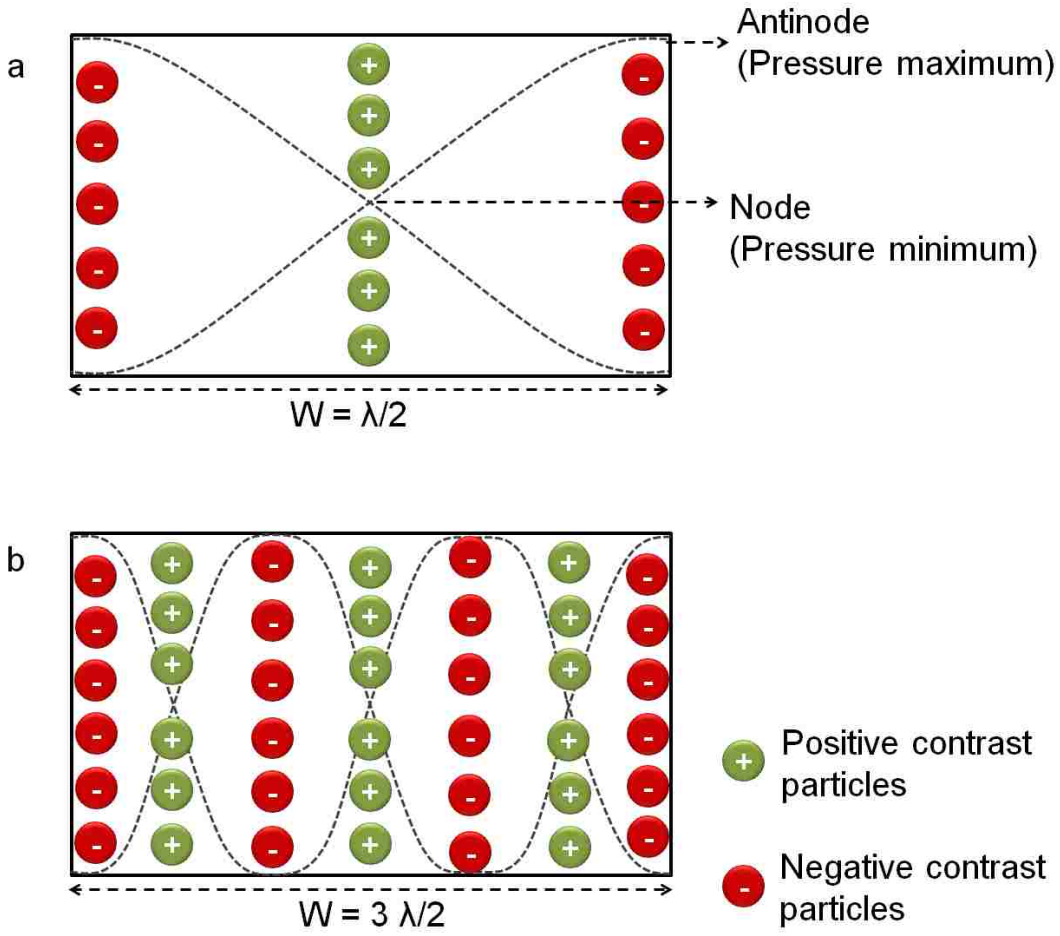

Fig. 7.1 (a) Principle of acoustic focusing: Positive contrast factor particles migrate to the single node at the center and negative contrast factor particles migrate to the two antinodes of the standing wave at the walls in a channel that is half-wavelength wide (b) Principle of multinode acoustic focusing: 3 nodes and 4 antinodes in a channel whose width is a third integer multiple of half-wavelength when the channel in (a) is driven at the third harmonic resonance frequency

The work with cylindrical capillary flow cells discussed above used fundamental resonance frequency to focus particles using acoustic radiation force into a single narrow stream. While providing accuracy and precision comparable to hydrodynamic focusing, it suffers from low throughput. To increase throughput, we have used the multinode acoustic principle that uses higher harmonics of the fundamental resonance frequency to focus particles and cells into highly parallel focused streams. The general relationship between velocity of sound through a medium (c), standing wave frequency (f) and wavelength (λ) is

$$c = f\lambda \qquad (7.2)$$

For multinode acoustic flow cells, the width of the flow channel (W) is an integer multiple (n) of half-wavelength, given by

$$W = \frac{n\lambda}{2} \qquad (7.3)$$

Hence, the number of nodes across channel of width is

$$n = \frac{2Wf}{c} \qquad (7.4)$$

Due to the harmonic relationship between the number of nodes and the flow channel width, the number of focused streams can be increased simply by driving the flow channel at higher harmonics of the fundamental resonance frequency[100]. Fig.7.1b

shows 3 nodes and 4 antinodes created when the flow channel is excited at the third harmonic of the resonance frequency.

Using this principle, we have previously demonstrated particle focusing in single wide channels into multiple focused streams using different fabrication approaches[100] [101]. Although they generated highly parallel focused streams, throughput had to be maintained low to optimize acoustic energy and keep the particles focused into nodes across the wide channel. However, diverting sample flow into multiple channels and focusing particles into fewer focused streams in each channel helped in overcoming issues with throughput, besides providing several focused streams. Using standard lithography and deep reactive ion etching techniques, we fabricated a flow cell consisting of 13 parallel channels where the width of each channel corresponded to the third harmonic resonance frequency. Besides generating 39 focused streams, this flow cell permitted flow rates upto 1.5mL/min[101]. Hence, we have pursued parallelizing flow channels resonating at third harmonic for the flow cell used in this work. However, to further enhance throughput to allow high volumes of samples, we have increased parallelization to include 100 channels such that this flow cell generates 300 focused particle streams at the resonance frequency of the transducer. In this work, we have demonstrated focusing particles at flow rates upto 25mL/min with appreciable particle focusing within individual streams confirmed by image analysis of focused particle streams in a few channels across the device. Furthermore, we have demonstrated focusing stained human whole blood and tumor microspheroids at 10mL/min in this flow cell. High sample throughput, tight particle focusing within individual streams in channels and

appreciable z-plane focusing make this multinode acoustic flow cell suitable for positioning cells in high volume samples such as those required for detecting circulating tumor cells.

7.3. Methods and Materials

7.3.1. Design of the flow cell

Parallelization of the flow channels is one of the ways to improve throughput for flow cytometry as well as for other cellular diagnostics. In order to allow very high sample throughput and to generate multiple focused particle streams, we have designed a flow cell that has a single inlet and outlet. However, the inlet splits the sample flow into 100 parallel channels. Each channel is 500μm wide, which approximately corresponds to the third-harmonic resonance frequency of 4.492MHz, meaning the particles will be focused into 3 parallel streams in each channel. As there are 100 channels, this flow cell can generate 300 parallel focused streams of particles at the resonance frequency.

7.3.2. Fabrication of the multinode acoustic flow cell

A number of techniques exist for microfabricating flow cells for acoustic focusing which include using both cylindrical and rectangular glass capillaries, wet etching in glass as well as silicon, micromachining approaches and deep reactive ion etching techniques. Previously we have demonstrated multinode acoustic focusing using micromachined flow cell[100], rectangular glass capillaries and deep reactive ion etching (DRIE) techniques[101]. Among these approaches, flow cells fabricated using DRIE have provided high flow rates and have also enabled parallelization of the multinode acoustic

technique. The steps involved in fabrication of these flow cells have been discussed in detail elsewhere[101], and include printing the flow cell design on silicon wafer by photolithography followed by etching the wafer by deep reactive ion etching. They have been summarized here for the convenience of the reader.

The flow cell design for printing on a photomask is first drawn in AutoCAD (Autodesk Inc., San Rafael, CA). This design is printed on a high resolution transparency (approximately 10,000 dpi) through a commercial vendor (CAD/Art Services Inc., Bandon, OR). The photomask is now ready for photolithography procedures. The first step in photolithography involves coating a layer of HMDS on the silicon wafer (WaferNet Inc., San Jose, CA, test grade, N or P type, 100mm diameter, any crystal orientation). Next, a uniform layer of positive photoresist (AZ 9260, Microchemicals GmbH, Germany) is coated onto the wafer using a spin coater (Cee® 200X, Brewer Science). Following this step, the coated wafer is heated at 120^0C on a hot-plate for 5 minutes and then allowed to cool at room temperature for nearly 20 minutes. The cooled wafer is aligned with the photomask in a mask aligner (Karl Suss MA6, SUSS MicroTec AG, Germany) . By exposing the wafer to high energy ultraviolet (UV) radiation, the design of the photomask is printed onto the wafer. After the exposure step, the wafer is developed using a suitable developer (AZ 400K, Microchemicals GmbH, Germany), diluted 4x using distilled water, for atleast 30 min. The development time depends on the surface area of the exposed region. As this design covers a 4” wafer, a longer development time is necessary. The exposure of the photoresist to high energy UV rays modifies its physical properties and hence causes the exposed photoresist to be removed during the development step. The developed wafer is then washed using water followed

by a short cycle of reactive ion etching to remove any developer residue. The next step involves etching the developed wafer in a deep reactive ion etcher (Alcatel AMS 100, Alcatel Micro Machining Systems, Annecy, France). The etching time depends on the etching depth. As we have observed uniform parabolic profile previously in channels etched to 100μm, we have retained those dimensions, which requires approximately 40 minutes for the etching cycle. The photoresist remaining after etching is lifted off the wafer during a short cycle of reactive ion etching followed by washing with acetone. The etched wafer is then washed using the Piranha etch step that uses a mixture of 30% hydrogen peroxide and 70% concentrated sulfuric acid. As this mixture is highly acidic, proper care is taken to perform Piranha etching following strict protocols that include wearing additional personnel protective equipments such as face shield and thick nitrile or latex gloves (in addition to lab coat, general laboratory gloves and safety glasses) and using a hood to avoid any injury to the experimenter. The next step involves bonding Pyrex® glass slide (Borofloat 33, Schott North America, Inc., Elmsford, NY) to the etched silicon wafer by using anodic bonding procedures. Before anodic bonding, small holes are drilled on the glass slide corresponding to the inlet and outlet of the flow cell using a hand drill (Dremel Rotary 300 series, Dremel). Once drilled, the glass slides are also cleaned using the Piranha etch step. Usually, both the etched wafer and the drilled glass slide are left for about 20 minutes in the bath containing the Piranha mixture. During the anodic bonding step, the wafer and glass slide are first aligned to match the inlet and outlet, and placed between two metal plates. These plates are carefully placed over a hot plate (at 60^0C or lower) and heated gradually to 400^0C. Once the steady high temperature is established, the current supply is turned on and the voltage is increased in

steps to about 1.2kV. At this high voltage and high temperature, the assembly is left undisturbed and the reaction is allowed to take place for atleast 90 min (longer reaction time is necessary when the voltage is less than 1kV). On completion of the reaction, the current supply is turned off, the temperature is lowered to nearly 60^0C and the metal plate assembly is carefully removed from the hot plate. The glass and silicon wafer are now bonded, and the inlet and outlet are fitted with flexible silicone tubing. The last step involves gluing a suitable piezo-electric transducer, such as lead zirconate titanate (PZT) crystal (5mm wide, 30mm long, APC International, Mackeyville, PA) underneath the silicon wafer and placed centrally, using commercially available super glue. As the flow channel dimensions correspond to the third-harmonic resonance frequency at 4.492MHz, we have used a PZT crystal that has a resonance frequency of 4.48MHz. Fig. 7.2 shows the top and side views of the finished microfabricated 100-channel flow cell.

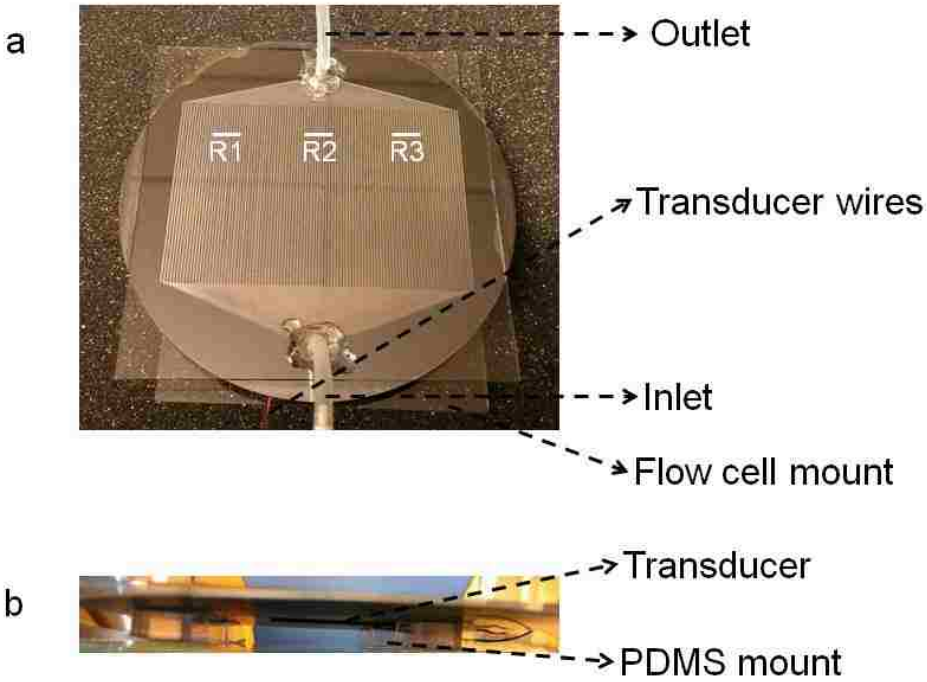

Fig. 7.2 Microfabricated 100-channel multinode acoustic flow cell (a) Top view showing the finished device mounted on a square glass slide and its 3 analysis regions (R1, R2 and R3) (b) Side view showing the transducer glued beneath the silicon wafer at its geometric center

7.3.3. Sample preparation

7.3.3.1 Polystyrene particles

For proof-of-concept demonstration of massive parallelization of the multinode acoustic focusing technique, we have used Nile Red labeled 10.2μm polystyrene particles (Spherotech Inc., Lake Forest, IL). 100μL of the sample stock was pipetted into 25mL of distilled Millipure water in a centrifuge tube. The sample suspension was mixed by shaking. For sample concentration measurements using Coulter counter, about 1μL of this suspension was diluted 10000x in distilled phosphate buffered saline (PBS).

7.3.3.2. Human whole blood

To demonstrate the ability of the multinode acoustic technique in focusing real world samples into massively parallel focused streams, we have used commercially available human whole blood sample and stained it using the lipophilic dye Nile Red. The dye, purchased from a commercial source and available at a concentration of 14mM, is diluted 14x to a final concentration of 1mM by suspending in phosphate buffered saline (PBS). 20μL of the diluted solution of Nile Red was added to 100μL of the human whole blood sample in a centrifuge tube and diluted to about 2mL using PBS. This suspension was mixed and shaken in a vortex rotator for atleast 4 hours. The sample was centrifuged and washed thrice (3x) after rotation to remove free dye in suspension. The final sample for multinode acoustic focusing experiments was prepared by suspending few hundred microliters of the washed and stained sample suspension in about 20μL's of PBS. Despite being free of pathogens, care was taken to follow the standard bio-safety protocols while staining and handling the blood sample.

7.3.3.3. Spheroids

To further evaluate the focusing of large samples, a sample of tumor microspheroids was cultured using standard protocols[103]. To initiate spheroid formation, exponentially growing cells of M1 cell line (1 x 10^6/mL) were inoculated into 100 mm dishes containing 15 mL of the complete medium on top of an underlayer of 0.5% agarose (Sigma-Aldrich). After about 96 hours, these spheroids were separated by decantation and pelleted by centrifugation (100 g, 5 min). The pelleted population was resuspended in phosphate buffered saline (PBS) (Life Technologies, Inc., Grand Island, NY) containing low concentration of green fluorescent protein (GFP) (EMD Millipore, Bedford, MA). From these spheroids, several aliquots were prepared and each aliquot was diluted further with PBS. To determine the size of these spheroids, images were recorded through a microscope interfaced with personal computer (Windows). The mean diameter of each spheroid in an aliquot was computed, and these measurements were calibrated against images of spheroids of known diameter. An aliquot of the spheroid suspension was pelleted, resuspended in the trypsin (Sigma-Aldrich) solution used earlier for monolayer cell culture and incubated at 37^0C for 10 minutes. After treating with trypsin, cell suspensions of spheroids were handled as above for suspensions of monolayer cells. The mean number of cells per spheroid was determined by measuring the number of cells recovered from known number of spheroids in the aliquot. Large spheroids were obtained by spin culturing cell aggregates. After culturing in agarose dishes, spheroids were separated based on size by sedimentation and transferred to 500 mL of complete medium in spinner flask (Belco) equilibrated with approximately 500 mL of 5% carbon dioxide in 95% air and spun at 200 rpm in a water bath maintained at 37^0C. The medium and gas

mixture were replaced frequently and aliquots of spheroids were removed regularly to maintain cell concentrations below 10^8/mL. The cultured microspheroids were suspended in PBS and their mean size distribution was counted using Coulter counter, and was found to be 65μm.

7.3.4. Experiment

The sample suspension of 10.2μm polystyrene particles were drawn using syringe pump and flowed through the massively parallel multinode acoustic flow cell. As our previous parallel microfabricated flow cell focused particles over 1mL/min[101], here we fixed our initial flow rate at 1mL/min. The sample flow rate was gradually increased in steps upto 25mL/min. At each flow rate, the images of the focused particle streams were recorded using an epifluorescence microscope (Zeiss Axio Imager) coupled with an electron multiplication-charge coupled device (EMCCD) camera (Luca S, Andor-Solis, Andor Technology, Belfast, N. Ireland). Later, we measured the intensity of the focused particle streams by following the procedure described below.

For image analysis, specific channels distributed over three different regions of the flow cell, one at the center above the transducer (R2) and two regions to the left (R1) and right (R3) of the transducer were chosen. For each flow rate, two images of the focused streams were recorded. In each image, three analysis points (AP1, AP2 and AP3), one each on the left, center and right of the image, were selected and intensity profiles of the focused particle streams were plotted using the EMCCD camera-supported image analysis software (Andor-Solis, Andor Technology, Belfast, N. Ireland). The raw data

from each intensity plot was imported and plotted in a spreadsheet in Microsoft Excel. In each intensity plot, the background was subtracted and the peak width at half maximum was measured. The procedure was repeated for each image obtained across the three regions of the flow cell and the mean value of peak-width at half-maximum was determined. The analysis procedures were repeated for each flow rate, and the mean values of intensity for each region were plotted against flow rate. Finally, for unit conversion from pixels to microns, known distances (in μm) between two points, for example the pixel distance between the channel walls (i.e. 500μm), were measured using ImageJ, the average of those values was obtained and the mean values of the peak widths at half maximum were divided by the corresponding conversion factor.

To determine focusing efficiencies with human samples and for different sample sizes, we have used stained whole blood sample and spheroids. Like the polystyrene particles, these were injected using a syringe pump. However, care was taken while handling the human whole blood sample to disinfect the experimental area using both 70% ethanol and bleach and also to avoid any spill. Initially the blood sample was flown at hundreds of μL/min and the sample flow rate was gradually increased in steps up to 10mL/min. Assuming large acoustic radiation forces owing to their size, we injected the sample of tumor microspheroids only at 10 mL/min.

7.4. Results

In multinode acoustic flow cells, the width of the flow cell is a multiple of half-wavelength, and hence the number of nodes depends on the multiple of half-wavelength.

We have previously fabricated a flow cell having 13 parallel flow channels, with each channel generating 3 tightly focused streams across 500μm wide channels, when excited using a single PZT glued beneath the etched silicon wafer having a natural resonance frequency equal to that of the third harmonic of the channel[101]. Here, we have retained those dimensions, both width and length, although resonance depends only on the width of the flow channel. However, we have increased the number of channels to 100, without increasing the dimensions, geometry or the number of transducers driving the flow cell. Thus, every channel in the flow cell is actuated using the single PZT. Hence, the positive-contrast particles and cells will be focused into 3 nodal streams in individual channels. With simultaneous excitation of 100 channels, the flow cell altogether generates 300 focused particle streams.

Upon turning on the acoustic field, the randomly dispersed polystyrene particles having a positive value of the contrast factor approached the nearest nodal position in the channel and remained focused into individual nodal streams until exiting the flow channel.. Increasing sample flow rates improved the particle arrival rate but did not have any effect on the efficiency of focusing. Fig.7.3 shows three focused streams in one of the flow channels at 5, 15 and 25 mL/min. Depending upon the flow rate, a drive voltage of 25-35 V_{pp} was required to focus the polystyrene particles. In addition to tight focusing within individual streams, these images indicate appreciable particle focusing in the z-plane, as continuous and bright fluorescent streaks are observed from each focused stream.

Fig.7.3 10.2µm Nile Red polystyrene particles focused into 3 nodes in one of the channels in the microfabricated 100-channel flow cell at 5,15 and 25 mL/min flow rates

In order to confirm our visual interpretation that the particles are focused tightly into the individual streams, we performed an image analysis of the focused streams at flow rates above 5mL/min. The rationale is that if the particles are tightly focused as expected into the individual streams, the intensity peaks will be narrow, and hence the peak-width-at-half-maximum should be low and relatively uniform for each stream at each flow rate and for every image at a particular flow rate. For analysis, we recorded images in uncompressed TIFF format (Fig. 7.4a) such that they were compatible with the camera-supported software and retain as much information of the images as possible. Fig. 7.4b shows the intensity plot of the focused streams at 10mL/min at 3 different analysis points (AP 1, 2 and 3) on the image. As seen in these images, the intensity peaks are narrow and centered about the same value on the x-axis for each stream (Fig. 7.4b). While a high background is observed in these plots, they do not affect significantly the peak intensity values of the individual streams. At higher flow rates of 15 (Fig. 7.4c) and 25 mL/min (Fig. 7.4d) also, the peak intensities and their position remain consistent. This shows that the acoustic energies are sufficient to focus particles tightly into the individual streams even at such high flow rates. Besides these, a decrease in background is observed with increasing flow rate for the same value of the image exposure time, with a corresponding

decrease in signal intensity. The average value of the pixel-micron conversion factor is 0.553 pixels/μm. Fig. 7.4e shows the plot of the average values of the peak widths of the individual streams, along with the standard deviation marked by error bars, for each region of the flow cell. For almost all flow rates, the peak width at half maximum values were less than 10μm, equal to the size of a polystyrene particle, with standard deviation values of few microns for the 3 regions of the flow cell. Calibration experiments performed by recording nine images of a stationary 10.2μm polystyrene bead at various locations in the field of view using a 10x objective produced a mean value of peak width at half maximum of approximately 5 μm, which closely matches with the value indicated by the graph. This shows that the particles are well focused into the individual streams at all flow rates. Hence, these results show that this microfabricated flow cell is efficient in focusing cells at high volumetric flow rates.

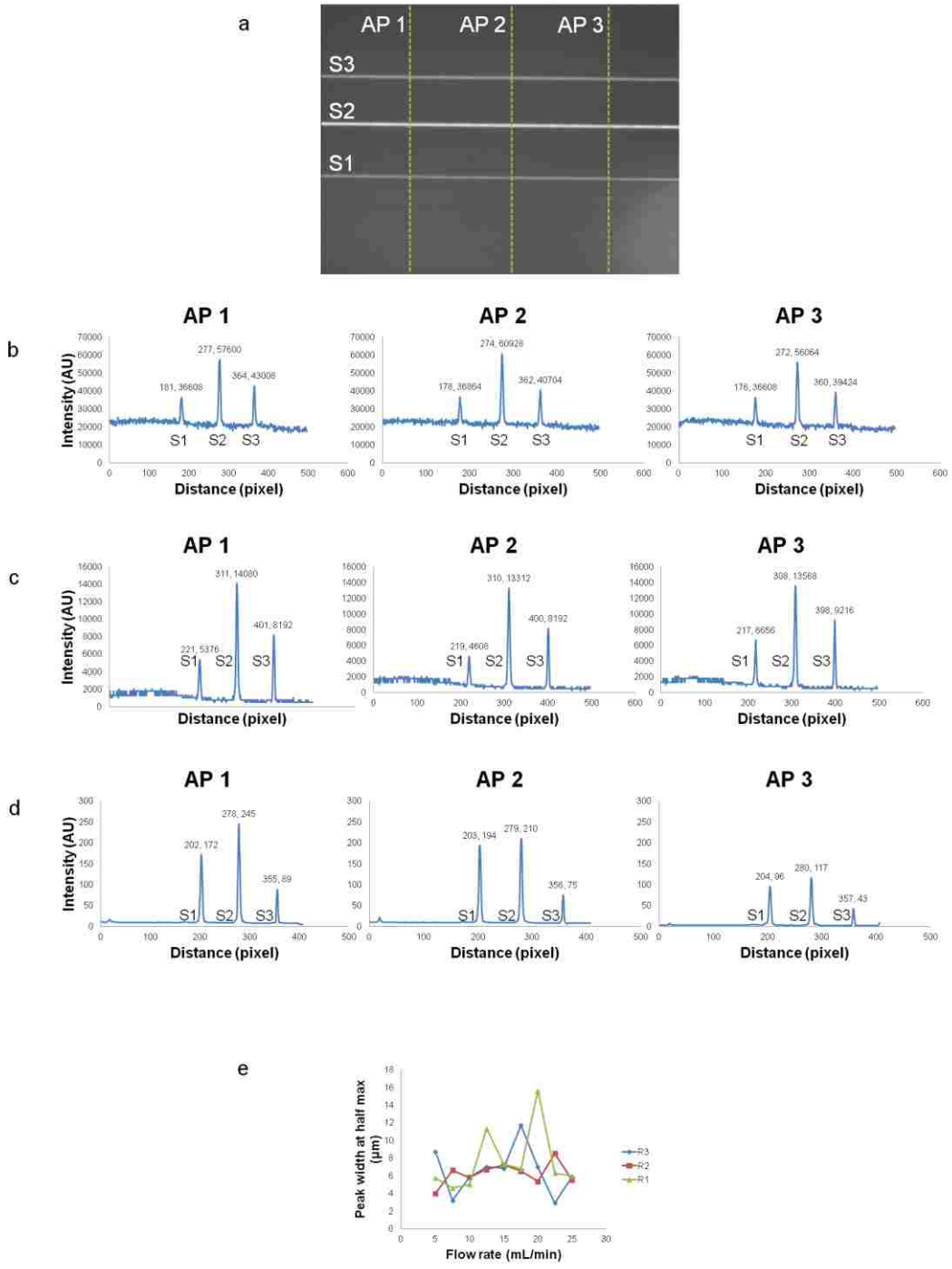

Fig. 7.4 Image analysis of focused particle streams (a) Snapshot of focused particle streams (S1, S2, S3) in a channel at 10mL/min showing the three analysis points (AP1, AP2, AP3) marked by green dotted lines. (b) Intensity plot of focused particle streams for the image in (a). (c),(d) Same as in (b) but for (c) 15mL/min and (d) 25mL/min. (e) Variation of peak width at half maximum for the three regions of the flow cell (R1, R2, R3) with flow rate

The particles (FP-10056-2, Spherotech Inc) used here are perfectly spherical and have a mean diameter of about 10 μm. As the acoustic radiation force on a particle scales with the volume of the particle, these particles in general experience high acoustic radiation force at all drive voltages. On the other hand, many cells are smaller and typically have an irregular shape. Therefore, for a particular frequency and drive voltage, the focusing efficiency of cells may be lower than polystyrene particles due to the lower acoustic radiation force on cells. . To evaluate the efficiency of focusing with biological samples, we have used stained human whole blood samples. While flowing the sample at 10mL/min, the red blood cells that were randomly distributed across the flow channel without acoustic excitation collected into the nodes within the individual flow channels, when driven at the resonance frequency of 4.492 MHz and a drive voltage of $46V_{pp}$ (Fig. 7.5).

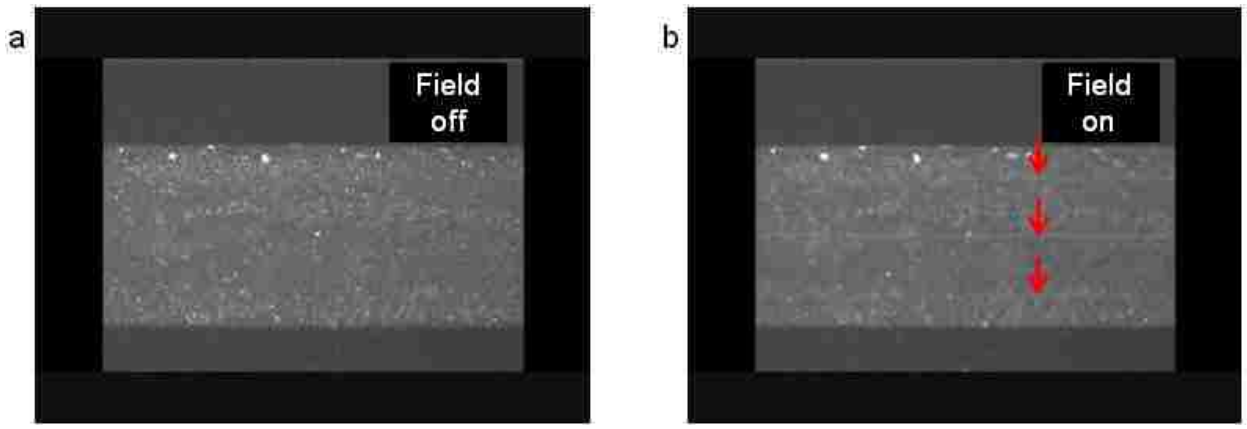

Fig. 7.5 Human whole blood stained with Nile Red (a) Randomly dispersed blood cells (b) focused into the 3 nodes (marked by red arrows) in one of the channels in the flow cell while flowing at 10mL/min when the acoustic field is turned on

Flow cytometry may also be used for analysis of large particles such as C. elegans and Drosophila embryos, multicellular structures such as islets cells of the pancreas and one-bead-one complex studies[1]. In commercial flow cytometers using the hydrodynamic focusing mechanism, particles of size few hundred microns in diameter clog the flow cells. Such issues were overcome by analyzing these particles in flow without focusing them in large flow cells[10]. Therefore, research efforts in recent years have focused on developing a true flow cytometer that can focus such large particles to enable precise optical measurements just like traditional flow cytometry. To demonstrate the ability of the multinode acoustic technique to focus such large particles, we have used spheroids, which usually range in size from tens of microns to few hundred microns in diameter. Here we have used spheroids having a mean diameter of 65μm that express green fluorescent protein (GFP) in culture. In comparison to the polystyrene particles and blood cells used previously, these spheroids experience greater acoustic radiation force due to their larger size. Fig.7.6 shows spheroids positioned into the nodes in one of the channels at 4.492 MHz and $35V_{pp}$ drive voltage. The lower sample concentration prevented arrival of spheroids simultaneously in all the 3 nodal positions in the channel. However, the series of images (Fig. 6) recorded at different time frames indicate tight focusing of these spheroids in the individual streams.

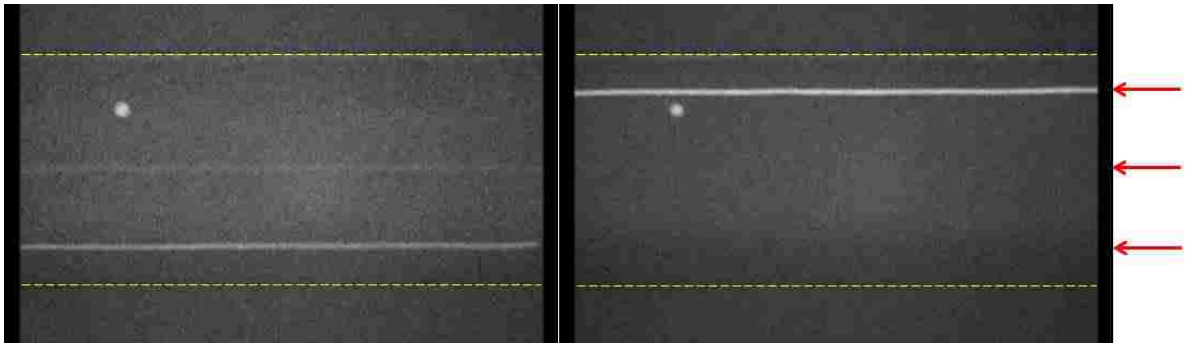

Fig. 7.6 Green fluorescent protein (GFP) expressing tumor microspheroids of mean diameter 65μm flowing at 10mL/min focus into 3 nodes (marked by red arrows) at two different time frames in one of the channels. The low sample concentration decreased the frequency of spheroid arriva l so that simultaneous detection of a spheroid in all 3 channels was rare.

7.5. Discussion

For decades, flow cytometry has been using the traditional hydrodynamic focusing technique that precisely positions particles and cells into the central plane of a sheathing fluid. Despite providing precise focusing, this approach suffers from low throughput, requiring longer analysis times for precisely measuring optical properties while handling large sample volumes. As sheath fluid is the limiting factor, only a suitable sheathless, alternate focusing technique will help in addressing issues with throughput. Although the main task of such an alternate mechanism is to increase throughput, it should retain the advantages of the hydrodynamic technique such as positioning the particles into a single plane, otherwise provided by sheathing. While several flow as well as field manipulation techniques exist, they have their own limitations. Hence, this paper presents an alternate focusing mechanism, which we call the multinode acoustic technique that permits parallelization of the fluidic channels as well as the focused streams, and hence allows handling of large sample volumes. We have previously designed and built microfabricated flow cells that are capable of generating multiple focused streams in a single wide channel as well as those that have several parallel channels with a smaller

number of focused streams within each channel. Among these two approaches, the latter has worked better, allowing particle focusing at lower magnitude of mL/min flow rate,due to relatively higher acoustic energy density within each flow channel. Hence, using the same fabrication approach, we have increased parallelization to focus particles and cells into hundreds of well-ordered streams.

While parallelization of the flow channels is common, not all focusing mechanisms support parallelization of the flow focused streams. In acoustic focusing in half-wavelength channels, the node is created at the center and two antinodes at the walls. The multinode acoustic technique focuses particles and cells in channels that are a multiple of half-wavelength, and hence multiple focused streams are generated within each channel. Each channel in the flow cell used in this work corresponds to the third multiple of one half-wavelength for 4.492MHz, and hence 3 nodal streams are established within each channel. All the samples used in this work have a positive value of the acoustic contrast factor and hence focus into the nodes. In addition to greater parallelization of the focused streams, this approach may also help in overcoming issues with inter-particle interaction due to their inherent physical properties due to relatively lower concentration of particles within each focused stream.

Using commercially available polystyrene particles, we have demonstrated particle focusing at flow rates up to 25 mL/min. For the channel dimensions (500 μm wide, 100 μm deep) used in this microfabricated flow cell, such high flow rates fall within the laminar range of fluid flow, with particle linear velocities approaching 8 cm/s in

individual focused streams at the highest flow rate. Such high linear velocities produce a significant lift on the particles, and focus the particles into a definite z-plane. Therefore, in the microfabricated flow cell, while acoustic radiation force alone regulates particle focusing in the transverse plane (channel width), an appreciable contribution of the particle lift force together with the acoustic force may contribute to the z-plane focusing of particles.

Image analyses of the focused particle streams justify the above claim. In Fig. 4b,c,d, we observe narrow peaks from each focused stream. In these plots, the peak height represents fluorescence intensity while the peak width represents the width of the focused particle stream. In flow cytometry, for accurately determining the optical parameters (forward and side scatter in addition to fluorescence) of every particle and cell in the focused stream, this width should be approximately equal to the dimensions of a single particle. Higher values represent either particle displacement away from the focused stream or particle coincidences at the interrogation point. Such discrepancies interfere with accuracy and precision of optical measurements and hence undesirable. Even though these images were recorded with a high exposure time setting, such particle displacements and coincidences would interfere with the peak width. The width of each peak in these plots is almost uniform, thus showing that there are no particle coincidences even at high flow rates. Here we observed a decrease in background with increasing flow rate. However, the fluorescence intensity also follows a similar trend. Such effects may be attributed to the mercury lamp source which do not produce a uniform intensity light unlike the laser sources used in flow cytometry. Besides the lamp source, we used a low

numerical aperture (NA 0.25) objective, to record these images, hence the photon collection efficiency is poor. Thus, poor illumination together with low NA objective may have reduced the actual intensity by a few orders of magnitude.

Although we used a transducer having a resonance frequency of 4.48 MHz, the flow channels do not resonate when driven at this frequency, despite matching dimensions to the third multiple of half-wavelength. Such discrepancies may be attributed to the effects of structural resonance. However, most transducers resonate and transmit sufficient energy at frequencies few hundreds of kHz from their resonance frequency, and hence despite using a 4.48 MHz transducer, the channels resonated with nearly-maximum energy at the third harmonic resonance frequency.

In addition to the polystyrene particles, we have demonstrated multinode acoustic focusing using stained whole blood as well as spheroids at flow rates as high as 10mL/min. Among these two biological samples, the spheroids, by virtue of their size, should have focused at lower drive voltages. However, we observed focusing only at $35V_{pp}$, compared to $46V_{pp}$ for the much smaller red blood cells for the same flow rate. Furthermore, the efficiency of focusing depends on the residence time of the particle in the acoustic field. Hence, for efficient focusing, a greater residence time is expected for the smaller sized red blood cells. In this case, as the flow rates are equal, their residence times are also equal. Such small differences in drive voltages may be due to the differences in interaction of ultrasound with individual cells and cell clusters.

While we have presented results upto 25mL/min flow rates, we observed focusing at flow rates as high as 60 mL/min (Fig. 7.7). However, such results were not reproducible in every channel in the flow cell, and disturbances in focusing were also observed occasionally. For particles to be positioned tightly into individual streams, there is a threshold value of the drag force. Beyond the threshold limit, such disturbances in focusing are certain. Hence future work with these flow cells will focus on increasing the acoustic energy in the flow channels which may include increasing the dimensions of the driving transducers or using driving frequencies approaching higher limits of the permissible range, without creating any energy-related streaming.

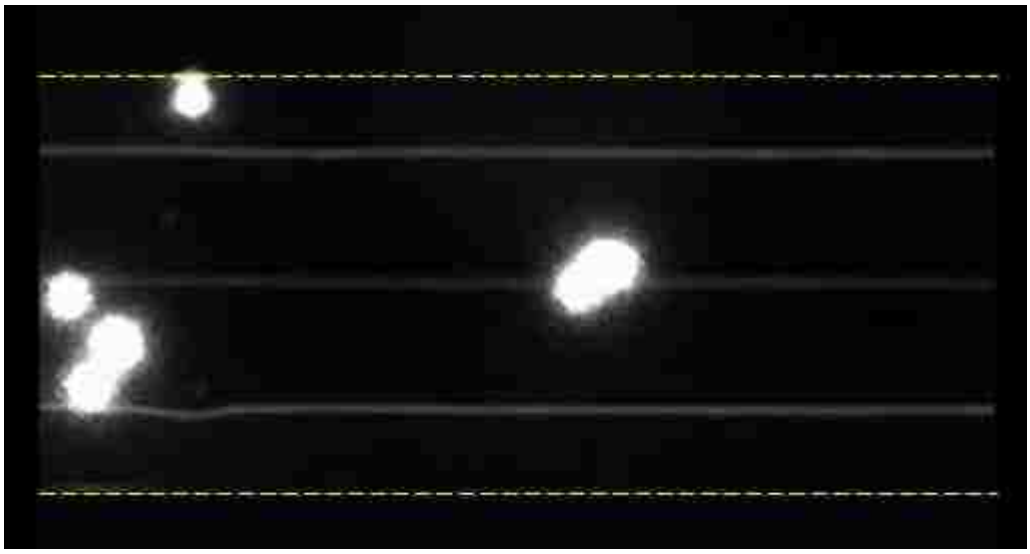

Fig. 7.7 10.2 μm Nile Red polystyrene particles focused into 3 streams in one channel in the microfabricated flow cell at 60 mL/min flow rate. Yellow dotted lines indicate the walls of the channel. Bright fluorescence is observed from polystyrene particles that settled at the bottom of the flow channel.

7.6. Conclusion

In this work, using a microfabricated flow cell having parallel fluidic channels, we have demonstrated focusing particles and cells in high volume samples into few hundreds of

focused streams at flow rates of few tens of mL/min. The appreciable particle focusing in both the x- and z-planes may be attributed to uniform parabolic flow in the flow channels. Besides uniform flow, high Reynolds number in channels provide high linear velocities, thus increasing cellular throughput by an order of magnitude and particle throughput by few orders compared to most commercial flow cytometers. Such high throughput positioning of cells is desired in flow cytometry for improving analysis rates while processing large sample volumes such as those used in rare event detection which include detecting circulating tumor cells and fetal cells in maternal cells. Thus, when integrated with suitable optics, detectors and real-time fast processors the 100-channel microfabricated multinode acoustic flow cell discussed in this work will provide high analysis rates for high throughput applications in flow cytometry.

Chapter 8

Acoustic technique for z-plane focusing

8.1. Introduction

In traditional flow cytometry, the sheath fluid used in hydrodynamic focusing technique precisely focuses particles as well as cells into the geometric center of the cylindrical tubing. Such precise focusing allows accurate determination of fluorescence and scatter properties from the focused cells, when excited using laser and interrogated using photon collection and detection optics. Furthermore, such two-dimensional positioning has allowed obtaining high resolution images of hydrodynamically focused particle streams[95]. However, the sheath fluid also accelerates the sample, which makes it necessary to use expensive optics and detectors in commercial flow cytometers. Efforts to obtain such precise positioning using alternate focusing mechanisms, namely inertial[9, 15-17], dielectrophoretic[4, 20] and acoustic[14, 36, 55] techniques have also demonstrated success.. Research in recent years focused on developing imaging flow cytometers that combine the strengths of traditional microscopy and flow cytometry has shown success in obtaining and analyzing high resolution images of individual particles with high precision. Although successful, these still use the conventional hydrodynamic focusing and hence suffer from limitations mentioned above. However, such image-based particle analyzers when integrated to high volume multinode acoustic flow cells can be used successfully even for rare event detection. This chapter proposes that two-dimensional focusing will be observed in multinode acoustic flow cells when the flow cell is driven using a transducer having driving frequency that creates a fundamental

harmonic standing wave (one node only) in the channel depth and an integer multiple of fundamental resonance (where the number of nodes equal that integer) across the channel width. A progressive methodology was adopted to demonstrate such precise two-dimensional focusing using multinode acoustic technique. First, the migration of particles into a single z-plane on acoustic actuation was demonstrated using a rectangular glass capillary driven at a frequency that corresponds to the fundamental resonance in the channel depth. Finally, two etched silicon devices, one each of type-1 and type-2 described in chapter 6, were used to demonstrate that particles can be positioned in two-dimensions by etching channels to one-half wavelength. . Besides improving throughput, such two-dimensional multinode acoustic flow cells will provide high precision and sensitivity similar to that of commercial flow cytometers when coupled to traditional optics and detectors.

8.2. Demonstration of acoustic focusing in the z-plane in rectangular capillaries

8.2.1. Methods

8.2.1.1. Proof-of-principle z-plane focusing in rectangular glass capillary

The proof-of-principle experiment to demonstrate precise z-plane focusing of particles using acoustic focusing technique was performed using a commercially available rectangular glass capillary. A glass capillary (Friedrich and Dimmock Inc, Millville, NJ), 8mm wide and 800μm deep, was fitted with flexible silicone tubing at both its ends to serve as fluidic inlet and outlet. A piezo transducer crystal (Boston Piezo-Optics Inc, Bellingham, MA), having resonance frequency of 871 kHz, was glued to one of the plane surfaces of the capillary, so that when it is excited acoustically, a standing wave is

generated in the depth of the flow cell, and the particles will be focused only into the capillary depth, while they will be dispersed across its width. The signal from the waveform generator (33250A, Agilent, Santa Clara, CA) was amplified using a radio-frequency amplifier (Empower RF Systems, Inglewood, CA). A sample of 10.2 μm Nile Red polystyrene particles (Spherotech Inc, Lake Forest, IL) of approximately 10^5/mL concentration was used. To confirm precise z-plane focusing in the glass capillary, the side view image of the focused stream was recorded using a video camera (JVC, Wayne, NJ), while the top view was recorded using an epifluorescence microscope (Axio Imager-2, Carl Zeiss, Inc) incorporating an EMCCD camera (Luca S, Andor Technology, Belfast, N.Ireland). Successful demonstration of focusing of particles to the mid-plane of the channel height will confirm the hypothesis that cells and particles can be precisely focused into a single z-plane using the acoustic focusing technique in rectangular channels.

8.2.1.2. Two-dimensional (2D) acoustic focusing by etching channels to half-wavelength dimensions

Particles can be precisely focused in rectangular channels in two ways. The first method is to use two piezo transducers, one each for focusing particles in each plane. The second method is to etch the rectangular channels to half-wavelength dimensions so that a single nodal plane is created at the geometric center of the depth of the channel (z-plane), similar to the glass capillary used in the previous sub-section, while the width is matched to either the fundamental or higher harmonics, depending upon the number of nodal

streams desired in the x-plane[104]. While using two transducers may successfully position particles in two dimensions, the resulting acoustic energy may be too high to be amenable to most cells. However, etching the channel to the fundamental harmonic (one-half wavelength) dimensions will definitely not have such harmful effects on cells as the particles will be positioned in both the channel width as well as its depth by a standing wave created using a single transducer.

In order to demonstrate two-dimensional acoustic focusing of particles, two designs used previously in Chapter 6, one each for type-1 (multinode flow cells having single wide channel) and type-2 (multinode flow cells having multiple parallel channels), were selected and those flow cells, namely the 2mm wide channel for type-1 and the massively parallel 100-channel for type-2, were fabricated by etching them to half-wavelength dimensions. For the resonance frequency of 4.48MHz, the corresponding etching depth is 167μm (Fig. 8.1). These devices were fabricated by photolithography and deep reactive ion etching techniques as described in section 6.1.2. However, the greater etching depth required longer etching time. A sample of 10.2μm Nile Red polystyrene particles (Spherotech Inc, Lake Forest, IL) was used to demonstrate two-dimensional acoustic focusing of particles in these devices.

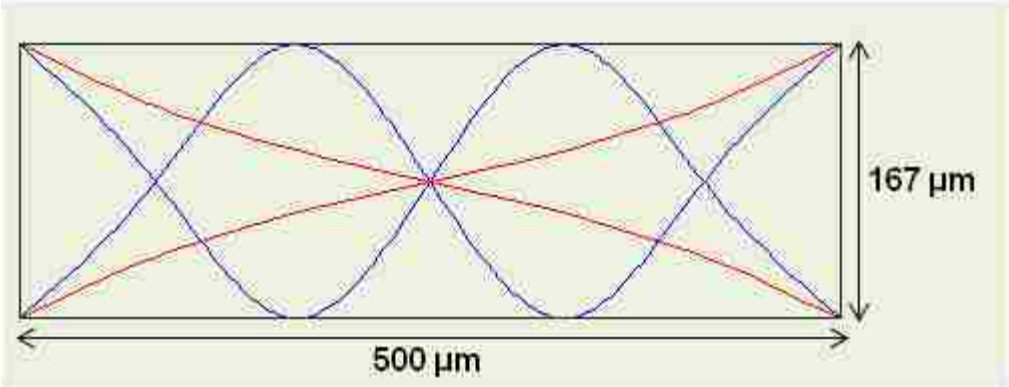

Fig. 8.1 Schematic representation of two-dimensional focusing by etching the 500µm wide channel to half-wavelength for 4.48 MHz

In the 2mm wide channel device, the focused streams across the channel width were imaged through a 4x objective lens fitted to the epifluorescence microscope (Axio Imager-2, Carl Zeiss, Inc) with the sample flowing at 500µL/min. However, to confirm precise focusing of particles into a single z-plane, images were recorded using a 10x objective limiting the field of view further to only 6 streams. Furthermore, the exposure time was suitably reduced to visualize individual particles in the focused stream. In the 100-channel device, images of the focused streams in individual channels were obtained using a 10x objective, and these images were analyzed visually to confirm precise two-dimensional focusing of particles in each channel in the device.

8.3. Results

In the proof-of-principle experiment with 800µm deep glass capillary, the driving frequency of the transducer was increased in steps to determine the optimum resonance frequency of the device for precise z-plane focusing of particles by imaging through the

side of the capillary. At 925 kHz, all the particles in the sample were focused precisely into the center, which is the z-plane for the glass capillary. VideoA4.1a in Appendix 1 better demonstrates this principle, i.e. the acoustically actuated migration of particles into the depth (z-plane) of the glass capillary. While imaging the focused stream via EMCCD camera in the epifluorescence microscope, the particles were found to be dispersed across the width of the capillary but in a single optical plane of focus. The single stream in the side view and single focal plane focusing in the top view confirm single z-plane acoustic focusing in the glass capillary (Fig. 8.2).

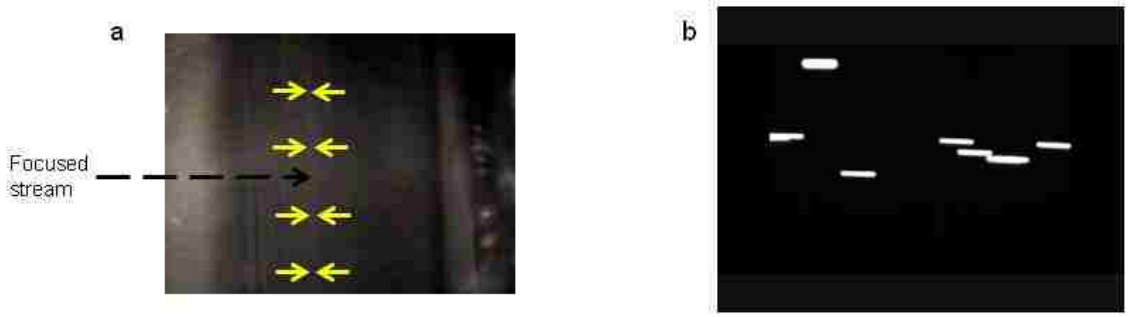

Fig. 8.2 (a) Side view of the glass capillary acoustic flow cell imaged using video camera shows 10.2 µm NR-PS particles focused to its center (marked by yellow arrows). (b) Top view imaged via epifluorescence microscope shows 10.2 µm NR-PS particles focused into a single z-plane

The 2 mm channel etched to half-wavelength dimensions generated 12 streams across the channel width at 4.485 MHz and at 500µL/min just like the type-1 device described in section 6.1.3.1. However, the z-plane focusing of particles was not quite satisfactory. Visual analysis of 6 streams through a 10x objective showed that the particles were focused into atleast two planes in the z-direction. To determine any change in resonance frequency due to deeper etching, the driving frequency was varied manually between 4.46 and 4.5 MHz. Such manual tuning had no effect as the particles were either focused in two planes or completely unfocused over this frequency range. Such imprecise z-plane

focusing was observed in the 100-channel device as well. While imaging focused streams in individual channels, not all channels resonated at the same frequency; there were atleast 4 resonance frequencies (Table 1) for the flow cell, with these frequencies increasing gradually in channels from one end of the device to the other. Furthermore, the maximum sample flow rate for appreciable focusing was lesser than that observed in the type-2 100-channel device described in section 6.1.3.1.

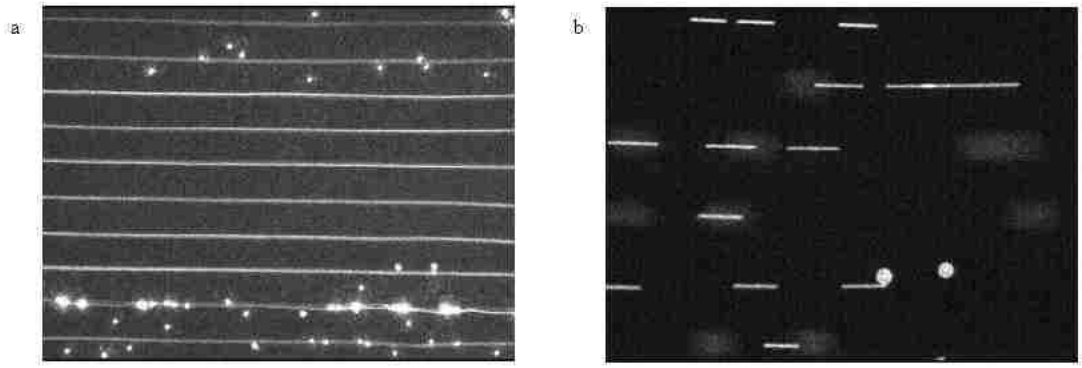

Fig. 8.3 (a) Image of 10 streams of 10.2 μm NR-PS particles flowing at 500 μL/min (b) Image of 6 streams obtained using 10x objective at low exposure time indicates more than one focusing plane in the z-direction

Channels	Resonating frequency (MHz)
1-12	4.492
13-30	4.483
31-82	4.468
83-100	4.455

Table 8.1 Four different resonating frequencies observed in the 100 channel device etched to a half-wavelength in the z-plane

8.4. Discussion

As mentioned earlier, precise focusing of particles into a single plane eliminates or minimizes the deviations in optical measurements in flow cytometry. In this chapter, an attempt was made to focus the particles not only in the x-plane but also the z-plane as well by etching the flow channels to half-wavelength dimensions. Although, a preliminary attempt to precisely focus particles into a single z-plane focusing of particles in the glass capillary was successful, the results when extended to multinode acoustic focusing were not satisfactory as more than one z-plane was observed in both types of devices etched to half-wavelength dimensions. Careful examination of this phenomenon however helps in giving a suitable explanation for the observations made here. First, at the resonance frequency, the acoustic energy in the system is a maximum. When resonance is established in the x-plane alone, such as applied to those devices used in chapter 6, the energy distribution is limited to the 3 nodal planes in the x-direction alone. However, when the channel is etched to half-wavelength dimensions, the energy is distributed (though not equally) between the x- and the z-planes, thus resulting in lower energy both these planes. This energy distribution in turn yields poor focusing in the z-plane, besides reducing the range of flow rates for appreciable x-plane focusing in the 100-channel device and establishing different resonance frequencies across the channels in the device. On the other hand, precise z-plane focusing of particles was observed in both the 2 mm wide channel as well as the 100-channel device used in Chapter 6. Such precise focusing observed in these channels could be attributed to the higher magnitude of lift force acting on the particles in the channel. Calculations showed that the lift force in channels etched to 100μm was comparable to those on particles focused using inertial

forces[11]. Thus the lift force together with the acoustic force on the particles precisely focuses the particles in two dimensions in both type-1 and type-2 devices etched to half-wavelength dimensions. Hence it can be concluded that cells and particles are not precisely focused into the z-plane when acoustic flow channels are etched to match half-wavelength in the z-direction despite theoretical predictions and that the shallow the channels the greater is the magnitude of both the acoustic as well as the inertial force acting on it.

Chapter 9

Optical analysis of parallel streams

9.1. Simultaneous analysis of parallel streams

Flow cytometry is a powerful analytical technique capable of measuring as many as 18 fluorescence parameters[105] from single cells. Despite its success, the hydrodynamic focusing mechanism used therein limits its use in rare event analysis such as the detection of circulating tumor cells, where one abnormal cell has to be counted in a population of a billion cells. Flow cytometry users often forego either precision or analysis time for such high throughput applications. Although using an array of high numerical aperture microball lenses to image focused particle streams individual channels has demonstrated success in improving analysis rate in hydrodynamic mechanism[74], issues related to the sheath fluid persist. However, such challenges can be overcome by using alternate high throughput focusing mechanisms instead of the conventional hydrodynamic focusing mechanisms. Most of these mechanisms have allowed parallelizing the focused particle streams[6, 9, 71-73]. Researchers have integrated such parallelized flow focusing systems with both conventional detectors[6, 71, 72] and advanced high frame-transfer image sensors integrating fast processors[9, 17, 73] to demonstrate their utility in high throughput applications. While these trials have shown success in appreciably high analysis rates, they suffer either from limitations in flow[9, 17] and channel dimensions limiting sample sizes, or present challenges in integrating optics[73]. However, the multinode acoustic focusing technique is free from such complexities and can handle a wide range of particle dimensions at high flow rates. While these flow cells may be

integrated with traditional flow cytometry optics, these do not permit interrogating multiple focused streams simultaneously, and hence may not achieve truly high analysis rates required for detecting rare events. This chapter presents proof-of-concept custom instrumentation that uses a laser line for interrogating the parallel focused streams and a microscope and camera for imaging them. Unlike the microball lens approach[74] that uses an array of expensive optical lenses to image individual channels, this system uses a single lens that is relatively inexpensive, allows interrogating multiple focused streams and multiple channels simultaneously and also can be integrated with beam laser source used commonly in flow cytometry.

9.2. Laser line generation using Powell lens

A number of optical elements, such as polygonal-prismatic lenses and cylindrical lenses, can be used to generate a laser line. The former requires complex rotating instrumentation. Although simple in construction and amenable to easy integration cylindrical lenses suffer from a non-uniform intensity profile. These issues can be overcome using the Powell lens[106] which is a modified cylindrical lens having a conical apex on one of its surfaces. The radius of curvature decreases from the center towards the edge, which results in a monotonic decrease in divergence, and hence establishes nearly uniform laser line that deviates less than 10% in intensity for almost 80% of its length[107]. However, the intensity profile of the laser line is sensitive to the alignment of the laser beam source. Besides intensity, the fan angle which is related to the conic constant of the prism surface and the beam size determines the length of the

laser line[108]. Previously, a Powell lens was successfully used to improve analysis rate in hyperspectral Raman imaging studies. While imaging using an intensified CCD, the uniformly intense laser line produced by the Powell lens allowed reading spectral signatures of fluorescently labeled polystyrene microspheres with high precision comparable to that of conventional beam spots used in such studies[107].. Furthermore, when used for gene expression studies by microarray scanning, the scanning rates, sensitivities and signal-to-noise ratios were comparable to that of a commercial instrument[108]. Such a uniform intensity laser line providing high sensitivities has advantages for flow cytometry analyses and hence the Powell lens is a suitable contender in the place of traditional optics for multinode acoustic flow cytometry.

9.3. Comparison of charge-coupled device (CCD) and complementary metal oxide semiconductor (CMOS) sensors

Both charge-coupled devices (CCD's) and complementary metal oxide semiconductors (CMOS) are used for scientific imaging. While both these devices convert the incident photons of light into electrical charges and further into electrical signals, they differ in their readout circuitry. The CCD can be considered as an array of photodiodes where the electrical charge is collected and stored in wells and later amplified and converted into digital signals by a single channel. The CCD provides high sensitivity and high quality images and may also use additional elements in its circuitry to reduce noise significantly. However, CCDs accumulate charges and suffer from low readout speed. CMOS differs from CCD in that each photo sensitive pixel is integrated with its own amplification,

noise cancellation and digital conversion circuitry. Although including these features increases complexity and reduces sensitivity, the read-out rates are higher than CCD's as signals are processed in more than one channel[109].

9.4. Methods

9.4.1. Flow cell

The proof-of-concept imaging system for multinode acoustic focusing was demonstrated using a 1mm wide glass capillary flow cell, fabricated using procedures discussed in Chapter 5, and driven using a piezo ceramic transducer having resonance frequency at 4.48MHz, which focuses the particles into 6 focused streams across the width of the capillary.

9.4.2. Experimental setup

Two designs that differ in the quality of the Powell lens and the type of the image sensor were developed to image the parallel focused streams generated within the glass capillary flow cell. This imaging system uses commercially available lens holders and stages and is built on a laboratory optical bench. A 150mW, 532nm laser light source (Coherent Inc., Santa Clara, CA), producing a beam spot of diameter 340μm, is used as excitation source. The laser beam passes through a neutral density filter (Thorlabs Inc, Newton, NJ) to reduce the beam intensity, followed by an iris for alignment, before entering the 2x beam expander (Thorlabs Inc, Newton, NJ) that increases the beam spot to twice its dimension.

The expanded beam spot is reflected off of a mirror into a 5^0 fan angle experimental grade Powell lens (Laserline Optics Canada, Canada), which diverges the incident expanded beam to produce a laser line of nearly uniform intensity. The laser line so produced is collimated using a plano-convex lens (Edmund Optics, Barrington, NJ), and passes through a dichroic filter that directs it into an objective aspheric lens (Thorlabs Inc, Newton, NJ) having a numerical aperture of 0.5. This high NA aspheric lens focuses the collimated laser line onto the flow cell and also collects the fluorescence emission from the sample. The emitted signal from the flow cell passes through the dichroic filter (Thorlabs Inc, Newton, NJ) and is directed through a plano-convex lens onto a high frame rate CMOS camera (Orca-Flash 4.0, Hamamatsu, Bridgewater, NJ). A bandpass filter (Thorlabs Inc, Newton, NJ) placed just in front of the camera allows only a narrow wavelength of the emitted light onto the camera (Fig. 9.1).

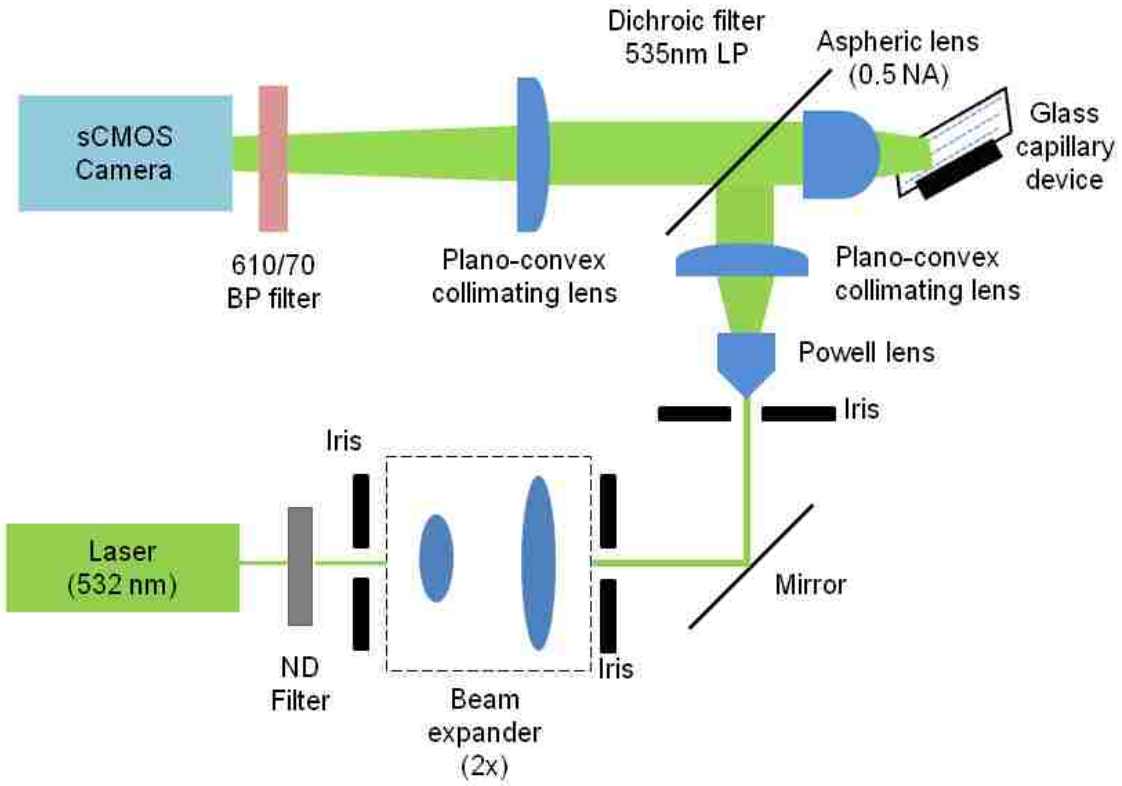

Fig. 9.1 Preliminary optical instrumentation using a beam expander, an experimental grade 5^0 fan angle Powell lens for laser line generation and a scientific complementary metal oxide semiconductor (CMOS) camera for imaging 6 parallel focused streams in a 1mm wide glass capillary device driven using a 4.48MHz piezo-ceramic transducer

The system described above was slightly modified to obtain a more uniform laser line. In this system, light from the source is reflected by two mirrors onto a plano-convex lens (Edmund Optics, Barrington, NJ) of focal length 50mm, which focuses the beam spot of original dimension onto a high quality 5^0 fan angle Powell lens (Laserline Optics Canada, Canada). This generates a uniform laser line which is collimated by plano-convex lens (Edmund Optics, Barrington, NJ) and directed into the flow cell using high NA aspheric lens. Finally, the emission signal from the flow cell is directed into a high sensitivity EMCCD camera (Luca S, Andor Technology, Belfast, N.Ireland) placed at the focal length of the imaging plano-convex lens (Thorlabs Inc, Newton, NJ) (Fig. 9.2).

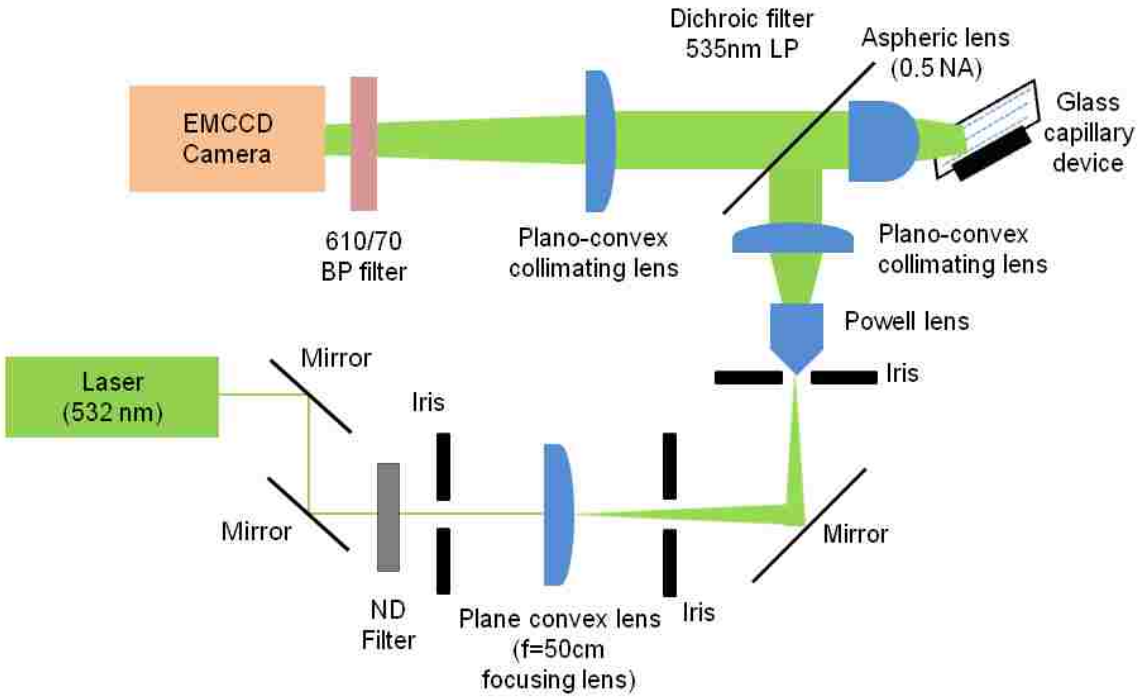

Fig. 9.2 Modified optical instrumentation using a plano-convex lens to focus the laser beam spot onto a 5^0 fan angle precision machined Powell lens and an electron multiplying charge-coupled device (EMCCD) camera for imaging 6 parallel focused streams in the 1mm wide glass capillary device driven using a 4.48MHz piezo-ceramic transducer

9.4.3. Experiment

For the preliminary setup, the dimensions of the laser line incident on the flow cell was measured by imaging a 1mm wide glass capillary filled with a diluted solution of 1mM Nile Red dye. For imaging, a complementary metal oxide semiconductor (CMOS) camera was placed at the focal length of the imaging plano-convex lens. The image of the laser lime was processed using ImageJ and the raw pixel intensity data were exported to a spreadsheet in Microsoft Excel and plotted. This procedure was repeated for the modified setup using an electron gain multiplying charge-coupled device (EMCCD) camera. However, instead of Nile Red, the glass capillary was filled with a very dilute solution of the polar dye Rhodamine.

Proof-of-concept analysis experiments were performed using a concentrated sample suspension (~10^6/mL) of 10.2μm Nile Red polystyrene particles (Spherotech Inc, Lake Forest, IL). To obtain high fluorescence intensity, the sample flow rate was limited to 500μL/min. Images of the focused particles streams were recorded at 450 frames/second using software supported by the high speed CMOS camera. For analyzing images using ImageJ, a rectangular region of interest was chosen and the pixel intensity data from the focused particle streams were plotted for stacks of images using the built-in Plot Profile too, which gives the one-dimensional spatial distribution of intensity of the individual particle streams.

For the modified setup, the same concentrated sample of 10.2μm Nile Red polystyrene sample was flowed through the glass capillary flow cell. Images of the focused streams were recorded using the EMCCD camera integrated into the setup. These images were later analyzed using the Surface Plot tool in ImageJ, which plots the pixel intensity of individual focused streams in two dimensions, after selecting the entire image frame, ~ 658 (y-pixels) x 498 (x-pixels), as the region of interest.

9.5. Results

A 1mm long laser line was obtained using the preliminary design that used an experimental grade Powell lens (Fig. 9.3a). The dimensions of both the laser line and the width of the flow cell are equal, and therefore allow imaging all 6 focused streams within the glass capillary flow cell. However, the intensity of the laser line was not uniform (Fig.

9.3b), with only about 50% of the intensity value at its ends. Furthermore, a variation in the width of the laser line (Fig. 9.3c), from its left to right, was observed.

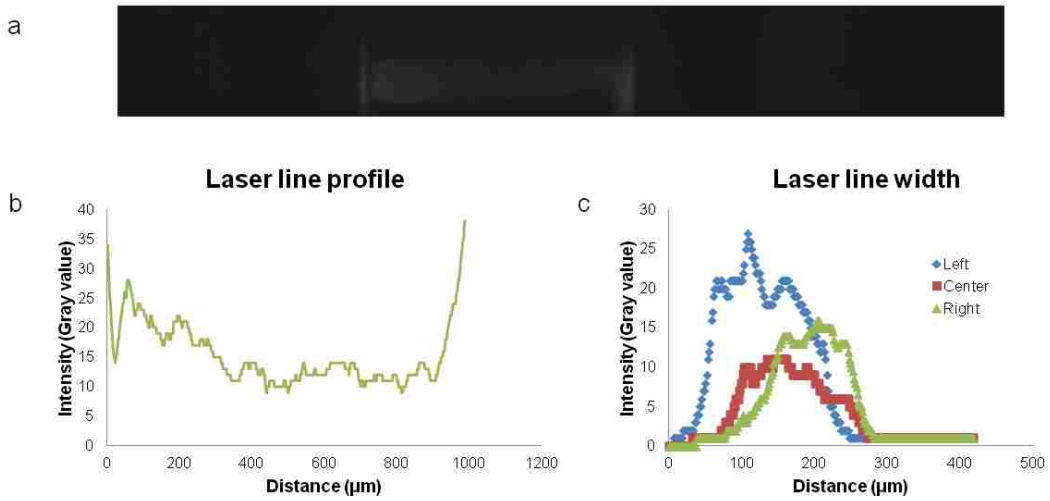

Fig. 9.3 (a) Image of the laser line obtained using the CMOS camera by imaging a 1mm wide glass capillary filled with 1mM solution of Nile Red dye (b) Intensity profile of the laser line in (a) plotted using ImageJ (c) Plot of width of the laser line in (a) at its left, center and right

Fig. 9.4 is the one-dimensional intensity plot of focused streams within the glass capillary flow cell. Although 6 peaks corresponding to the 6 focused streams (S1-6) are visible, the peak intensities are not uniform and too low.

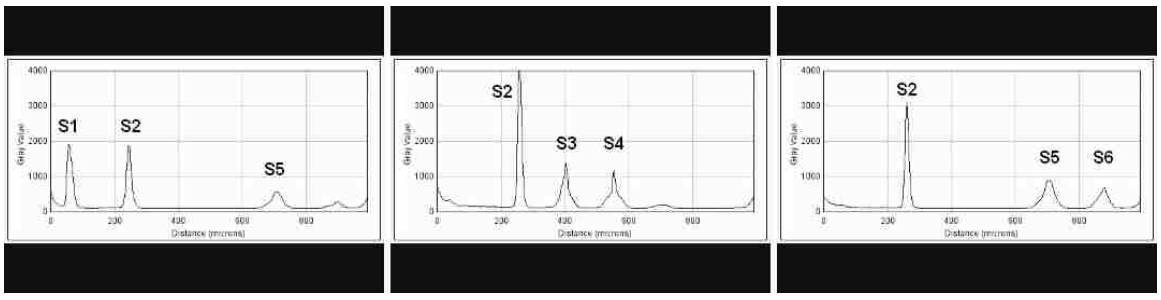

Fig. 9.4 Intensity plot of the focused particle streams (S1-6) in the glass capillary device plotted using Plot Profile tool in ImageJ

The laser line generated using the second design was more uniform in both intensity (Fig. 9.5a) and width (Fig. 9.5b). While all the 6 focused streams (S1-6) were detected, high background (noise) from the EMCCD interfered with detection of peak signal intensities despite processing the stacks of images to reduce background (Fig. 9.5c).

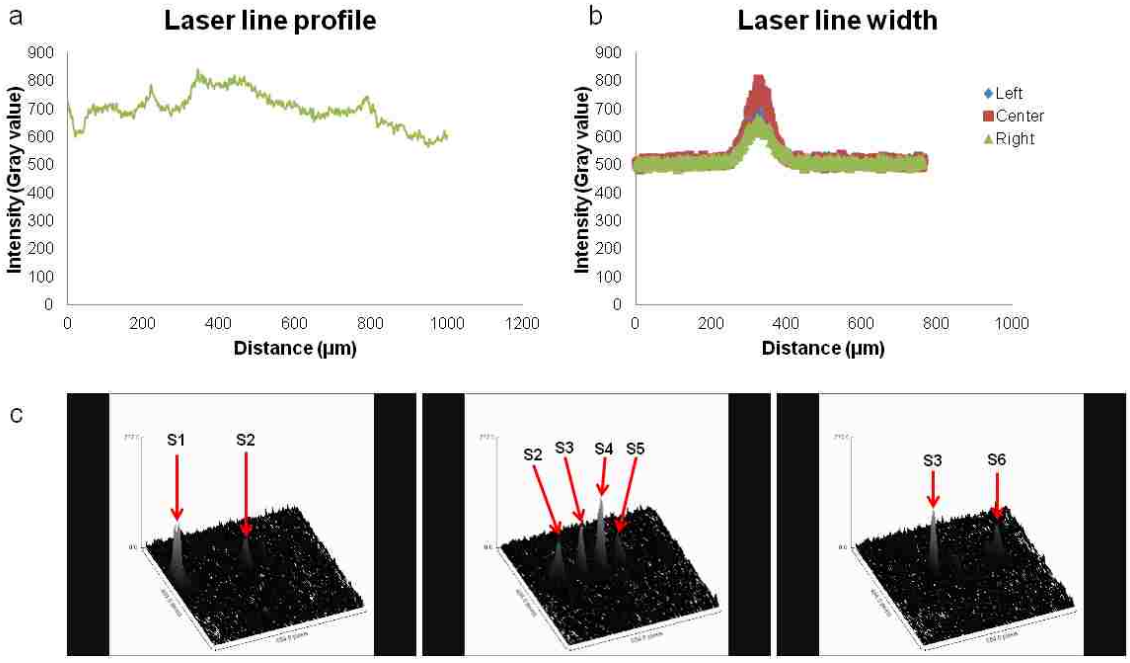

Fig. 9.5 (a) Plot of intensity along the length (x-direction) of the laser line obtained by imaging a 1mm wide glass capillary filled with dilute solution of Rhodamine using an EMCCD camera (b) Plot of intensity in the y-direction at the left, center and right of the laser line (c) Surface intensity plot of 6 focused particle streams (S1-6) within the 1mm wide glass capillary plotted using ImageJ

9.6. Discussion

The results observed herein show that the highly parallel streams generated using multinode acoustic focusing can be interrogated simultaneously using a laser line produced using a Powell lens. While these linear diverging lenses have not been previously used in flow cytometry, they allow interrogating multiple particle focused streams, and hence may find use in a flow cytometer using multinode acoustic flow cells.

Although both these systems generate only a marginally uniform laser line, optimizing the incident beam diameter and point of incidence in the prism face of the Powell lens will help in overcoming such issues. Thus, it can be concluded that the Powell lens will be an appropriate replacement for traditional optics in a multinode acoustic flow cytometer.

Besides their optical layout, the two designs differ in the type of sensor used for photon collection. Although both CCD and CMOS have been successful, the CMOS camera was capable of acquiring images faster and with lower background than the EMCCD camera. While this acquisition rate (450 frames per second) is relatively higher than most image sensors, it is capable of acquiring at even higher rates and limited only by computer hardware specifications. Such high rates cannot be achieved using the EMCCD camera. Besides acquisition rate, the signal-to-noise ratio is clearly higher as compared to the EMCCD sensor.

Proof-of-concept experiments were performed using both Nile Red particles. Rainbow calibration beads were also tested in the instrumentation design using beam expanding optics and CMOS camera. These rainbow beads have a fixed amount of fluorophore and hence can be used to characterize sensitivity of commercial flow cytometers. Rainbow beads up to peak-5 (starting with peak-13 that has the highest concentration of fluorophore) could be detected in this system. However, the images were not processed to reduce background, which could have limited the minimum concentration of the bound fluorophore for detection, which is an indirect measure of sensitivity.

Thus, these results confirm that the highly parallel focused streams of particles generated using multinode acoustic focusing technique can be interrogated simultaneously using diverging optical elements such as Powell lens and imaged using microscopy image sensors. Although the glass capillary flow cells consume more power, they are easy to integrate with optical elements and hence used in this imaging system. Here, the images obtained with these microscopy cameras were processed after capturing them. While this is sufficient for proof-of-principle experimentation, real flow cytometers use fast data acquisition systems incorporating real time signal processors. Furthermore, high analysis rates can be achieved only by using such systems. Therefore, when integrated with suitable optics, detectors and signal processing elements, multinode acoustic focusing will provide high analysis rates required for the detection of rare events.

Chapter 10

Conclusions and Future Directions

Flow cytometry is a versatile tool that finds broad applications ranging from clinical research to environmental monitoring, and invariably used for single cell analysis. Single cell characterization includes measuring absorbance, fluorescence and membrane potential. While absorbance measurements give information about the chemical composition of cells, measuring absorption spectra of microorganisms may present challenges. While Coulter counters can be used to measure size and volume of single cells based on electrical impedance measurements as they pass through the orifice, the orifice dimensions limit the size range of the particles under analysis, i.e. measuring such parameters accurately for particles of size < 2% of the orifice dimension is extremely difficult whereas particles whose size approach the orifice dimension clogs the orifice. Flow cytometry combines the power of both these techniques and enables determining both intrinsic and extrinsic properties of stained single cells by measuring optical parameters such as fluorescence, orthogonal and side scatter signals, to characterize their size and nuclear constituents, that are invaluable in determining the pathogenic state of any disease. Furthermore, flow cytometry sorts the heterogeneous cell population into a number of homogeneous groups. In flow cytometry, fluorescently labeled cell markers and appropriate excitation sources enabled distinguishing different cell types in a heterogeneous cell population and determining the relationship between the cellular variables, while the detectors and processing electronics enabled reading cell signatures and sorting cells at high speeds. Besides, flow cytometry distinguishes free from bound fluorophore, and hence unlike most fluorescence analysis techniques, does not require

washing cell suspensions. Even early flow cytometers were capable of analyzing at rates as high as 10^8 events per second by trading-off precision for appreciably high analysis rates[110-112]. While advances in photodetectors and high-speed processors have provided the necessary precision and sensitivity, these have increased the cost of commercial flow cytometers, and still require several hours of operation for sorting rare cell populations. However, such increase in analysis time is primarily due to the traditional hydrodynamic focusing mechanism that accelerates particles while focusing them using the sheath fluid, and results in short particle transit times at the detection region.

This dissertation has addressed these challenges by presenting an alternate focusing technique called the multinode acoustic focusing technique which precludes particle acceleration and focuses particles and cells into highly parallel streams depending on driving requency and harmonics of resonance, and therefore supports parallel flow cytometry. Such parallelization using the hydrodynamic mechanism introduces complications in fluidics requiring multiple sheath fluid ports for each focused stream. Besides eliminating sheath, this technique is also free of concentration effects, such as those observed in fundamental half-wavelength acoustic focusing, as particles and cells migrate into more than one stream. Furthermore, multimode acoustic focusing focuses both cells and particles at flow rates of tens of mL/min that have never been achieved using hydrodynamic and other alternate focusing techniques. Since this technique allows parallelizing flow channels and flow streams besides focusing particles at high flow rates, it is a suitable alternative to the conventional hydrodynamic technique for high throughput flow cytometry.

To demonstrate multinode acoustic focusing, flow cells were fabricated using three different approaches. Table 10.1 summarizes the design and drive parameters of the different types of multinode acoustic flow cells used in this dissertation.

Type of flow cell	No. of channels	Channel dimensions (Width / Height)	Frequency (MHz)	Drive voltage (V_{pp})	No. of nodes	Maximum flow rate (mL/min)
Machined (Glass-metal)	1	1.6 cm / 730 μm	0.8-1.7	35-50	17-37	1
Glass capillary	1	2 mm / 200 μm	3.12	50	8	1.5
Etched silicon	1	2 cm / 100 μm	2.91	20-30	40	12.5
Etched silicon	1	2 mm / 100 μm	4.48	30	12	0.5
Etched silicon	13	500 μm / 100 μm	4.492	35	39	1.5
Etched silicon	100	500 μm / 100 μm	4.492	30-42	300	25
Etched silicon	1	2 mm / 167 μm	4.48	30	12	0.5
Etched silicon	100	500 μm / 167 μm	4.455-4.492	45	300	10
Glass capillary	6	1 mm / 100 μm	4.492	30	6	0.5

Table 10.1 Summary of design and drive parameters of multinode acoustic flow cells

While all these flow cells have shown success in focusing particles into parallel focused streams, they differ in their volumetric throughput, and hence the maximum analysis rate that can be achieved when these flow cells are integrated with suitable optics and detection systems. The machined glass-metal flow cell was driven using a high bandwidth transducer coupled using ultrasound gel. Although using such a transducer enabled driving the flow cell at varying harmonics of the fundamental resonance frequenct of the transducer and hence generate different numbers of focused particle streams, its low Q-factor value required high drive voltage for focusing particles tightly into individual streams at higher harmonics despite gel-coupling. While both particles and cells were focused into highly parallel streams at flow rates up to 1 mL/min, throughput is only comparable to commercial flow cytometers using hydrodynamic focusing and too low for detecting rare events. Furthermore, fabrication technique is crude and involves using epoxy glue which contributes to additional acoustic attenuation besides fourth-power scattering losses in the aluminum metal. For this reason, fabrication of flow cells made homogeneously of material having lower acoustic losses was pursued using commercially available rectangular glass capillary flow cells. While throughput was higher than the micromachined flow cell, focusing precision was sensitive to accuracy of fabrication, i.e. the particles were not focused tightly unless the transducer was glued perpendicular to the wall of the channel. Furthermore, the walls of the glass capillary were curved, which presented additional challenges in orienting the transducer as mentioned above. While such difficulties can be overcome by using glass capillaries having walls with no curvature, they are not cost effective. Although the glass capillary flow cell is optically transparent and allows integrating into flow cytometry systems

using both conventional and advanced optics and detectors, it requires very high power despite having relatively low inherent acoustic attenuation. Such high drive voltage limits its use for flow cytometry analysis of live cells and microorganisms. However, flow cells etched in silicon are easy to fabricate also provide better efficiency of focusing. For example, while comparing single channel etched devices with the machined glass-metal flow cell, the 2 cm wide etched silicon flow cell focused particles at flow rates up to 12.5 mL/min whereas the 1.6 cm wide machined flow cell provided such precise focusing only up to 1 mL/min, and unlike the glass capillary, these flow cells required much lower power. Furthermore, design flexibility using the microfabrication approach allowed fabricating flow cells having highly parallel channels, which not only improved throughput but also increased the acoustic energy density within individual channels, thus focusing particles tightly into the individual streams. Such tight focusing allowed focusing both particles and cells at flow rates up to tens of mL/min, therefore improving throughput by few orders of magnitude than hydrodynamic focusing flow cytometers for rare event analysis such as the detection of circulating tumor cells and fetal cells in maternal blood

A qualitative study of the acoustic losses in multinode acoustic flow cells justifies the observations made with these flow cells. Acoustic losses occur in almost every component of the flow cell that includes the transducer, the fabrication material, the suspension medium and also the interfaces between each. While the transducer and medium losses are inherent and hence inevitable, the material losses can be minimized by proper selection of material of fabrication, therefore reducing the total acoustic loss significantly. Among the three fabrication materials, silicon has the least acoustic loss,

and hence the net losses in flow cells fabricated using silicon wafers is relatively lower, thus permitting focusing particles at high flow rates and with high efficiency. However, the study described here is purely qualitative. Only a quantitative description of acoustic losses in multinode acoustic flow cells can confirm these claims.

While selection of fabricating material having lower losses increases the net acoustic energy into the flow cell, uniform parabolic flow profile within channels precisely focuses particles into the channel depth, allowing precise measurement of optical parameters. The success of etched silicon flow cells in focusing particles with high efficiency even at high flow rates is partly due to such uniform flow profiles established within rectangular flow channels. At flow rates of tens of mL/min in channels etched to 100μm, the Reynolds number of flow is laminar, which establishes a parabolic profile that lifts the particles into the region of high velocity and hence positions them precisely into the center of the flow channel. Although the magnitude of inertial forces on particles in these flow cells is comparable to those in inertial focusing flow channels, such forces may only contribute to particle positioning into the channel depth, and have no influence on particle focusing into individual streams as those forces are primarily dependent on the particle as well as channel dimensions; neither particle size nor channel dimensions used here conform to those needed for inertial focusing.

Although the flow cells etched in silicon have performed better than other multinode acoustic flow cells, they still have certain limitations. First, most of the channels etched in silicon do not have a smooth surface, despite deep reactive ion etching being anisotropic having the highest etching rate in the direction of the channel depth. Such imprecision is mainly due to the etching parameters. Such irregularity in smoothness

results in particle settling as observed in most flow cells etched in silicon. Furthermore, surface roughness could also interfere with focusing precision within channels besides limiting the sample flow rate due to disturbances in flow profile. Although challenging, such irregularities in etching can be overcome by adjusting the etching parameters suitably.

Besides etching, these etched flow cells could present challenges in integrating them with laser optics. Unlike glass, silicon is opaque and absorbs incident photons. Therefore, for flow cytometry interrogation, these flow cells will have to be etched through the wafer. Although possible, they require relatively expensive wafers besides longer etching times as the rate of etching decreases gradually with etching depth.

While the discussion so far concludes that these multinode flow cells provide throughput much higher than almost all commercial flow cytometers, they will not provide high analysis rates if integrated with traditional flow cytometry optics and detectors, as most flow cytometers use optics that interrogate only one focused stream. Hence, it is necessary to develop a custom flow cytometry system specially for these multinode acoustic flow cells. While designing a complete flow cytometry system for multinode acoustic focusing is beyond the scope of this dissertation, a proof-of-concept imaging system was developed to show that these flow cells will provide high analysis rates as proposed when integrated with suitable optics and detectors. This proof-of-principle instrumentation uses a Powell lens to generate a laser line that interrogates the parallel focused streams, which are imaged using microscopy and cameras fabricated using high gain and high speed sensors. Besides a Powell lens, crossed cylindrical lenses also generate a laser line. However, these lenses provide uniform intensity only for smaller

line dimensions, and may be unforgiving for very long laser lines that may have to be used with multinode acoustic flow cells. For the Powell lens, the dimension of the laser line depends on the fan angle and the dimension of the incident beam spot, and hence can produce a high and uniform intensity laser line of any dimension. Another way of interrogating the individual focused streams may be to scan them at high frequencies. However, this approach involves using complex optics which eventually increases the cost and complexity of operation. Thus, for a true multinode acoustic flow cytometer, the Powell lens is preferred to conventional optics. Besides interrogation optics, the analysis rate of any flow cytometer depends on the speed of the processing electronics at the detection end. While microscopy sensors used herein have proved successful in imaging the focused particle streams, future work with these imagers should be directed towards interfacing them with real time signal processing tools and also detectors that are capable of processing and generating data in real time, such as multi anode photomultiplier tubes (PMT's). Unlike the traditional PMT's, these have multiple channels for processing optical information, which not only increases speed of acquisition and processing, but also preserves spatial optical information. The success of flow cytometry is mainly due to its ability to sort the cells of interest, post detection. In most rare event analyses, confirmation studies are performed with the homogeneous sorted population using standard cytometry techniques. Thus, just like the conventional fluorescence activated cell sorter, the multinode acoustic flow cytometer should also include sorting capabilities. Hence, future work should also focus on developing suitable sorting mechanisms for these multinode acoustic flow cells. However, this work proves that multinode acoustic focusing will help flow cytometry reach new strides in throughput and analysis rates and

hence replace hydrodynamic focusing technique for the detection of rare events in flow cytometry.

List of Appendices

List of videos in Appendix

Appendix1. Demonstration of multinode acoustic focusing using videos

A1. Micromachined multinode acoustic flow cell

The micromachined flow cell is the first among the three types of flow cells used to demonstrate multinode acoustic focusing for high throughput flow cytometry. This flow cell is fabricated using micromachined aluminum frame and commercially available glass slides. This flow cell has a 1.6cm wide flow channel that is 700µm deep. A 1" circular transducer was used to drive the acoustic signal and a 0.5" across it was used to measure the strength of the acoustic signal. Both these transducers were gel-coupled to the flow cell. Section A1 demonstrates multinode acoustic focusing through videos recorded using Windows Movie Maker® tool by a commercially available video camera that was interfaced with a computer running on Microsoft Windows®.

A1.1. Multinode acoustic focusing of 10.2µm polystyrene particles

VideoA1.1.1 shows the 10.2µm Nile Red polystyrene particles, flowing at 250µL/min, focusing into 33 parallel focused streams when driven at 1.54MHz using a 1" circular transducer. This frequency corresponds to the 33rd harmonic of the resonance frequency of the transducer. Hence, on applying acoustic field, the particles focus into 33 parallel streams. This video was recorded by placing the camera at a distance sufficient to capture all the focused streams in the field of view. Although the particles focused into individual streams on entering the region of the transducer, this video was recorded immediately above the transducer. VideoA1.1.2 is a magnified image of 3 focused streams of 10.2µm Nile Red polystyrene particles. This video was recorded using a 4x objective placed in

the optical path of the camera. The particles flow randomly when the acoustic field is off. However, when the acoustic field is turned on, these randomly flowing particles gradually migrate into the nodes in the field of view.

A1.2. Multinode acoustic focusing of mixture of positive and negative acoustic contrast factor particles

VideoA1.2. demonstrates multinode acoustic focusing of a sample consisting of a mixture of positive and negative acoustic contrast factor particles. The sample used here consists of 10.2μm Nile Red polystyrene particles that have positive value of the acoustic contrast factor and few drops of 2% milk that has negative acoustic contrast factor. Therefore when the acoustic field is turned on, the polystyrene particles migrate into the nodes while the lipids in 2% milk solution migrate into the antinode of the acoustic standing wave. The flow cell was driven at 1.54MHz, and hence 33 streams of 10.2μm Nile Red polystyrene particles and 34 streams of lipids were observed. However, these alternating streams were not clear when imaged using the camera alone. Hence the field of view was restricted to include few focused streams of 10.2μm particles and lipids using a 4x objective placed in the optical path of the video camera.

A1.3. Multinode acoustic focusing of human whole blood

VideoA1.3. shows the sample of human whole blood focused into 33 parallel streams in at the driving frequency of 1.54MHz. The sample was hand-pumped at ~1mL/min. The

blood cells have a positive value of the acoustic contrast factor and hence on acoustic excitation, they migrate to the nodes of the acoustic standing wave. This video was recorded by placing the video camera at a distance sufficient to capture all the focused streams of blood cells within the flow cell.

A1.4. Multinode acoustic focusing of tumor microspheroids

VideoA1.4. shows the sample of tumor microspheroids focused into 33 parallel streams, when driven at 1.54MHz. The sample was flown at 250μL/min. These spheroids were prepared using standard protocols. The size of these spheroids were measured using Coulter counter and were found to have a mean diameter of approximately 95μm. Like the blood cells, spheroids also have positive value of contrast factor and hence move to the nodes in the presence of the acoustic field. This video was also recorded by placing the camera at a distance sufficient to image the 33 focused streams within the flow cell.

A1.5. Multinode acoustic focusing of algae

VideoA1.5. shows a concentrated sample of the algae Dunaliella focused into 33 parallel streams when the flow cell was driven at 1.54MHz. These algae were grown at room temperature under bright light. High lipid concentration, inherent of algae, restricted the flow rate to 100μL/min. Besides lipid concentration, they are very small and hence the acoustic radiation force on algae is much lower than blood cells and spheroids. Therefore,

by flowing at a relatively lower flow rate, these algae were allowed to reside longer in the acoustic field. This video was recorded 30 minutes after turning the field on.

A2. Demonstration of multinode acoustic focusing using rectangular glass capillary flow cell

VideoA2 demonstrates multinode acoustic focusing in the rectangular glass capillary flow cell. The glass capillary is 2mm wide and 200μm deep, and driven using a lead zirconate titanate (PZT) transducer crystal glued to one if its walls. The natural frequency of the driving transducer is 2.91MHz. A similar PZT crystal was glued across the driving transducer to measure the strength of the applied acoustic field. A sample of 10.2μm Nile Red polystyrene particles suspended in distilled water was flown through the glass capillary flow cell at 1mL/min. This video was recorded through a 4x objective lens in an epifluorescence microscope incorporating an electron-multiplying charge-coupled device (EMCCD) camera. Two bandpass filters, 545/25 and 605/70, were used for excitation and emission respectively. In this video, the particles are seen flowing randomly in the absence of the acoustic field. However, when the flow cell was driven at 3.12MHz with peak-to-peak drive voltage of $50V_{pp}$, the particles focus into 8 streams. However, the limited field of view through the 4x objective allows capturing only 7 focused streams at any given time.

A3. Demonstration of multinode acoustic focusing using etched silicon flow cells

This section demonstrates multinode acoustic focusing using flow cells fabricated by photolithography and deep reactive ion etching techniques. The fabrication procedure for these flow cells are comprehensively discussed in Chapter 6. Two different designs were adopted for fabricating these flow cells, which may be broadly classified as follows:

Type-1: Multinode flow cells having a single wide channel generating multiple focused streams

Type-2: Multinode flow cells having several parallel channels with each channel generating fewer focused streams

A lead zirconate titanate (PZT) crystal, 3cm long, 0.5cm wide and of thickness corresponding to its natural frequency, glued beneath the etched silicon wafer was used to drive these flow cells.

A3.1. Type-1: Multinode flow cells having a single wide channel

Two flow cells of different dimension (width) were fabricated to demonstrate multinode acoustic focusing for type-1 flow cells that focus particles into multiple streams in a single side channel. These include a 2cm wide flow cell, which when driven using a 2.91 MHz frequency generates 40 nodes, and a 2mm wide flow cell that 12 nodes when driven using a 4.48MHz transducer. The videos for both these flow cells were recorded, while flowing the sample consisting of 10.2μm Nile Red polystyrene particles through them, using 4x objective for imaging and 545/25 and 605/70 bandpass filter sets for excitation

and emission respectively. VideoA3.1.1 shows 10.2µm Nile Red polystyrene particles flowing at 12.5mL/min and focused into the nodes when the 2cm flow cell was driven at 2.875MHz. This video was recorded, using the Andor Luca S EMCCD camera that has a 10 x 10µm detector pixel size. While recording this video, the exposure time was set to 0.1s and gain to 100. Limited field of view using a 4x objective lens restricts imaging only 7 streams in a frame. VideoA3.1.2 shows 10.2µm Nile Red polystyrene particles focused into the nodes while flowing at 500µL/min in the 2mm wide flow cell when it was driven at 4.492MHz. This video was recorded using the Andor Luca R EMCCD camera that has a high-aspect rectangular field of view by virtue of its pixel dimensions. This video was recorded with an exposure time of 0.2s and a gain of 100.

A3.2. Type-2: Multinode acoustic flow cells having multiple parallel channels

This sub-section demonstrates multinode acoustic focusing using etched silicon flow cells having multiple parallel channels. These channels are designed to resonate at the 3rd harmonic, therefore generating 3 focused streams, when driven using a 4.48MHz PZT transducer crystal. First, a flow cell having 13 parallel channels, therefore generating 39 nodal streams at the resonance frequency, was fabricated and tested. In this flow cell, multinode acoustic focusing was demonstrated by flowing 10.2µm Nile Red polystyrene particles at 1.5mL/min. The video of the focused particle streams was recorded by imaging one channel at a time through a 10x objective lens in an epifluorescence microscope fitted with the Andor Luca S EMCCD camera. Bandpass filter sets, 545/25 for excitation and 605/70 for emission, which fall within the fluorescence spectrum of

Nile Red, were used for imaging the focused particle streams. In Video 3.2.1, the randomly flowing polystyrene particles in the absence of the acoustic field are seen focusing into 3 nodes in 3 channels in the 13-channel flow cell when the acoustic field is turned on.

To further increase parallelization, a massively parallel flow cell consisting of 100 parallel channels was fabricated. The dimensions of the channels were retained and driven at the same driving frequency as the 13-channel flow cell. Therefore, this flow cell generates 300 nodal streams when driven at the resonance frequency of the transducer. This massively parallel flow cell allowed focusing polystyrene particles at flow rates of tens of mL/min with appreciable precision. To demonstrate massively parallel focusing using multinode acoustic technique, videos were recorded using a 10x objective lens fitted in an epifluorescence microscope incorporating the Andor Luca-S EMCCD camera after adjusting the exposure time to 0.1s and gain to 100. VideoA3.2.2a shows randomly moving particles at 10mL/min in one of the channels in the absence of the acoustic field focusing into 3 nodes upon turning the acoustic field on. This video shows focused streams in 4 channels. The polystyrene particles were focused atleast upto 25mL/min. Video A3.2.2b shows polystyrene particles focusing into 3 nodes in two different channels in the massively parallel multinode flow cell while flowing at at 25mL/min. To test the efficiency of focusing of biological samples, Nile Red-stained human whole blood and green fluorescent protein (GFP)-stained tumor microspheroids (of mean size 65μm) were flown through this flow cell. The blood cells as well as the tumor microspheroids were stained using standard protocols. While recording the video of focused streams of both whole blood and spheroids, the exposure time was adjusted to

0.1s and the gain was set to 100. VideoA3.2.2c shows blood cells focusing into the nodal streams in one of the channels while flowing at at 10mL/min. This video clearly shows an increase in fluorescence due to high concentration of the focused blood cells in the 3 nodal regions in the channel. VideoA3.2.2d shows GFP-stained spheroids focused into 3 nodal regions in one of the channels while flowing at 10mL/min. Low sample concentration interfered with arrival of spheroids at the imaging point.

A4. Demonstration of z-plane focusing for mutlinode acoustic technique

In flow cytometry, hydrodynamic focusing precisely focuses particles into the z-plane which enables accurate measurement of the particle's optical properties. Hence any alternate technique for flow cytometry should mimic the hydrodynamic mechanism in z-plane focusing. To demonstrate z-plane focusing using acoustic mechanism, a rectangular glass capillary 8mm wide and 800μm deep was used. A lead zirconate titanate (PZT) crystal having resonance frequency at 871 kHz was used to drive this flow cell. The transducer was glued to the horizontal face so that it creates a fundamental harmonic standing wave in the depth of the flow cell. Hence, upon turning the acoustic field on, all the particles focus into a single plane. This phenomenon is seen in VideoA4.1a, which was recorded using a video camera (used in section A1) through the wall of the glass capillary and hence represents the side view of the flow cell. A single narrow focused stream is seen at the center of the glass capillary, confirming precise focusing into the z-plane. Furthermore, the top view of the flow cell, seen in VideoA4.1b, recorded using a 10x objective lens using the epifluorescence microscope and Andor Luca S EMCCD

camera shows particles dispersed across the width of the capillary but in a single plane. These two videos confirm that particles can be focused into a single z-plane in rectangular flow channels, when driven at resonance frequency that matches to one half-wavelength for the channel depth, using the acoustic focusing mechanism.

While glass capillaries having depth corresponding to one half-wavelength are used to focus particles into a single z-plane, similar focusing can be obtained with microfabricated silicon flow cells by etching them to one-half wavelength. For a transducer having natural frequency of 4.48MHz, the etch depth equals 167μm approximately. Toward the aim of focusing particles into a single z-plane in etched flow cells, one flow cell from each type, the 2mm wide flow cell for type-1 and the 100-channel flow cell for type-2, were fabricated by etching channels to 167μm. Videos of focused streams in these flow cells were recorded using the epifluorescence microscope and the EMCCD camera with suitable magnifying objective lenses. For the 2mm device etched to one half-wavelength, the video of the focused streams was recorded after setting the exposure time to 0.5s. In VideoA4.2.1a, the polystyrene particles flowing at 500μL/min focus into the nodal streams at 4.485MHz. Although 12 focused streams were observed, the field of view using a 4x objective lens limits capturing only 10 streams in the frame. To determine if the particles are precisely focused into the z-plane, the field of view was further restricted to image 6 focused streams using a 10x objective lens, and the exposure time was reduced to 0.005. As seen in VideoA4.2.1b, particles focused into more than one z-plane. This video shows focusing into atleast two z-planes. However, in VideoA4.2.1c recorded with the 2mm wide flow cell etched to 100μm used previously after adjusting the exposure time to 0.003s and gain to 200, the particles are focused

nearly into a single z-plane. For the 100-channel device etched to one-half wavelength, the videos were recorded using a 4x objective lens in the epifluorescence microscope with EMCCD camera in order to image 2 channels simultaneously, and the exposure time was set to 0.1s. VideoA4.2.2a shows 10.2μm Nile Red polystyrene particles focused tightly into 3 streams in channels 5-8 of the flow cell at the driving frequency of 4.492MHz. However, in VideoA4.2.2b recorded over channels 17-20 in the same flow cell and driven at the same frequency of 4.492MHz, constant migration of nodes is observed in atleast the center focused stream in channels 17 and 19 (the first channel from the bottom in image frames). After exhaustive experimentation, it was found that not all channels in this 100-channel flow cell resonate at the same frequency. For example, VideoA4.2.2c was recorded over channels 49 and 50 in this device with the driving frequency set to 4.468MHz. Here, the polystyrene particles are focused tightly into individual streams in both the channels. Hence, these prove that the 100-channel etched to half-wavelength dimension has more than one resonance frequency, and hence particles cannot be focused in two dimensions (across channel width and into channel depth) by etching channels in multinode acoustic flow cells to half-wavelength dimensions.

A5. Optical analysis of parallel streams in a glass capillary flow cell using custom instrumentation setup

Having fabricated multinode acoustic flow cells that provide throughput ranging from few hundreds of μL/min to few tens of mL/min, it is necessary to analyze these streams

simultaneously using advanced optics and high speed detectors to achieve analysis rates approaching a billion events per second. Toward this aim, proof-of-concept custom imaging flow cytometry instrumentation setup (Fig. 8.1) was developed. This system uses a laser line produced by an experimental grade Powell lens to interrogate the parallel focused streams and a high frame rate complementary metal oxide semiconductor (CMOS) camera to image them. A 532nm laser was used as the excitation source. The laser beam spot from the source which was approximately 340μm was expanded 2x using beam expanding optics. This expanded beam, when incident on the experimental grade Powell lens, diverges in one dimension to produce a laser line of length 1mm. However, the width of this laser line was not uniform, and using an experimental grade Powell lens was found to interfere with the quality and dimensions of the laser line. Using collimating optics and high numerical aperture (0.5 NA) objective aspheric lens, the laser line was focused onto a rectangular glass capillary flow cell, 1mm wide and 100μm deep and driven using a 4.48 MHz transducer. This flow cell generates 6 focused streams when driven at the transducer's resonance frequency. The focused particle streams within the glass capillary were imaged onto the CMOS camera placed at the focal length of a second plano-convex collimating lens. The images were recorded as stacks of TIFF formatted files using camera-supported software. Video5.1a is the screen capture of a few frames from these images. These images were later analyzed using ImageJ, a Java-coded image analysis tool. For analysis, a rectangular region of interest was selected in the image of the focused streams. The range of intensity was adjusted suitably using ImageJ without interfering with the raw fluorescence intensity data. Finally, the intensity data were obtained by running stacks of images using the Plot Profile function in ImageJ.

VideoA5.1b is the screen capture of the plot of intensity data of the rectangular region of interest in VideoA5.1a. Next, the imaging system just described was modified to include a high quality 5^0 fan angle Powell lens and an electron-multiplying charge-coupled device (EMCCD) camera instead of CMOS camera. Furthermore, the beam expander was replaced with beam focusing optics. Therefore, the size of the beam spot incident on the Powell lens was the same as that generated by the laser source. The laser line generated by modifying the previous design was relatively thinner and of uniform intensity. Here also, the images were recorded as stacks of 100 TIFF images, which were processed to reduce background significantly using ImageJ. After selecting the entire frame, 658 (y-pixels) x 498 (x-pixels), as the region of interest, the intensity data were plotted using Surface Plot function in ImageJ which gives a two-dimensional intensity profile. VideoA5.1c is a screen capture of 100 TIFF images after background subtraction using ImageJ. In this video, the positions of the peaks corresponding to the 6 focused streams within the glass capillary flow cell are consistent, which indicate tight focusing of particles within individual streams. Despite correcting for background, it still appears in this plot. However, the signal-to-noise ratio is appreciable.

References

1. Shapiro, H.M., *Practical flow cytometry*. 2005: Wiley. com.

2. Kachel, V., H. Fellner-Feldegg, and E. Menke, *Hydrodynamic properties of flow cytometry instruments.* Flow cytometry and sorting, 1990: p. 27-44.

3. Davies, D., *Cell sorting by flow cytometry.* Flow Cytometry: Principles and Applications, 2007: p. 257-276.

4. Ateya, D.A., et al., *The good, the bad, and the tiny: a review of microflow cytometry.* Analytical and bioanalytical chemistry, 2008. **391**(5): p. 1485-1498.

5. Yang, A.-S. and W.-H. Hsieh, *Hydrodynamic focusing investigation in a micro-flow cytometer.* Biomedical microdevices, 2007. **9**(2): p. 113-122.

6. Preffer, F. and D. Dombkowski, *Advances in complex multiparameter flow cytometry technology: Applications in stem cell research.* Cytometry Part B: Clinical Cytometry, 2009. **76**(5): p. 295-314.

7. Wlodkowic, D. and Z. Darzynkiewicz, *Rise of the micromachines: microfluidics and the future of cytometry.* Methods in cell biology, 2011. **102**: p. 105.

8. Janossy, G. and H. Shapiro, *Simplified cytometry for routine monitoring of infectious diseases.* Cytometry Part B: Clinical Cytometry, 2008. **74**(S1): p. S6-S10.

9. Hur, S.C., H.T.K. Tse, and D. Di Carlo, *Sheathless inertial cell ordering for extreme throughput flow cytometry.* Lab on a Chip, 2010. **10**(3): p. 274-280.

10. King, D., et al., *Progress in Capillary Flow Cytometry.* The Microflow Cytometer, 2010: p. 69.

11. Di Carlo, D., *Inertial microfluidics.* Lab on a Chip, 2009. **9**(21): p. 3038-3046.

12. Gascoyne, P.R. and J. Vykoukal, *Particle separation by dielectrophoresis.* Electrophoresis, 2002. **23**(13): p. 1973.

13. Laurell, T., F. Petersson, and A. Nilsson, *Chip integrated strategies for acoustic separation and manipulation of cells and particles.* Chemical Society Reviews, 2007. **36**(3): p. 492-506.

14. Goddard, G., et al., *Ultrasonic particle-concentration for sheathless focusing of particles for analysis in a flow cytometer.* Cytometry Part A, 2006. **69**(2): p. 66-74.

15. Edd, J.F., et al., *Controlled encapsulation of single-cells into monodisperse picolitre drops.* Lab on a Chip, 2008. **8**(8): p. 1262-1264.

16. Oakey, J., et al., *Particle focusing in staged inertial microfluidic devices for flow cytometry.* Analytical chemistry, 2010. **82**(9): p. 3862-3867.

17. Goda, K., et al., *High-throughput single-microparticle imaging flow analyzer*. Proceedings of the National Academy of Sciences, 2012. **109**(29): p. 11630-11635.

18. Piacentini, N., et al., *Separation of platelets from other blood cells in continuous-flow by dielectrophoresis field-flow-fractionation.* Biomicrofluidics, 2011. **5**: p. 034122.

19. Mernier, G., et al., *Cell viability assessment by flow cytometry using yeast as cell model.* Sensors and Actuators B: Chemical, 2011. **154**(2): p. 160-163.

20. Lin, C.-H., et al., *Vertical focusing device utilizing dielectrophoretic force and its application on microflow cytometer.* Microelectromechanical Systems, Journal of, 2004. **13**(6): p. 923-932.

21. Holmes, D., H. Morgan, and N.G. Green, *High throughput particle analysis: Combining dielectrophoretic particle focussing with confocal optical detection.* Biosensors and Bioelectronics, 2006. **21**(8): p. 1621-1630.

22. Kundt, A. and O. Lehmann, *Longitudinal vibrations and acoustic figures in cylindrical columns of liquids.* Annalen der Physik und Chemie (Poggendorff's Annalen), 1874. **153**(1874): p. 1-12.

23. King, L.V., *On the acoustic radiation pressure on spheres.* Proceedings of the Royal Society of London. Series A-Mathematical and Physical Sciences, 1934. **147**(861): p. 212-240.

24. Gor'Kov, L. *On the forces acting on a small particle in an acoustical field in an ideal fluid*. in *Soviet Physics Doklady*. 1962.

25. Nilsson, A., et al., *Acoustic control of suspended particles in micro fluidic chips.* Lab on a Chip, 2004. **4**(2): p. 131-135.

26. Whitworth, G., M. Grundy, and W. Coakley, *Transport and harvesting of suspended particles using modulated ultrasound.* Ultrasonics, 1991. **29**(6): p. 439-444.

27. Coakley, W., et al., *Ultrasonic manipulation of particles and cells. Ultrasonic separation of cells.* Bioseparation, 1994. **4**(2): p. 73.

28. Allman, R. and W. Coakley, *Ultrasound enhanced phase partition of microorganisms.* Bioseparation, 1994. **4**(1): p. 29.

29. Hawkes, J.J., D. Barrow, and W.T. Coakley, *Microparticle manipulation in millimetre scale ultrasonic standing wave chambers.* Ultrasonics, 1998. **36**(9): p. 925-931.

30. Limaye, M., J. Hawkes, and W. Coakley, *Ultrasonic standing wave removal of microorganisms from suspension in small batch systems.* Journal of microbiological methods, 1996. **27**(2): p. 211-220.

31. Grundy, M., K. Moore, and W. Coakley, *Increased sensitivity of diagnostic latex agglutination tests in an ultrasonic standing wave field.* Journal of immunological methods, 1994. **176**(2): p. 169-177.

32. Thomas, N.E., M.A. Sobanski, and W.T. Coakley, *Ultrasonic enhancement of coated particle agglutination immunoassays: Influence of particle density and compressibility.* Ultrasound in medicine & biology, 1999. **25**(3): p. 443-450.

33. Barnes, R., P. Jenkins, and W. Coakley, *Preliminary clinical evaluation of meningococcal disease and bacterial meningitis by ultrasonic enhancement.* Archives of disease in childhood, 1998. **78**(1): p. 58-60.

34. Coakley, W., et al., *Analytical scale ultrasonic standing wave manipulation of cells and microparticles.* Ultrasonics, 2000. **38**(1): p. 638-641.

35. Goddard, G. and G. Kaduchak, *Ultrasonic particle concentration in a line-driven cylindrical tube.* The Journal of the Acoustical Society of America, 2005. **117**: p. 3440.

36. Goddard, G.R., et al., *Analytical performance of an ultrasonic particle focusing flow cytometer.* Analytical chemistry, 2007. **79**(22): p. 8740-8746.

37. Petersson, F., et al., *Separation of lipids from blood utilizing ultrasonic standing waves in microfluidic channels.* Analyst, 2004. **129**(10): p. 938-943.

38. Jönsson, H., et al., *Particle separation using ultrasound can radically reduce embolic load to brain after cardiac surgery.* The Annals of thoracic surgery, 2004. **78**(5): p. 1572-1577.

39. Jönsson, H., et al., *Particle separation using ultrasound can be used with human shed mediastinal blood.* Perfusion, 2005. **20**(1): p. 39-43.

40. Lenshof, A., et al., *Acoustic whole blood plasmapheresis chip for prostate specific antigen microarray diagnostics.* Analytical chemistry, 2009. **81**(15): p. 6030-6037.

41. Petersson, F., et al. *Particle flow switch utilizing ultrasonic particle switching in microfluidic channels*. in *7th International Conf on Miniaturizing Chem and Biochem Analysis Systems*. 2003.

42. Petersson, F., et al., *Carrier medium exchange through ultrasonic particle switching in microfluidic channels.* Analytical chemistry, 2005. **77**(5): p. 1216-1221.

43. Augustsson, P., et al., *Decomplexing biofluids using microchip based acoustophoresis.* Lab on a Chip, 2009. **9**(6): p. 810-818.

44. Thévoz, P., et al., *Acoustophoretic synchronization of mammalian cells in microchannels.* Analytical chemistry, 2010. **82**(7): p. 3094-3098.

45. Augustsson, P., et al., *Buffer medium exchange in continuous cell and particle streams using ultrasonic standing wave focusing.* Microchimica Acta, 2009. **164**(3-4): p. 269-277.

46. Grenvall, C., et al., *Label-free somatic cell cytometry in raw milk using acoustophoresis.* Cytometry Part A, 2012. **81**(12): p. 1076-1083.

47. Petersson, F., et al., *Free flow acoustophoresis: microfluidic-based mode of particle and cell separation.* Analytical chemistry, 2007. **79**(14): p. 5117-5123.

48. Augustsson, P., et al. *Extraction of circulating tumor cells from blood using acoustophoresis*. in *Micro Total Analysis Systems*. 2010.

49. Adams, J.D. and H.T. Soh, *Tunable acoustophoretic band-pass particle sorter*. Applied physics letters, 2010. **97**(6): p. 064103-064103-3.

50. Lenshof, A. and T. Laurell, *Continuous separation of cells and particles in microfluidic systems.* Chemical Society Reviews, 2010. **39**(3): p. 1203-1217.

51. Evander, M., et al., *Acoustophoresis in wet-etched glass chips.* Analytical chemistry, 2008. **80**(13): p. 5178-5185.

52. Grenvall, C., et al., *Harmonic microchip acoustophoresis: a route to online raw milk sample precondition in protein and lipid content quality control.* Analytical chemistry, 2009. **81**(15): p. 6195-6200.

53. Adams, J.D., et al., *High-throughput, temperature-controlled microchannel acoustophoresis device made with rapid prototyping.* Journal of Micromechanics and Microengineering, 2012. **22**(7): p. 075017.

54. Kapishnikov, S., V. Kantsler, and V. Steinberg, *Continuous particle size separation and size sorting using ultrasound in a microchannel.* Journal of Statistical Mechanics: Theory and Experiment, 2006. **2006**(01): p. P01012.

55. Nordin, M. and T. Laurell, *Two-hundredfold volume concentration of dilute cell and particle suspensions using chip integrated multistage acoustophoresis.* Lab on a Chip, 2012. **12**(22): p. 4610-4616.

56. Shi, J., et al., *Acoustic tweezers: patterning cells and microparticles using standing surface acoustic waves (SSAW).* Lab on a Chip, 2009. **9**(20): p. 2890-2895.

57. Haake, A., et al., *Manipulation of cells using an ultrasonic pressure field.* Ultrasound in medicine & biology, 2005. **31**(6): p. 857-864.

58. Haake, A., et al., *Positioning, displacement, and localization of cells using ultrasonic forces.* Biotechnology and bioengineering, 2005. **92**(1): p. 8-14.

59. Lilliehorn, T., et al., *Dynamic arraying of microbeads for bioassays in microfluidic channels.* Sensors and Actuators B: Chemical, 2005. **106**(2): p. 851-858.

60. Evander, M., et al., *Noninvasive acoustic cell trapping in a microfluidic perfusion system for online bioassays.* Analytical chemistry, 2007. **79**(7): p. 2984-2991.

61. Neild, A., et al., *Simultaneous positioning of cells into two-dimensional arrays using ultrasound.* Biotechnology and bioengineering, 2007. **97**(5): p. 1335-1339.

62. Hammarström, B., T. Laurell, and J. Nilsson, *Seed particle-enabled acoustic trapping of bacteria and nanoparticles in continuous flow systems.* Lab on a Chip, 2012. **12**(21): p. 4296-4304.

63. Woodside, S.M., et al., *Acoustic force distribution in resonators for ultrasonic particle separation.* AIChE journal, 1998. **44**(9): p. 1976-1984.

64. Hagsäter, S.M., et al., *Acoustic resonances in microfluidic chips: full-image micro-PIV experiments and numerical simulations.* Lab on a Chip, 2007. **7**(10): p. 1336-1344.

65. Coakley, W.T., et al., *Cell manipulation in ultrasonic standing wave fields.* Journal of Chemical Technology and Biotechnology, 1989. **44**(1): p. 43-62.

66. Harris, N., et al., *A silicon microfluidic ultrasonic separator.* Sensors and Actuators B: Chemical, 2003. **95**(1): p. 425-434.

67. Hill, M., *The selection of layer thicknesses to control acoustic radiation force profiles in layered resonators.* The Journal of the Acoustical Society of America, 2003. **114**: p. 2654.

68. Hill, M., R.J. Townsend, and N.R. Harris, *Modelling for the robust design of layered resonators for ultrasonic particle manipulation.* Ultrasonics, 2008. **48**(6): p. 521-528.

69. Townsend, R., et al., *Investigation of two-dimensional acoustic resonant modes in a particle separator.* Ultrasonics, 2006. **44**: p. e467-e471.

70. Basiji, D.A., et al., *Cellular image analysis and imaging by flow cytometry.* Clinics in laboratory medicine, 2007. **27**(3): p. 653-670.

71. McKenna, B.K., et al., *A parallel microfluidic flow cytometer for high-content screening.* Nature methods, 2011. **8**(5): p. 401-403.

72. Mckenna, B.K., et al., *384-Channel parallel microfluidic cytometer for rare-cell screening.* Lab on a Chip, 2009. **9**(2): p. 305-310.

73. Schonbrun, E., S.S. Gorthi, and D. Schaak, *Microfabricated multiple field of view imaging flow cytometry.* Lab on a Chip, 2012. **12**(2): p. 268-273.

74. Fan, Y., et al., *Three dimensional microfluidics with embedded microball lenses for parallel and high throughput multicolor fluorescence detection.* Biomicrofluidics, 2013. **7**: p. 044121.

75. Pridmore-Brown, D., *Sound propagation in a fluid flowing through an attenuating duct.* J. Fluid Mech, 1958. **4**(pt 4): p. 393-406.

76. Szabo, T.L., *Causal theories and data for acoustic attenuation obeying a frequency power law.* The Journal of the Acoustical Society of America, 1995. **97**: p. 14.

77. Duck, F.A., A.C. Baker, and H.C. Starritt, *Ultrasound in medicine*. 2002: CRC Press.

78. Mason, W. and H. McSkimin, *Energy losses of sound waves in metals due to scattering and diffusion.* Journal of Applied Physics, 1948. **19**(10): p. 940-946.

79. Fabian, J. and P.B. Allen, *Theory of sound attenuation in glasses: the role of thermal vibrations.* Physical Review Letters, 1999. **82**: p. 1478-1481.

80. Treeby, B.E., et al., *Measurement of the ultrasound attenuation and dispersion in whole human blood and its components from 0–70 MHz.* Ultrasound in medicine & biology, 2011. **37**(2): p. 289-300.

81. Dai, H. and R. Feng, *Ultrasonic attenuation in red blood cell suspensions.* Ultrasonics, 1988. **26**(3): p. 168-170.

82. Hirai, N. and H. Eyring, *Bulk viscosity of liquids.* Journal of Applied Physics, 1958. **29**(5): p. 810-816.

83. Yuan, Y. and K. Shung, *Ultrasonic backscatter from flowing whole blood. I: Dependence on shear rate and hematocrit.* The Journal of the Acoustical Society of America, 1988. **84**: p. 52.

84. Yuan, Y. and K. Shung, *Ultrasonic backscatter from flowing whole blood. II: Dependence on frequency and fibrinogen concentration.* The Journal of the Acoustical Society of America, 1988. **84**: p. 1195.

85. Morfey, C., *Sound transmission and generation in ducts with flow.* Journal of Sound and Vibration, 1971. **14**(1): p. 37-55.

86. Pagneux, V. and B. Froelich, *Influence of low Mach number shear flow on acoustic propagation in ducts.* Journal of Sound and Vibration, 2001. **246**(1): p. 137-155.

87. Brand, R. and R. Nagel, *Reflection of sound by a boundary layer.* Journal of Sound and Vibration, 1982. **85**(1): p. 31-38.

88. Gammell, P., D. Le Croissette, and R. Heyser, *Temperature and frequency dependence of ultrasonic attenuation in selected tissues.* Ultrasound in medicine & biology, 1979. **5**(3): p. 269-277.

89. Straube, W. and R.M. Arthur, *Theoretical estimation of the temperature dependence of backscattered ultrasonic power for noninvasive thermometry.* Ultrasound in medicine & biology, 1994. **20**(9): p. 915-922.

90. Arthur, R.M., et al., *Noninvasive temperature estimation based on the energy of backscattered ultrasound.* Medical physics, 2003. **30**: p. 1021.

91. Muir, T. and E. Carstensen, *Prediction of nonlinear acoustic effects at biomedical frequencies and intensities.* Ultrasound in medicine & biology, 1980. **6**(4): p. 345-357.

92. Gong, X.f., et al., *Determination of the acoustic nonlinearity parameter in biological media using FAIS and ITD methods.* The Journal of the Acoustical Society of America, 1989. **86**: p. 1.

93. Davies, D., *Cell sorting by flow cytometry*. 2007: Springer. 257-276.

94. Suthanthiraraj, A., P. Pearlson, and S.W. Graves, *Fluidics.* Current Protocols in Cytometry: p. 1.2. 1-1.2. 14.

95. Simonnet, C. and A. Groisman, *High-throughput and high-resolution flow cytometry in molded microfluidic devices.* Analytical chemistry, 2006. **78**(16): p. 5653-5663.

96. Howell Jr, P.B., *Two simple and rugged designs for creating microfluidic sheath flow*. Lab on a Chip, 2008. **8**(7): p. 1097-1103.

97. Di Carlo, D., et al., *Continuous inertial focusing, ordering, and separation of particles in microchannels.* Proceedings of the National Academy of Sciences, 2007. **104**(48): p. 18892-18897.

98. Di Carlo, D., et al., *Equilibrium separation and filtration of particles using differential inertial focusing.* Analytical chemistry, 2008. **80**(6): p. 2204-2211.

99. Goda, K., K. Tsia, and B. Jalali, *Serial time-encoded amplified imaging for real-time observation of fast dynamic phenomena.* Nature, 2009. **458**(7242): p. 1145-1149.

100. Piyasena, M.E., et al., *Multinode acoustic focusing for parallel flow cytometry.* Analytical chemistry, 2012. **84**(4): p. 1831-1839.

101. Austin Suthanthiraraj, P.P., et al., *One-dimensional acoustic standing waves in rectangular channels for flow cytometry.* Methods, 2012. **57**(3): p. 259-271.

102. Cushing, K.W., et al., *Elastomeric Negative Acoustic Contrast Particles for Affinity Capture Assays.* Analytical chemistry, 2013. **85**(4): p. 2208-2215.

103. LaRue, K.E., E.M. Bradbury, and J.P. Freyer, *Differential regulation of cyclin-dependent kinase inhibitors in monolayer and spheroid cultures of tumorigenic and nontumorigenic fibroblasts.* Cancer research, 1998. **58**(6): p. 1305-1314.

104. O. Jakobsson, C.G.a.T.L., *Acoustic actuated fluorescence activated cell sorting*, in *CYTO 2012*. 2012: Leipzig, Germany.

105. Perfetto, S.P., P.K. Chattopadhyay, and M. Roederer, *Seventeen-colour flow cytometry: unravelling the immune system.* Nature Reviews Immunology, 2004. **4**(8): p. 648-655.

106. Powell, I., *Linear diverging lens*, U.S. Patent, Editor. 1989, Canadian Patents and Development Limited, Ottawa, Canada.

107. Christensen, K.A. and M.D. Morris, *Hyperspectral Raman microscopic imaging using Powell lens line illumination.* Applied spectroscopy, 1998. **52**(9): p. 1145-1147.

108. Sinclair, M.B., et al., *Design, construction, characterization, and application of a hyperspectral microarray scanner.* Applied Optics, 2004. **43**(10): p. 2079-2088.

109. Kaufmann, K., *CMOS Technology for Scientific Imaging.* Spectroscopy, 2011: p. 26-30.

110. Horan, P.K. and L.L. Wheeless, *Quantitative single cell analysis and sorting.* Science, 1977. **198**(4313): p. 149-157.

111. Shapiro, H.M., *Microbial analysis at the single-cell level: tasks and techniques.* Journal of microbiological methods, 2000. **42**(1): p. 3-16.

112. Davey, H.M. and D.B. Kell, *Flow cytometry and cell sorting of heterogeneous microbial populations: the importance of single-cell analyses.* Microbiological reviews, 1996. **60**(4): p. 641-696.